

ANALYSIS OF POTENTIAL SEDIMENTATION EFFECTS OF PROPOSED CYLINDRICAL WEDGEWIRE SCREENS FOR INTAKE OF COOLING WATER AT INDIAN POINT ENERGY CENTER

ASA Project 2011-292

PREPARED FOR:

Goodwin Procter
Boston, MA

PREPARED BY

Craig
Swanson Chris
Galagan Daniel
Mendelsohn
Lauren Decker
Deborah Crowley
Yong Kim



Applied Science Associates, Inc.
55 Village Square Drive
South Kingstown, RI 02879 USA
phone: +1 401 789-6224
fax: +1 401 789-1932

ASA Offices:
São Paulo, Brazil
Shanghai, China
Gold Coast, Australia
Perth, Australia

www.asascience.com

DATE SUBMITTED

29 March 2013

TABLE OF CONTENTS

Table of Contents.....	ii
List of Figures	iii
List of Tables.....	v
1. Introduction.....	1
2. Characterization of Rates of Sediment Deposition in the Hudson River in the Vicinity of IPEC 4	
3. Analysis of Sedimentation Effects from Proposed CWW Screen System	6
3.1 Computer Modeling of River Currents Using BFHYDRO Model.....	6
3.1.1 Model Results Incorporating the Plenum Structures	6
3.1.1.1 Velocity.....	7
3.1.1.2 Bottom Shear Stress.....	9
3.1.2 Model Results Incorporating CWW Screen Intake Flow.....	10
3.1.2.1 Velocity.....	10
3.1.2.2 Bottom Shear Stress.....	16
3.2 Computer Modeling of Flow Around CWW Screens Using FLUENT Model.....	23
3.2.1 Description of Model and Application	23
3.2.2 Model Velocity Results	24
3.2.3 Bottom Shear Stress Calculation	31
3.3 Integration of BFHYDRO and FLUENT Model Results	38
3.3.1 Results of CWW Screen Array Operation	38
4. Summary and Conclusions	42
5. References.....	45
Appendix A: Description of Proposed Use of Cylindrical Wedgewire Screen Array System to Supply IPEC Cooling Water	
Appendix B: Data Collection Activities in Proposed Area of CWW Screens	
Appendix C: Shear Stress and Erosion/Deposition of Bottom Sediments	
Appendix D: Estimation of Bottom Stress	
Appendix E: Computer Modeling of River Currents Using BFHYDRO	

LIST OF FIGURES

Figure 1-1. Plan view of IPEC site on the Hudson River with present intake and discharge structures called out	2
Figure 3-1. Example bottom speed difference distribution for the Unit 2 and Unit 3 CWW intake plenum structures.....	8
Figure 3-2. Example slack before flood tide bottom currents in the CWW screen intake array area.	11
Figure 3-3. Example maximum ebb tide bottom currents in the CWW screen intake array area.	11
Figure 3-4. Example maximum ebb tide bottom current speeds in the CWW screen intake array area.	12
Figure 3-5. Example slack before ebb tide bottom currents in the CWW screen intake array area.	13
Figure 3-6. Example maximum flood tide bottom currents in the CWW screen intake array area.	13
Figure 3-7. Example maximum flood tide bottom current speeds in the CWW screen intake array area.....	14
Figure 3-8. Example ebb tide bottom current speed difference in the CWW screen intake array area.	15
Figure 3-9. Example near slack tide bottom current speed difference in the CWW intake array area.	16
Figure 3-10. Study domain for assessment of the bottom shear stress difference.	17
Figure 3-11. Time series of study domain area coverage time series of bottom shear stress less than the critical value in the CWW intake array area.....	18
Figure 3-12. Time series of example area coverage time series of bottom shear stress less than the critical value zoom to one half a tidal cycle.....	19
Figure 3-13. Time series of example area coverage difference and free stream bottom current velocity.	20
Figure 3-14. Scatterplot of area coverage for bottom stress below the critical threshold level as a function of the free stream bottom velocity.	21
Figure 3-15. Scatterplot of difference in area coverage between the with CWW intake flow and without CWW intake flow cases for bottom stress below the critical threshold level as a function of the free stream bottom velocity.	22
Figure 3-16. Frequency distribution of free stream bottom velocities in the study domain during the evaluation period	22
Figure 3-17. Grid mesh detail around the CWW screen array (reproduced from Enercon [2012b] Figure 5.8) for a typical unit.....	24
Figure 3-18. Velocity variations at Unit 2 during ebb tide at the 50th percentile of River velocity (0.2724 m/s [0.8936 ft/s]). Ebb tide velocity is generally moving left and slightly up towards the top of the figure.	26

Figure 3-19. Velocity variations at Unit 2 during flood tide at the 50th percentile of River velocity (0.2007 m/s [0.6584 ft/s]). Flood tide velocity is generally moving right and slightly down towards the bottom of the figure.	27
Figure 3-20. Velocity variations at Unit 3 during flood tide at the 10th percentile of River velocity (0.0489 m/s [0.1605 ft/s]). Flood tide velocity is generally moving right and slightly down towards the bottom of the figure.	28
Figure 3-21. Velocity variations at Unit 3 during flood tide at the 50th percentile of River velocity (0.1913 m/s [0.6275 ft/s]). Flood tide velocity is generally moving right and slightly down towards the bottom of the figure.	29
Figure 3-22. Velocity variations at Unit 3 during flood tide at the 90th percentile of River velocity (0.4489 m/s [1.4728 ft/s]). Flood tide velocity is generally moving right and slightly down towards the bottom of the figure.	30
.....	31
Figure 3-23. Calculated shear (from velocity at 1 m (3.3 ft) in the CWW model) on the left and shear output directly from the FLUENT model on the right. Both are for Unit 2 during ebb tide at the 50 th percentile of River velocity. Ebb tide velocity is generally moving left and slightly up towards the top of the figure	31
Figure 3-24. Change in shear stress from ambient (present) conditions due to the risers at Unit 3 with 10 th percentile velocities during flood (0.0489 m/s [0.1605 ft/s]). Flood tide velocity is generally moving right and slightly down towards the bottom of the figure	33
Figure 3-25. Change in shear stress from ambient (present) conditions due to the risers at Unit 3 with 50 th percentile velocities during flood (0.1913 m/s [0.6275 ft/s]). Flood tide velocity is generally moving right and slightly down towards the bottom of the figure	34
Figure 3-26. Change in shear stress from ambient (present) conditions due to the risers at Unit 3 with 90 th percentile velocities during flood (0.4489 m/s [1.4728 ft/s]). Flood tide velocity is generally moving right and slightly down towards the bottom of the figure	35
Figure 3-27. Excess shear stress experienced at Unit 3 during flood tide at the 50th percentile (0.1913 m/s [0.6275 ft/s]). Flood tide velocity is generally moving right and slightly down towards the bottom of the figure	36
Figure 3-28. Excess shear stress experienced at Unit 3 during flood tide at the 90th percentile (0.4489 m/s [1.4728 ft/s]). Flood tide velocity is generally moving right and slightly down towards the bottom of the figure	37
Figure 3-29. Excess shear stress experienced at Unit 3 CWW array during ebb tide at the 50 th percentile velocity, with added stress from Table 3-6. Ebb tide velocity is generally moving left and slightly up towards the top of the figure.	39
Figure 3-30. Excess shear stress experienced at Unit 3 CWW array during ebb tide at the 90 th percentile velocity, with added stress from Table 3-6. Ebb tide velocity is generally moving left and slightly up towards the top of the figure.	40

LIST OF TABLES

Table 3-1. Summary of bottom speed and shear stress for the "with" and "without" CWW plenum structure cas	9
Table 3-2. Summary of area coverage for model predicted bottom shear stress less than the critical threshold for resuspension	19
Table 3-3. Percentiles of velocity observations for each unit and river tidal flow direction.....	25
Table 3-4. Summary of ambient shear stress in (N/m ²) associated with unaltered conditions at selected percentiles for the free stream River velocity. Bolded green text indicates ambient shear stress is greater than the critical shear stress.....	32
Table 3-5. Unit 2 incremental stress from BFHYDRO model results for various locations in the area of the CWW screen array.....	38
Table 3-6. Unit 3 incremental stress from BFHYDRO model results for various locations in the area of the CWW screen array.....	38
Table 3-7. Area (acres) with shear stress below resuspension threshold values for scenarios using the 50 th and 90 th velocity percentiles.	41

1. INTRODUCTION

The Indian Point Energy Center (IPEC) consists of two operating nuclear power plants, referred to as Units 2 and 3, owned respectively by Entergy Nuclear Indian Point 2, LLC and Entergy Nuclear Indian Point 3, LLC (collectively, Entergy). Unit 1 is no longer in service. IPEC is located along the eastern side of the Hudson River (River) in the village of Buchanan, New York; approximately 68 km (42 mi) upstream of the Battery (located at the southern tip of Manhattan and defined as the mouth of the River).

IPEC presently uses a once-through cooling water system that consists of two screened intake structures located at the shoreline on the River, each serving one unit. Maximum cooling water flow is 9.36 Mm³/day (1,740 Kgpm or 2.5 Bgal/day). The circulating water intake structures (CWIS) are essentially box culverts that span the water column. The water depth at the intakes is 8.2 m (27 ft) relative to Mean Sea Level (MSL). Each CWIS is made up of six individual bays. Bar screens and traveling screens prevent debris and fish from entering the intakes, respectively. Comparatively minimal service water (SW) pumps are in SW bays that are part of the same CWIS as the CW bays and pumps.

Once water passes through the condensers in each plant, the water travels through a common canal and is discharged through submerged slots in a structure located in the River downstream of the closest intake. A head between water level in the discharge structure and the River level maintains an approximately 3 m/s (10 ft/s) discharge velocity oriented offshore perpendicular to the shoreline. Figure 1-1 shows a photograph of IPEC with the intakes and discharge structures called out.

On behalf of Entergy, Applied Science Associates, Inc. (ASA) previously developed a hydrothermal model of the River that incorporated environmental and plant characteristics in support of a triaxial thermal study requested by the New York State Department of Environmental Conservation. Extensive field data sets from 2009 and 2010 were used for model calibration and validation. The background, assumptions and findings, which included field data analysis as well as model calibration and validation, was documented in two ASA reports (Swanson et al., 2010 and Swanson et al., 2011). These data are employed here.

More recently, Entergy contracted with ASA to assess the sedimentation potential associated with the proposed use of an array of cylindrical wedgewire (CWW) screens to be located approximately 100 to 150 m (300 to 500 ft) offshore of the present shoreline intake structures. The 144 CWW screens would be installed in sets of 12 connected to 12 plenums. Descriptions of the CWW screens, the layout of the arrays and other structures required for the proposed system, is documented in Enercon (2012a) and Appendix A of this report.

This assessment reviews the literature on sedimentation rates in the general vicinity of IPEC. It also assesses whether the planned installation reasonably can be expected to: (1) change the probability of resuspension of sediment post-construction; and (2) change local current patterns in a manner that may alter sediment deposition.

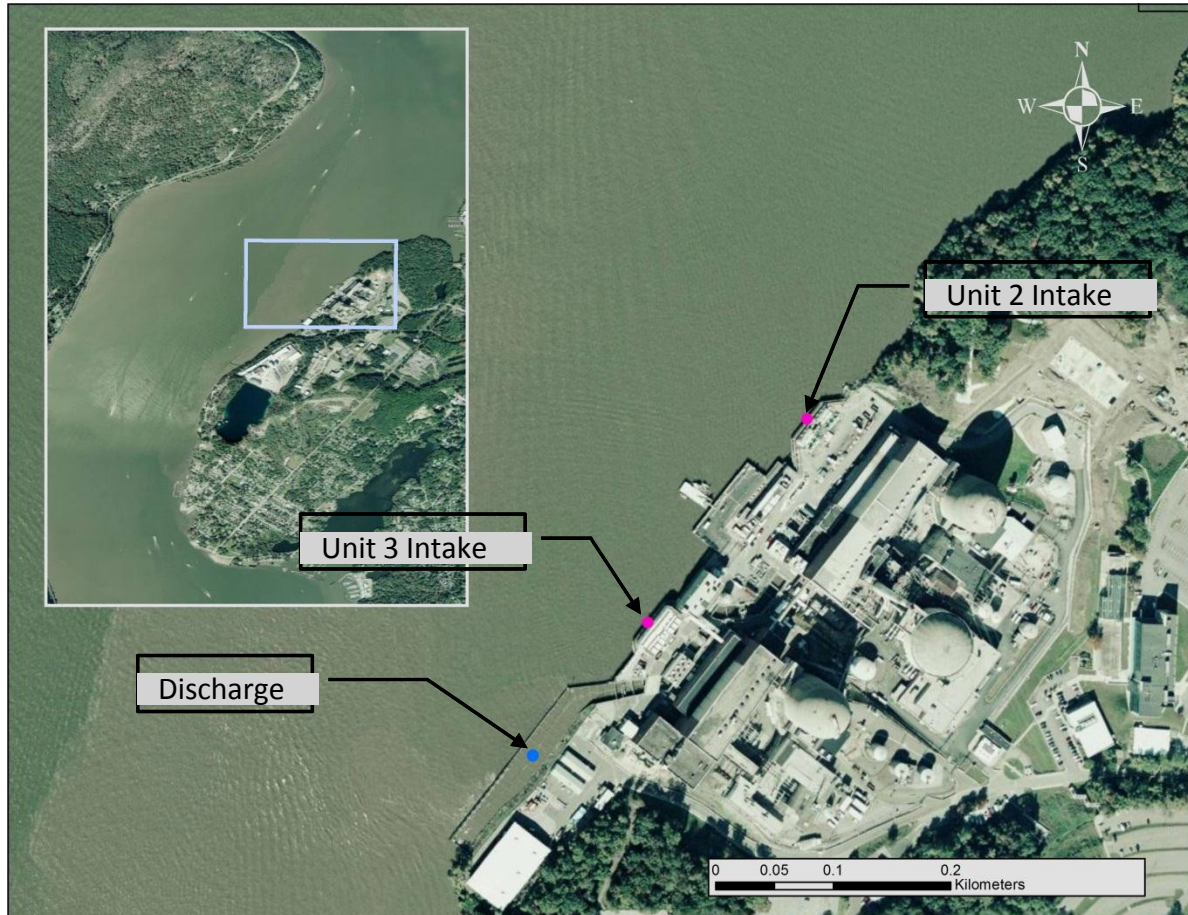


Figure 1-1. Plan view of IPEC site on the Hudson River with present intake and discharge structures called out.

This report documents these analyses. Section 1 provides background information and defines the purpose of the study. Section 2 characterizes sediment deposition patterns and rates in the area. Section 3 provides results of modeling the sedimentation effects from the proposed CWW screen system. This section includes the results from two different computer models used as part of this analysis. First, a large scale computer model, BFHYDRO, of the River (Swanson et al., 1010; Swanson et al., 2011) simulated the current velocity structure in the vicinity of the CWW screen arrays. The BFHYDRO model investigated potential effects of the CWW screen plenums and the withdrawal of intake water associated with the proposed intakes. Associated post processing was conducted to estimate areas with changes in bottom stress and thus changes in sedimentation and scour. Second, a high resolution computational fluid dynamics (CFD) model (FLUENT) prepared by Enercon (2012b) was used to perform

detailed analyses of the local bottom stress around the CWW screen arrays. The FLUENT model analyzed the effects of the risers and post processing was conducted to estimate areas with changes in bottom stress. Section 3 concludes with the integration of the results from the two models. Finally, Section 4 summarizes the analyses and results used to estimate potential deposition and/or scour due to the operation of the CWW screen system. References follow. Appendix A describes with additional detail the CWW screens proposed and the expected layout of the screen arrays. Appendix B summarizes the data collection activities recently conducted to support the system design process. Appendix C provides information on shear stress and how it affects erosion/deposition of bottom sediments followed by Appendix D that estimates bottom stress based on velocity data collected in the vicinity of IPEC and a local wave analysis. Appendix E provides details on the application of the large scale BFHYDRO model to the River and comparison with measured River currents.

2. CHARACTERIZATION OF RATES OF SEDIMENT DEPOSITION IN THE HUDSON RIVER IN THE VICINITY OF IPEC

Substantial information is available on the transport, deposition and erosion of sediment within the Hudson River Estuary, based on studies performed over several decades. The collection of bathymetric data, sidescan sonar imagery, sub-bottom profiles and samples of surface and subsurface sediment provide substantial information concerning the large scale sedimentary environments and the ongoing processes responsible.

Sediment enters the Hudson River estuary in two ways. First, it is carried by surface water runoff including from tributaries such as the Mohawk River, and the multiple small rivers within the Hudson River watershed. The annual sediment load may vary from year to year, depending on the strength of the spring freshet. Second, although net sediment flux is primarily downstream, upstream sediment movement can occur from NY Harbor (Bokuniewicz, 2005) as fine grained suspended sediment is transported by estuarine circulation and tides. Sediment entering the River from downstream is typically deposited and resuspended multiple times before it is permanently deposited (Bokuniewicz, 2005). Sediment transported up and down the River by reversing tidal currents and turbidity maxima (elevated levels of suspended particulates, including sediment) driven by saltwater circulation can occur when the freshwater flow high in the water column makes contact with the saltwater flow coming up the River below it. The location of the maximum is identified by decreasing suspended sediment concentrations up- and downstream and elevated concentrations where the two water masses interact. The elevated concentrations are a result of two processes: turbulence within the area where these two water masses mix and flocculation of suspended sediment particles coming downstream in freshwater when they encounter elevated salinity. The location of the maximum moves up and down the River depending on the balance between freshwater and tidal flows and can extend as far as Newburgh Bay, 90 km north of the Battery (Geyer and Chant, 2006). Within the turbidity maximum, elevated suspended sediment concentrations may enhance sediment accumulation.

Rates of sediment accumulation in the Hudson River are highly variable over short time frames (days to years), but relatively consistent over long time periods (decades). Klingbeil and Sommerfield (2005) reported annual accumulation rates for the entire estuary of up to 10 cm/yr (4 in/yr), 100-year accumulation rates up to 1 cm/yr (0.4 in/yr), and 1000-yr accumulation rates up to 1 mm/yr (0.04 in/yr). It should be noted that these sediment accumulation rates are based on calculations of a sediment budget for the entire Hudson estuary drainage, with the result that large variation from these rates can be seen within small areas of the river.

The Hudson River Estuary Program sponsored a number of studies that characterized the dynamics of sediment movement within the estuary. Sediment in the Indian Point reach of the River is predominantly muddy (silt and clay >90%) with areas of sandy mud (sand >10%) in

elongated patches (Nitsche et al., 2004). Nitsche et al. (2004) characterized the eastern half of the Indian Point reach as either dominated by sediment scour or an area of deposition with total sediment thickness less than 0.5 m (1.6 ft). The delineation of these environments is based on interpretation of sidescan sonar imagery, sub-bottom profiles, and multi-beam bathymetry data and with direct evidence from sediment samples obtained from the top 5-10 cm of bottom sediment.

Estimates of the sediment accumulation rates within the Indian Point reach of the Hudson Estuary have been calculated using two different methods. One method, reported by Nitsche and Kenna (2007), compared bathymetric data from 1930-1940 with data from 2001 to derive a sediment accumulation rate over that period. The second method (Nitsche et al., 2010) used a combination of radiocarbon dates from sediment cores in conjunction with sub-bottom profiles to determine a rate of sediment accumulation for the 20th century.

Nitsche and Kenna (2007) reported that sediment accumulated to thicknesses between 0 and 1.5 m from 1930-1940 to 2001 within the IP reach. The area directly in front of IPEC shows the complete thickness range. In the area of Unit 2 the thickness ranged from 0 to 0.5 m (0 to 1.6 ft) thick, and at the site of Unit 3 thicknesses were from 0.05 to 1.5 m (0.16 to 5 ft). These sediment thicknesses translate into average annual accumulation rates between 0.0 and 2.2 cm/yr (0.0 and 0.9 in/yr).

3. ANALYSIS OF SEDIMENTATION EFFECTS FROM PROPOSED CWW SCREEN SYSTEM

This section addresses whether rates of sedimentation are likely to be altered by the installation of the CWW screen arrays. The analysis uses two computer models to make this evaluation: BFHYDRO, a large scale model of the currents in the River; and FLUENT, a high resolution computational fluid dynamics (CFD) model used to perform detailed analyses of the local velocities and bottom stress around the CWW screen arrays.

3.1 COMPUTER MODELING OF RIVER CURRENTS USING BFHYDRO MODEL

The present model application is based on the BFHYDRO hydrothermal model previously developed for the assessment of the potential effects of the IPEC thermal effluent plume (Swanson et al., 2010; Swanson et al., 2011). BFHYDRO is a three dimensional hydrodynamic model which uses a non-orthogonal curvilinear grid in the horizontal direction and a sigma stretch coordinate system in the vertical, which maximizes flexibility in model grid design. For this application, the model used 11 layers in the vertical, identical to the hydrothermal application cited above. This application further refined the near field area model grid close to the IPEC intake structures and planned CWW screen intakes. The fine grid resolution model application was then used to predict currents for both the present and planned intake configurations. Further details of the model application and comparison of results to measured currents in the area are found in Appendix E.

The BFHYDRO model was used to investigate the effects of two characteristics of the CWW screen array. First, BFHYDRO was used to determine the effect of the plenum structures on velocity near the riverbed and corresponding bottom shear stress. Second, BFHYDRO was used to investigate whether simulated water withdrawal materially affected velocity and bottom shear stress. This section presents results of the extent of the expected changes in currents and bottom shear stress due to the plenum chambers installed in the River bottom and the effects of the cooling water flow into the CWW screen intakes.

3.1.1 MODEL RESULTS INCORPORATING THE PLENUM STRUCTURES

The configuration of the proposed CWW screen intakes includes a concrete foundation and plenums that would have a level top generally coincident with the approximate bottom depth of the intake site. However, bathymetry at the sites is not level, with the result that some portions of the plenums would be buried and other portions exposed.

The first purpose of the study was to assess the potential influence of the exposed parts of the Unit 2 and Unit 3 CWW screen plenums on local currents (and resulting bottom stress discussed in Appendix D), which defined the sediment deposition / resuspension environment in the River at these locations. The model was used to predict both the bottom currents for the present bathymetry and the hypothetical case where the bathymetry reflected installed plenum

structures. The difference in the velocity field between the two cases was then calculated by subtracting the results of the “without CWW plenums” simulation from the “with CWW plenums”.

In order to simulate the difference between the, “with” and “without” CWW plenum cases, two different model bathymetries were developed to represent each condition appropriately. The first grid used the present bathymetry as shown in Appendix E, and the second used an altered bathymetry to represent the flat, plenum chamber tops at 20.4 m [67 ft]) and (15.9 m [52 ft]) depths for Units 2 and Unit 3, respectively. The depth reference datum is taken as Mean Sea Level (MSL) at Sandy Hook, NJ, to correspond with the Entergy technical drawings for the local bathymetry and CWW design. The screens and risers are not explicitly modeled using the BFHYDRO model but instead were modeled using the finer resolution FLUENT model described in the next section.

3.1.1.1 VELOCITY

The model was run for various tidal cycles for both bathymetric configurations, one with and one without the CWW plenums as described above, then the model-predicted values stored for subsequent analysis. The predicted bottom current vectors of the simulation using present bathymetry were then numerically subtracted from the predicted bottom currents from the case with the CWW plenums included, in order to develop speed differences at every cell over the entire simulated time period. For the present analysis, the bottom layer of the model predictions was of interest because it is proximate to the bottom and includes the CWW screen plenums. Since BFHYDRO is a terrain-following approach and 11 equally spaced layers were used in the model application, the local water depth controls the layer thickness. An example model predicted speed difference between the two cases is presented in Figure 3-1.

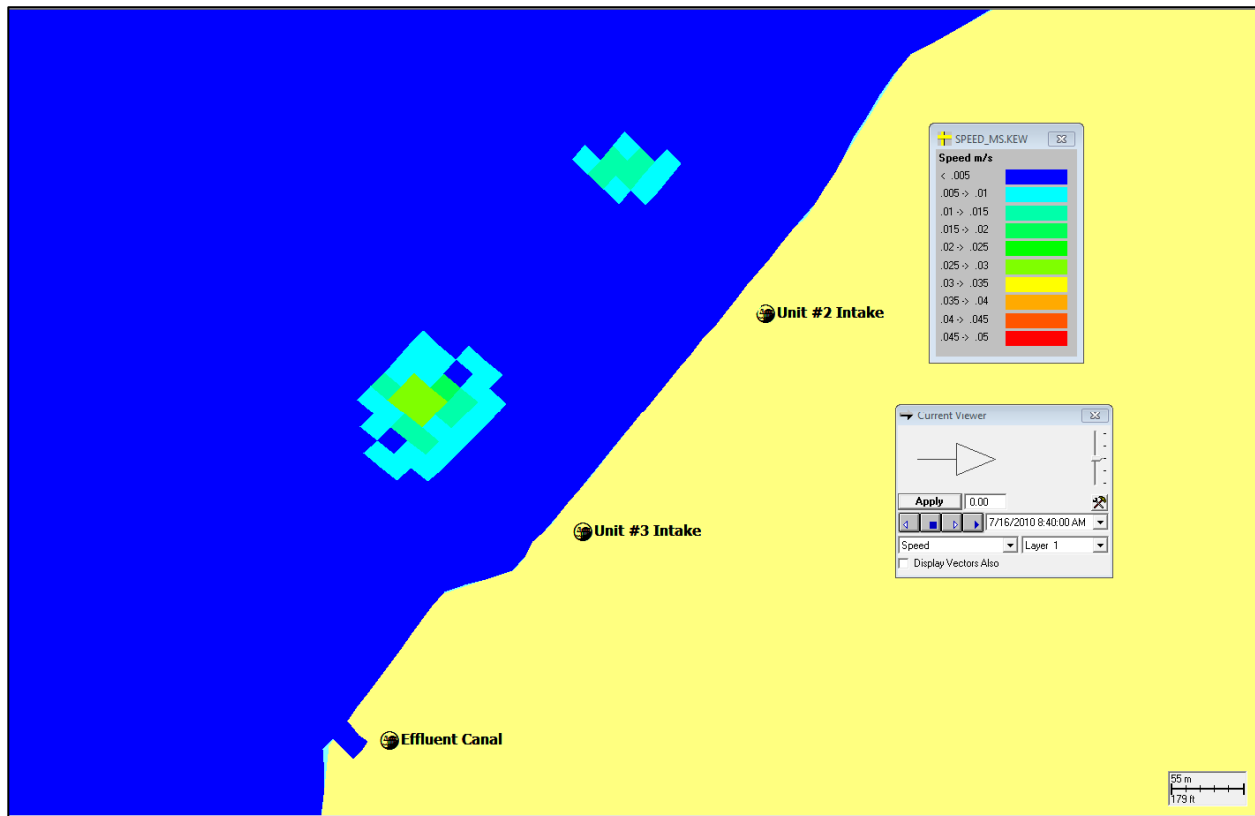


Figure 3-1. Example bottom speed difference distribution for the Unit 2 and Unit 3 CWW intake plenum structures.

As the figure illustrates, there was only a very small difference between the case with the CWW plenum structures included and that without. The maximum difference was approximately 0.014 m/s (0.046 ft/s) for the Unit 2 plenums and 0.028 m/s (0.092 ft/s) for Unit 3, which would be roughly 2% and 4% of the approximately 0.7 m/s (2.3 ft/s) peak speeds. This small difference reflected the plenum effects only, and did not include the CWW intake screens themselves. The area covered by a difference of 0.01 m/s (0.033 ft/s) or greater was approximately 1,200 m² (0.3 ac) in the Unit 2 area and 3,000 m² (0.74 ac) in the Unit 3 area. For the same locations, the associated maximum bottom speed for the CWW case was 0.650 and 0.732 m/s (2.1 and 2.4 ft/s) for the Unit 2 and 3 areas, respectively. The corresponding present bathymetric conditions bottom speeds were 0.625 and 0.725 m/s (2.05 and 2.38 ft/s), respectively. The difference between the Unit 2 and Unit 3 areas was primarily due to the difference in water depths at the two sites, where the Unit 2 intake was situated in significantly deeper waters. In addition, the bottom slope in the Unit 3 area was somewhat steeper and slightly more of the CWW plenum chamber was exposed than that of Unit 2. A summary of the speeds is presented in Table 3-1 below.

Table 3-1. Summary of bottom speed and shear stress for the "with" and "without" CWW plenum structure cas

Parameter	Unit 2	Unit 3
Present maximum bottom speed	0.630 m/s (2.07 ft/s)	0.725 m/s (2.38 ft/s)
CWW plenum maximum bottom speed	0.650 m/s (2.13 ft/s)	0.732 m/s (2.40 ft/s)
Maximum bottom speed difference	0.014 m/s (0.046 ft/s)	0.028 m/s (0.092 ft/s)
Present maximum bottom stress	0.784 N/m ² (1.14x 10 ⁻⁴ psi)	0.984 N/m ² (1.43 x 10 ⁻⁴ psi)
CWW plenum maximum bottom stress	0.819 N/m ² (1.18x 10 ⁻⁴ psi)	1.063 N/m ² (1.54x 10 ⁻⁴ psi)
Maximum bottom stress difference	0.035 N/m ² (0.51x 10 ⁻⁵ psi)	0.079 N/m ² (1.15 x 10 ⁻⁵ psi)

3.1.1.2 BOTTOM SHEAR STRESS

The change in bottom stress was estimated for the area of maximum current speed difference around the CWW plenum structure for each unit. The bottom stress calculations used the standard log law boundary layer equation (presented also in Appendix C) as follows:

where the density $\rho = 1014 \text{ kg/m}^3$ (63.30 lb/ft³), bottom drag coefficient $C_D = 0.0019$ and $U =$ (m/s) is the current speed 1 m (3.3 ft) above the bottom (see Appendix C and D for details).

The maximum bottom stress estimates for the configuration with the potential CWW plenum structures in place were 0.819 and 1.063 N/m² (1.18 and 1.54 x 10⁻⁴ psi) for Units 2 and Unit 3, respectively. The corresponding bottom stress estimates for the present bathymetry were 0.784 and 0.984 N/m² (1.14 and 1.43 x 10⁻⁴ psi), respectively. The resulting change in the bottom shear stress was a small increase of 0.035 N/m² (0.51 x 10⁻⁵ psi) for Unit 2 and a larger increase of 0.079 N/m² (1.15 x 10⁻⁵ psi) for Unit 3, equating to 4% and 8% of the peak values estimated for present conditions. The difference between the Unit 2 and Unit 3 bottom stress values was primarily due to the speed differences due to depths as described above. The drag coefficients presented were calculated from ADCP data obtained from the Normandeau field study characterizing the potential CWW locations. These values were previously described in detail in Section 6. A summary of the model predicted bottom shear stress and stress differences is presented in Table 3-1. The maximum speed difference was not coincident in time with the maximum speeds at either of the sites, but rather occurred during lower speed regimes.

3.1.2 MODEL RESULTS INCORPORATING CWW SCREEN INTAKE FLOW

The BFHYDRO modeling study was then run to simulate the CWW screen intake flow. The incorporation of the intake flow in the BFHYDRO model did not include the CWW screens, but simulated intake flow by withdrawing water from the bottom two layers of the water cells. For each intake, eight cells were used to represent the shape and extent of the array, for a total of 16 intake cells. The intake flow was held constant at $100 \text{ m}^3/\text{s}$ (2,280 MGD) distributed evenly over all 16 cells and the two layers. The purpose of this analysis was to determine whether the presence of the intake flow would affect velocity and bottom shear stress on (or near) the riverbed.

The model was run for two sets of cases, evaluating the “with CWW screen intake flow” and “without CWW screen intake flow” conditions for a spring tide and a neap tide regime over both flood and ebb portions of the tidal cycles, respectively. This selection of tidal regimes bounds the current speeds in the river and will cover all but anomalous conditions. The bottom layer velocities, which were approximately 1 m (3.3 ft) above the bottom, were then extracted for each grid cell over the model runtime period, and the bottom stress was evaluated using the equation presented in Appendix C. The cooling water discharge was included in this simulation and modeled as a flow oriented offshore perpendicular to the shoreline in the upper water column for both cases while the present intake flow was approximated with shoreline withdrawals over the water column at the present CWIS locations.

The area affected by the CWW intake flow was then estimated in two manners. The first used the velocity difference between the “with CWW intakes flow” case and the “without CWW intake flow” case, created by subtracting the “without” case from the “with” CWW intake flow case. The second used the calculated bottom stress in comparison with a threshold stress for sediment resuspension to evaluate the difference in the variability, over time, of the area covered by stresses lower than the threshold value, between the “with” and “without” CWW intake flow cases. The results are discussed in the following sections.

3.1.2.1 VELOCITY

Example plots of the model predicted bottom velocities are presented for the slack before flood and maximum ebb currents tidal conditions for visual comparison in Figure 3-2 and Figure 3-3. The model predicted speed contours for the max ebb case are presented in Figure 3-4. The bottom velocity used was based on the bottom model layer whose thickness is defined as $1/11^{\text{th}}$ of the local water depth.

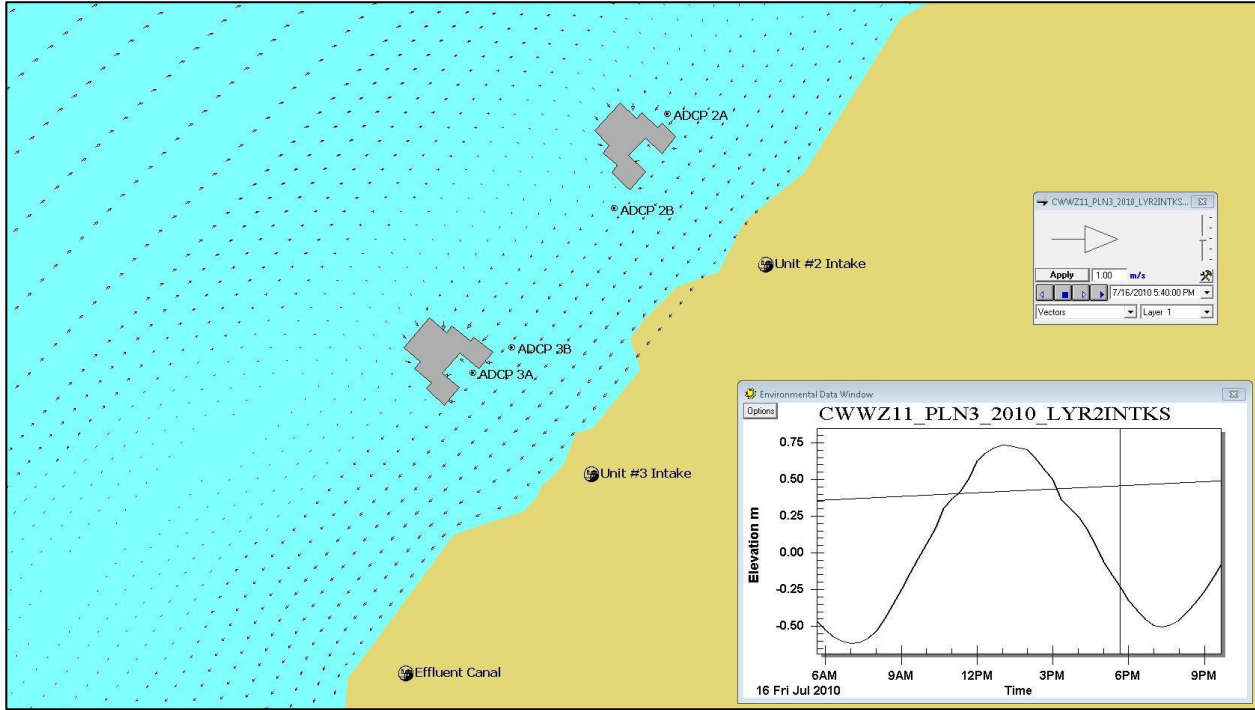


Figure 3-2. Example slack before flood tide bottom currents in the CWW screen intake array area.

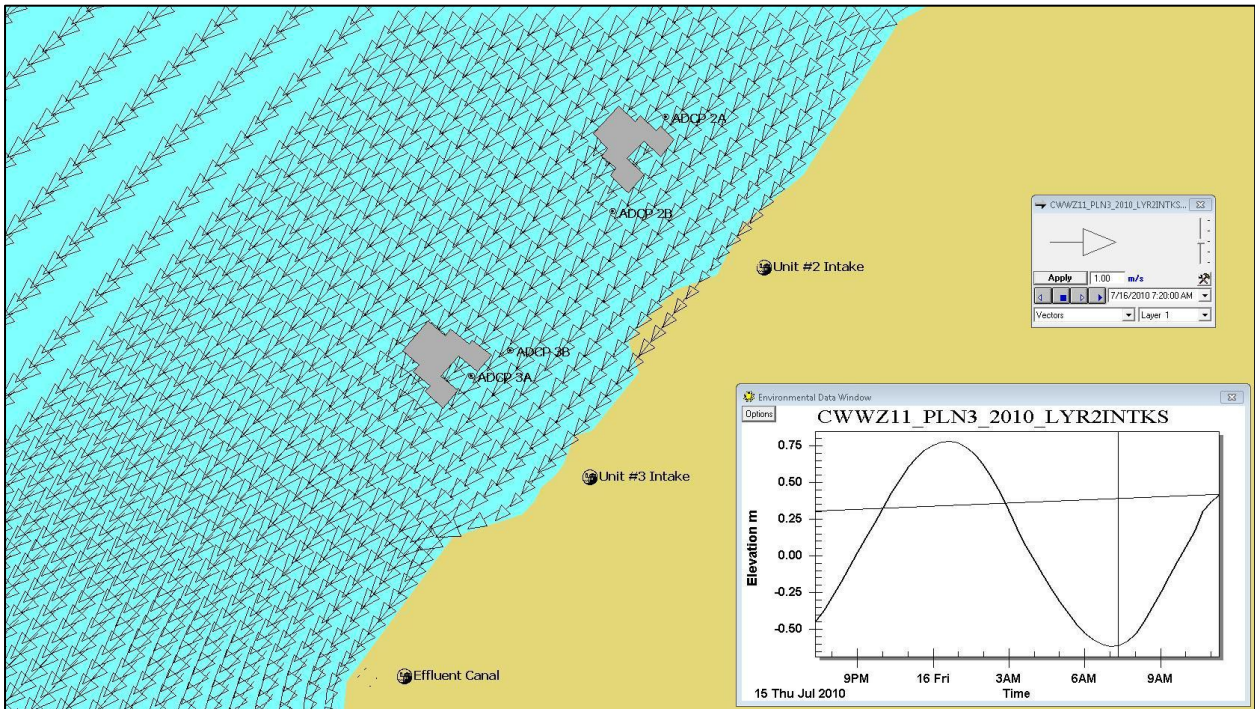


Figure 3-3. Example maximum ebb tide bottom currents in the CWW screen intake array area.

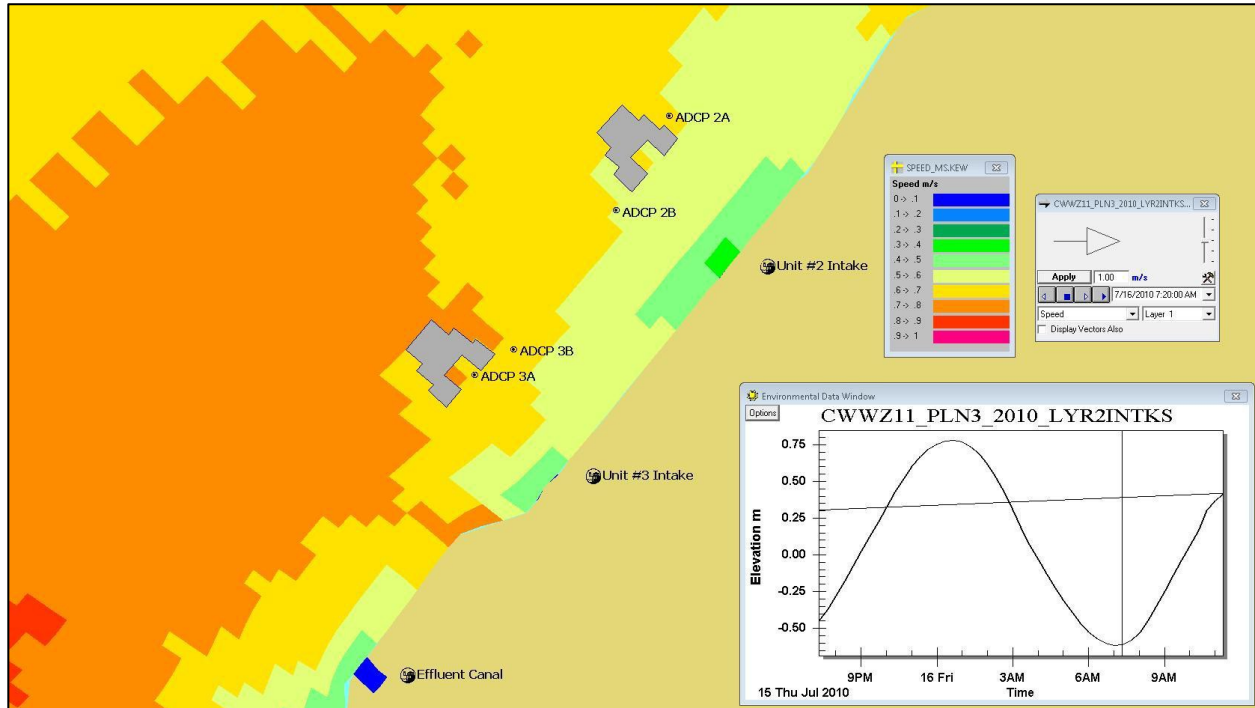


Figure 3-4. Example maximum ebb tide bottom current speeds in the CWW screen intake array area.

The slack tide bottom current plot (Figure 3-2) is presented to show the relative magnitude of the intake induced currents with respect to the free stream flow (Figure 3-3). The small intake currents (< 0.1 m/s [< 0.33 ft/s]) visible in the slack tide figure were completely overwhelmed under full ebb tide current velocities. The model predicted bottom speeds, presented for the same ebb tide time (Figure 3-4), showed the influence of the arrays. An increase in speed just upstream of both arrays is visible in the color coded speed contours. Each color band represents a 0.1 m/s (0.33 ft/s) range; therefore the speed differences are up to 0.1 m/s (0.33 ft/s). A corresponding decrease in speed was also seen immediately downstream of the arrays. This pattern was seen over the entire tidal cycle, though the increase and decrease in speeds occurred on the opposite sides of the arrays for the flood tide. This can be seen in a similar set of plots showing the slack before ebb and maximum flood tide bottom current vectors as well as a color coded contour, speed plot at the same maximum flood, presented in Figure 3-5, Figure 3-6 and Figure 3-7, respectively. Again the bottom velocity vector and speed estimates are based on the bottom model layer whose thickness is defined as $1/11^{\text{th}}$ of the local water depth.

As with the slack before ebb condition, at slack before flood the bottom currents in the river slow to near zero, (although never really stop) and the small influence of the intake can be seen as very small vectors. Although the flood tide currents never quite reach the same magnitude as the ebb (the additional Hudson River flow offsets the flow pattern), the intake induced flow of < 0.1 m/s (< 0.33 ft/s) is not discernible in the maximum flood tide plot, where the river flow approaches 1 m/s (3.3 ft/s) as was also seen in the maximum ebb tide current plots.

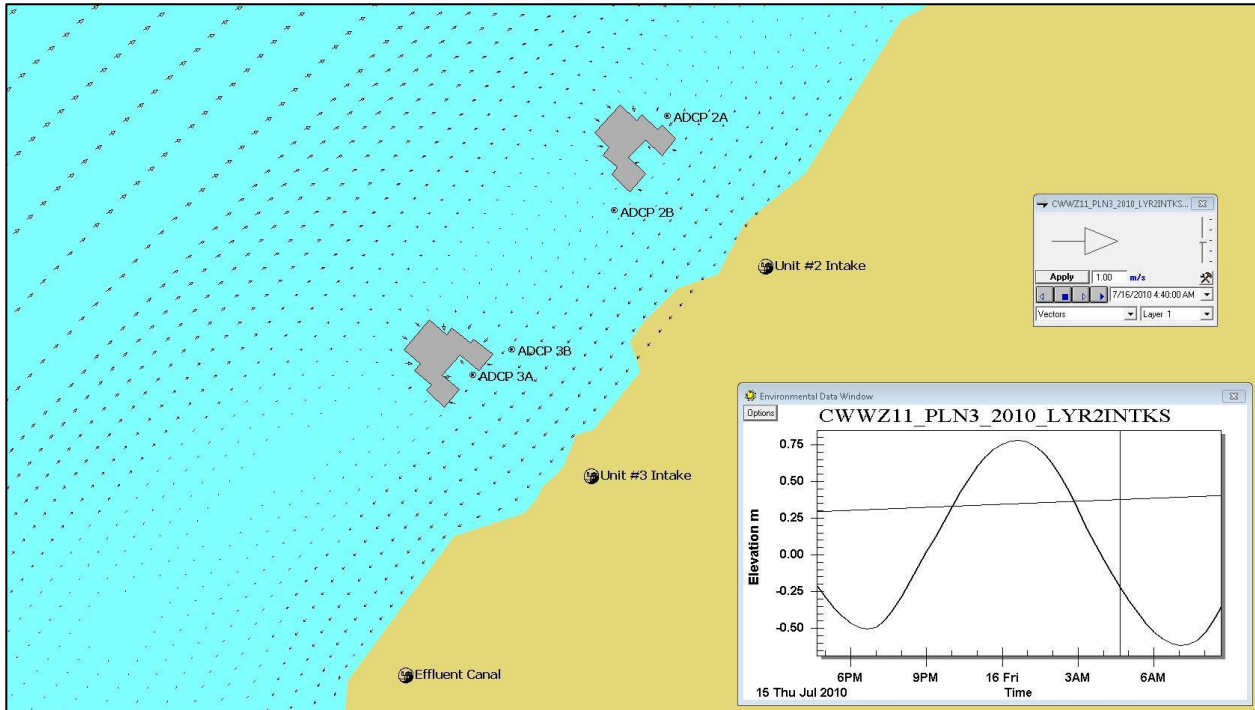


Figure 3-5. Example slack before ebb tide bottom currents in the CWW screen intake array area.

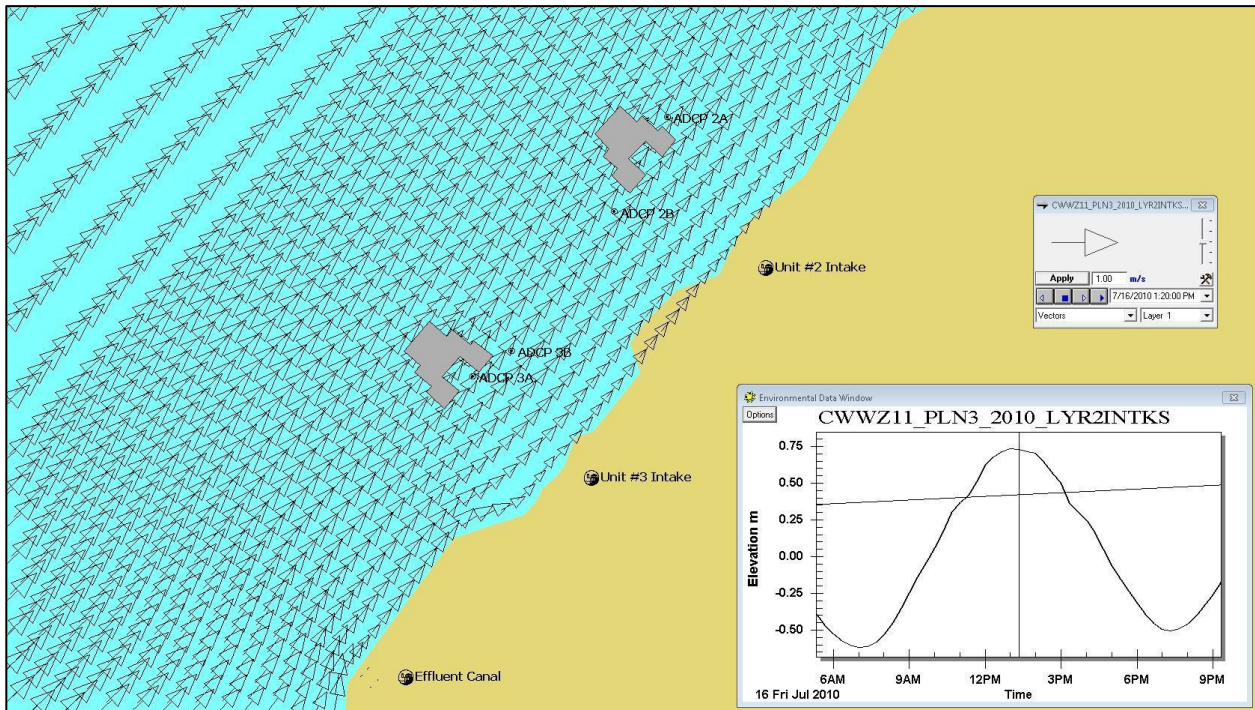


Figure 3-6. Example maximum flood tide bottom currents in the CWW screen intake array area.

Referring to the maximum flood speeds plot (Figure 3-7), it can be seen that there is a slight increase, on the order of 0.1 m/s (0.33 ft/s) on the downstream, (lower left) side of both the Unit 2 and 3 CWW intakes. Conversely, a slight decrease in speed can be seen on the upstream side of the units. In both the ebb tide and flood tide cases, there is an increase of flow on the upstream side of the Units and a decrease on the downstream side, indicating that there would be an increased propensity for resuspension of sediments on the upstream and deposition on the downstream.

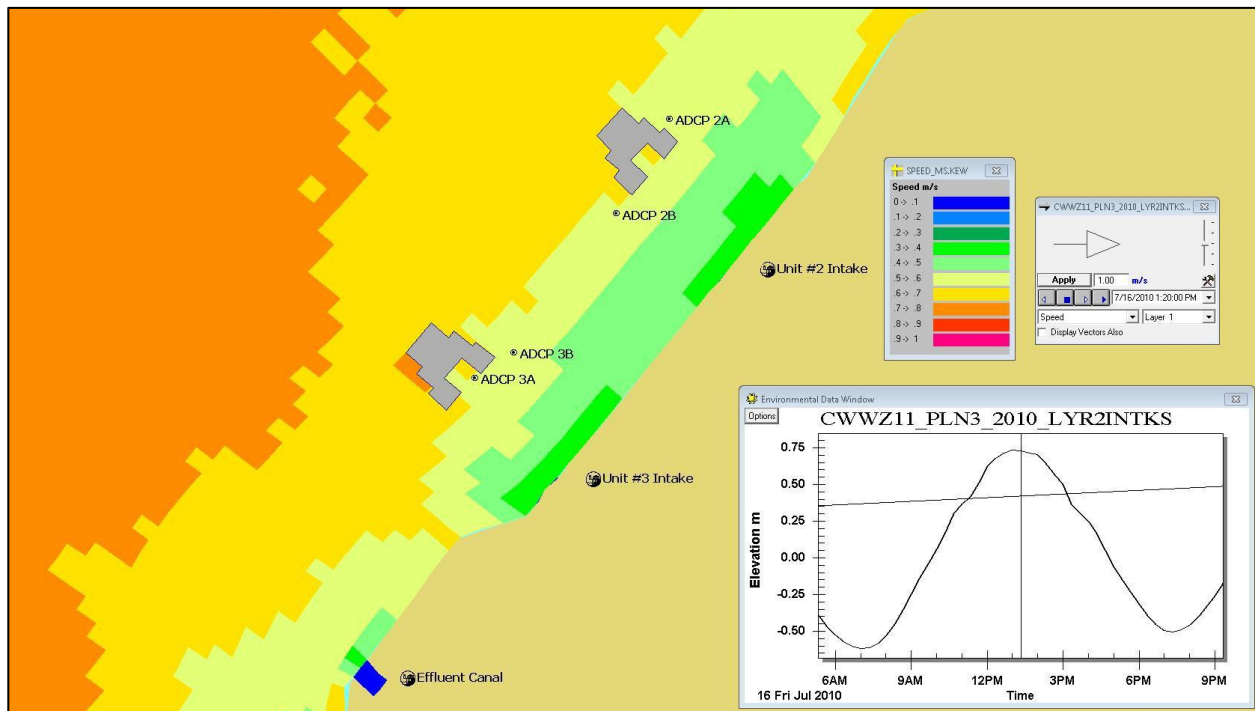


Figure 3-7. Example maximum flood tide bottom current speeds in the CWW screen intake array area.

The difference in bottom current speeds between the “with” and “without” CWW intake flow conditions is presented in Figure 3-8 for the same time step as the two figures representing maximum ebb tide currents (Figure 3-3 and Figure 3-4). The impacted area can be seen to be on the order of 0.1 m/s (0.33 ft/s) as described above. The tidal regime in the present figure is representative of the fully developed, spring ebb current speeds. For comparison, as the speeds decreased a short time later, nearing slack tide, the difference area increased, particularly in the shallower area around the Unit 3 CWW array as can be seen in Figure 3-9. Therefore, the figures illustrate that as the current speeds decrease the influence of the plenum structures on the currents increases. As seen in the previous figures depicting the current speeds, the difference would be an increase on the upstream side of the structure and a decrease on the downstream side.

This spatial and temporal speed variation will be subsequently used in conjunction with the FLUENT model predictions discussed in a later section.

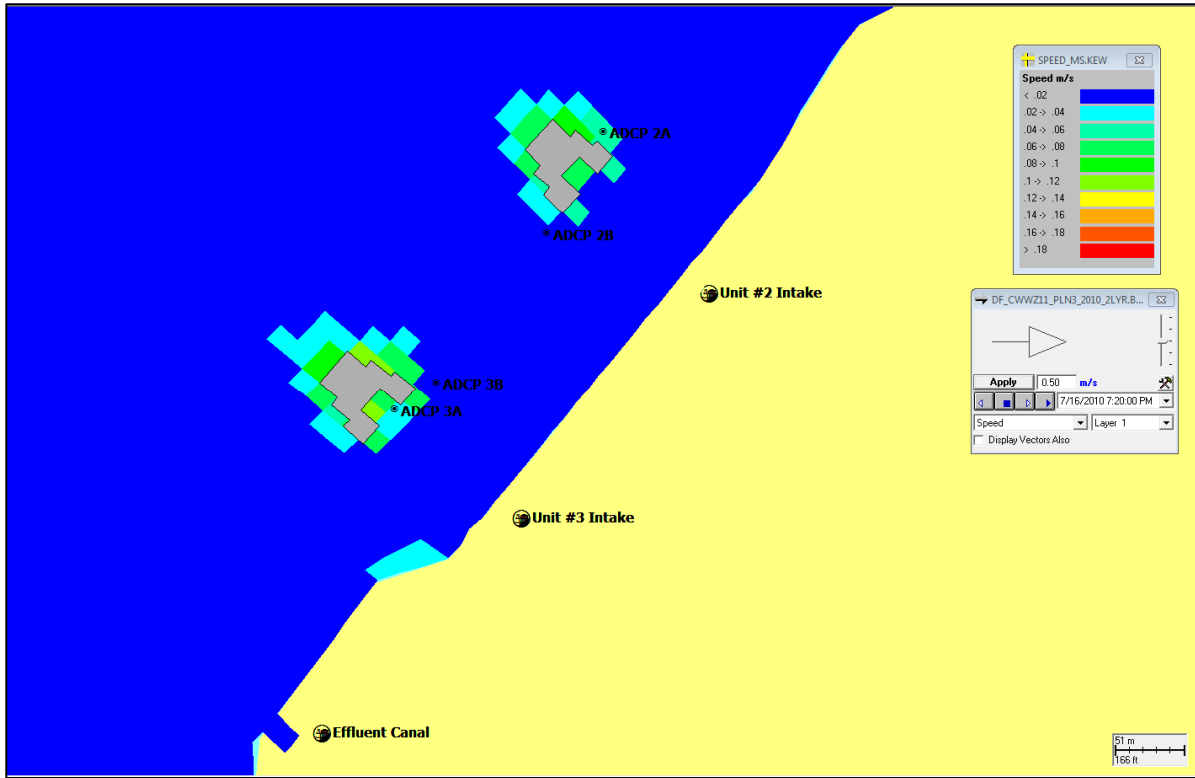


Figure 3-8. Example ebb tide bottom current speed difference in the CWW screen intake array area.

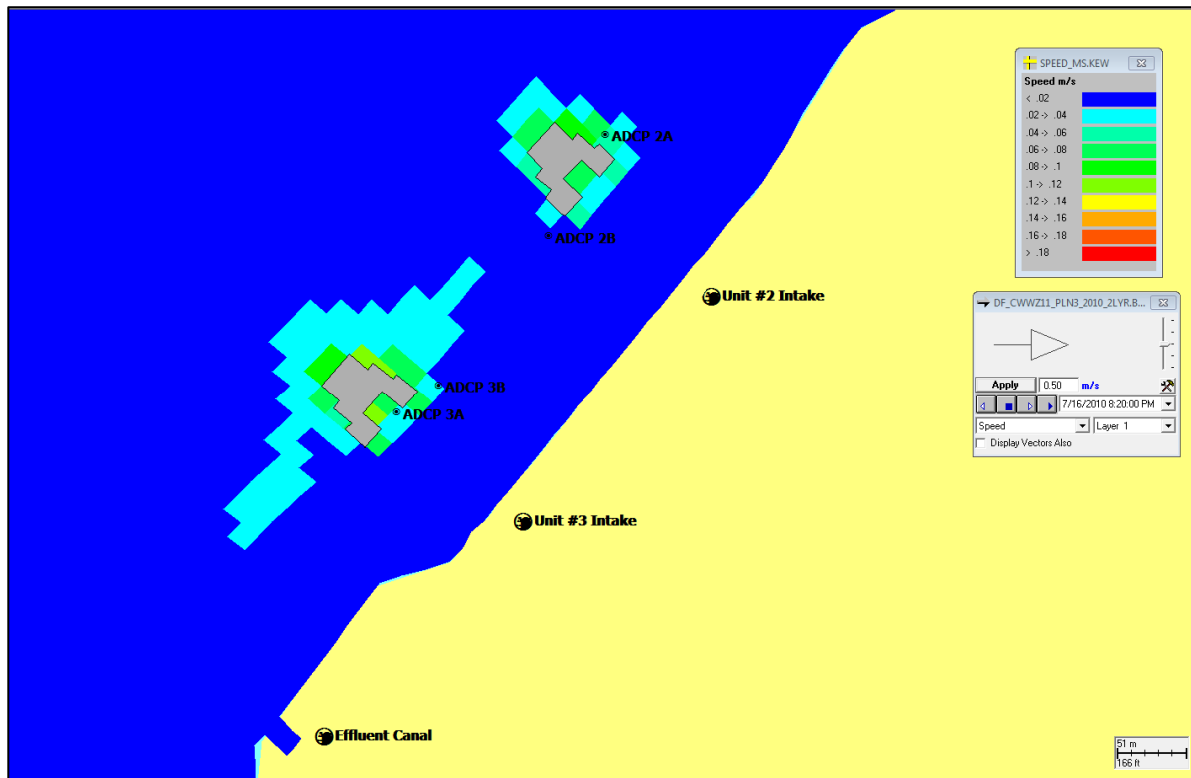


Figure 3-9. Example near slack tide bottom current speed difference in the CWW intake array area.

3.1.2.2 BOTTOM SHEAR STRESS

To determine whether the presence of the CWW screen intake flow affects the sediment erosion / deposition patterns in the area, the bottom shear stress was calculated from the model predicted velocities at each bottom cell for each time step over the model simulation. The bottom stress was then compared to a critical shear stress resuspension threshold value of 0.077 N/m^2 ($1.117 \times 10^{-5} \text{ psi}$) to determine the status of that cell (see Appendix C and D for details). If the predicted bottom stress was less than the critical value, that cell was assumed to be depositional. The comparison was made for every cell in the domain, over the tidal cycle and the area summed for all cells. This calculation was performed for both the “with CWW” and “without CWW” cases for the spring and neap tide scenarios. Finally, a difference was taken subtracting the depositional area for the “without” case from the depositional area for the case with the CWW’s intake flow in place, over the simulation period to determine if the net area less than the critical threshold increased between the “without CWW intake flow” and the “with CWW intake flow” case.

A plot of the area used to evaluate whether the bottom shear stress is less than the critical threshold over time is presented in Figure 3-10. Figure 3-11 presents time histories (time series) for both the spring and neap tidal forcing with the model results presented as bottom area in the study domain having less than the critical shear stress, overlain, over two tidal cycles

(the times along the x-axis are specified to line up the two cases and are arbitrary). The area differences between the “with CWW intake flow” cases and “without CWW intake flow” cases are also shown. A zoomed in plot showing a half tidal cycle is presented in Figure 3-11 to reveal more detail in the time series.

It should be noted that zero area coverage, which occurs the majority of the simulation time, indicates times when the bottom current velocity generates a shear stress greater than the critical value everywhere in the study domain (Figure 3-10), and therefore no area is covered by shear stress lower than the threshold. Conversely, the peaks of the curves represent very low velocities, where the entire study domain has shear stress less than the critical value. The actual area coverage of the peaks is not of particular interest, rather the area coverage between the zero values and the peaks indicate the difference between the cases.

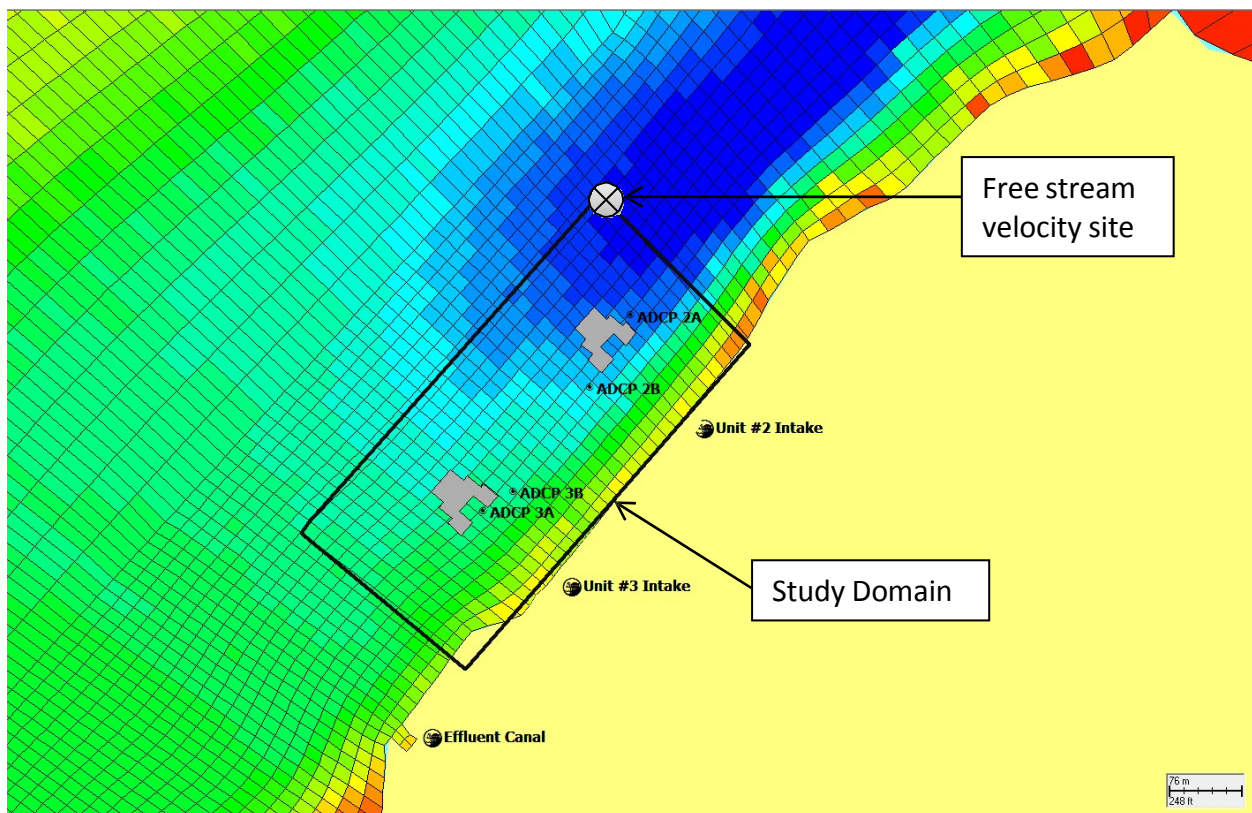


Figure 3-10. Study domain for assessment of the bottom shear stress difference.

There were only short time periods during the tidal cycle when there were any differences between the “with CWW intake flow” and “without CWW intake flow” conditions, and the affected areas were relatively small (not much different than the “without CWW” conditions). This can be seen more clearly in the time series of both the area difference and the free stream bottom current velocities (Figure 3-13). The differences varied both positively and negatively, indicating that the overall impact (net difference) was small and balanced; sometimes more erosional, sometimes more depositional. The cumulative effect was a difference of

approximately +/-2,000 m² (+/-0.5 acres) for spring and neap, respectively, with an overall insignificant net difference. A summary of the predicted areas for each case and the differences between cases is presented in Table 3-2.

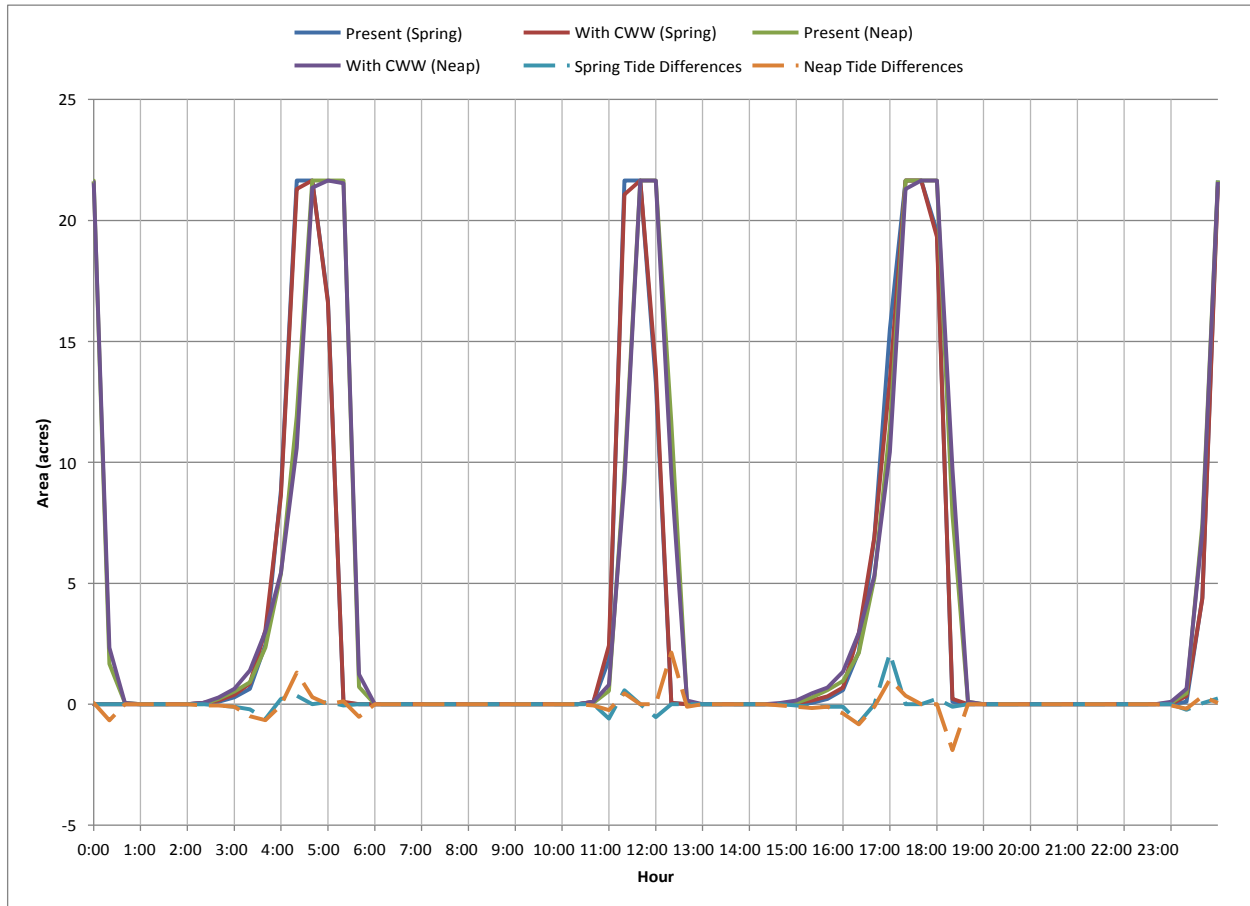


Figure 3-11. Time series of study domain area coverage time series of bottom shear stress less than the critical value in the CWW intake array area.

In addition, there was a greater difference between the spring and neap tidal response in area, with averages of 15,500 m² and 19,000 m² (3.83 and 4.73 ac), respectively, than between the “with” and “without” CWW intake flow cases (less than 40 m² [0.01 ac]) as can be seen in the summary of area coverages presented in Table 3-2. As the peak bottom current speeds for the neap case were lower than for the spring tides, there was a longer transition period around the critical shear stress current speeds.

Table 3-2. Summary of area coverage for model predicted bottom shear stress less than the critical threshold for resuspension.

	Spring Tide			Neap Tide		
	Without CWW (acres)	With CWW (acres)	Difference (acres)	Without CWW (acres)	With CWW (acres)	Difference (acres)
Average	3.83	3.82	0.007	4.73	4.73	-0.005
Maximum	21.7	21.7	2.1	21.7	21.7	2.1
Cumulative	-	-	0.73	-	-	-0.48

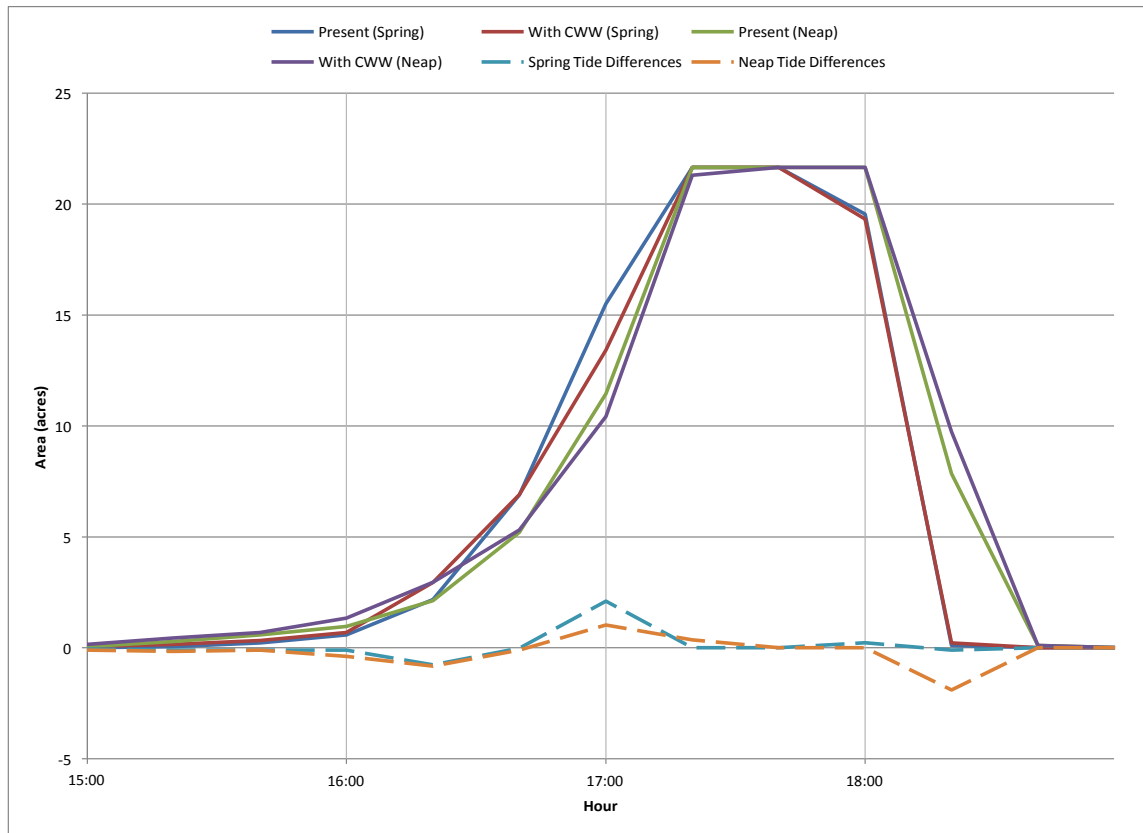


Figure 3-12. Time series of example area coverage time series of bottom shear stress less than the critical value zoom to one half a tidal cycle.

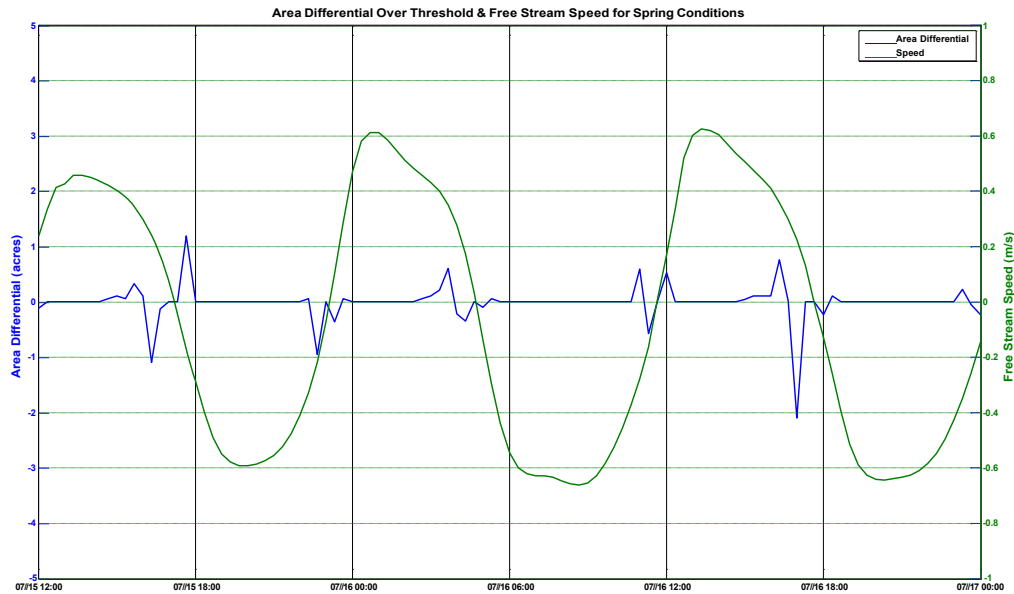


Figure 3-13. Time series of example area coverage difference and free stream bottom current velocity.

To better understand the dynamics of the differences, an assessment of the area coverage as a function of the free stream velocity was made. Figure 3-14 shows a scatterplot of the area coverage of bottom stress below critical shear stress for resuspension as a function of the free stream current speed, as taken at the upstream end of the IPEC area study domain. Positive current velocities represent upstream (flood) flow and negative represent ebb flows. The relationship between the current speeds and area coverage described above can now be clearly seen; low speeds (less than 0.2 m/s [0.66 ft/s]) produced large areas below critical shear and higher speeds quickly reduced the area to zero, which is reached at approximately 0.4 m/s (1.31 ft/s).

This current speed influence can also be seen in a scatter plot of the differences between the “with” CWW intake flow and “without” as shown in Figure 3-15. Both the spring and neap tidal regimes are shown. In the area difference detail analysis, the relationship to free stream current velocity had a slightly different focal point, centered on critical shear stress velocity threshold of 0.2 m/s (0.66 ft/s) developed in Appendix C. For free stream velocities less than +/- 0.2 m/s (0.66 ft/s), the trend in the model predictions implied that the “without CWW” intake flow cases had the larger associated areas (negative difference) whereas for velocities greater than +/- 0.2 m/s (0.66 ft/s) the “with CWW” cases had larger areas (positive difference). This result implied that the CWW intake flow were increasing the local velocities slightly when compared to the “without” cases and conversely a potential obstruction to flow produced a local decrease in bottom current speeds in the higher free stream current regimes.

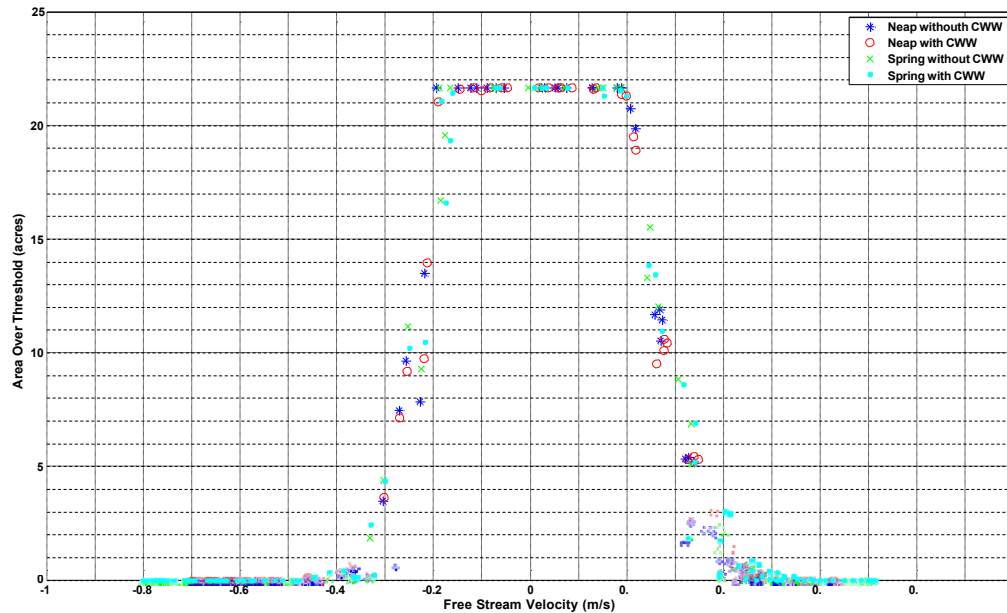


Figure 3-14. Scatterplot of area coverage for bottom stress below the critical threshold level as a function of the free stream bottom velocity.

As an indication of the amount of time that the particular relationships between the bottom velocity and shear stress difference occurred, a frequency distribution of the free stream velocities is presented in Figure 3-16. The distribution indicates that the current velocities in the IPEC area were predominantly greater than the ± 0.2 m/s (0.66 ft/s) critical threshold value with speeds less than 0.2 m/s (0.66 ft/s) only 18% of the time, calculated as the sum of the percentage occurrences shown in green.

The results of the foregoing analysis indicate that while there is a detectable influence of the CWW screen plenum and intake flow on the current speeds and patterns, it is small, localized and transient. The greatest effects are seen in the area immediately surrounding the CWW array but due to the oscillating nature of the tides reflect both an increase and a decrease depending on the stage of the tide and direction of the currents. There is a slight offset in the pattern forced by the uneven tides, with the higher currents experienced on the ebb tide (influenced by the river flow) and lower current speeds on the flood. This results in a slightly higher propensity of the current speeds to remain below the critical shear stress threshold speed of approximately 0.2 m/s (0.66 ft/s) on the flood tide slack before ebb, also increasing the influenced area.

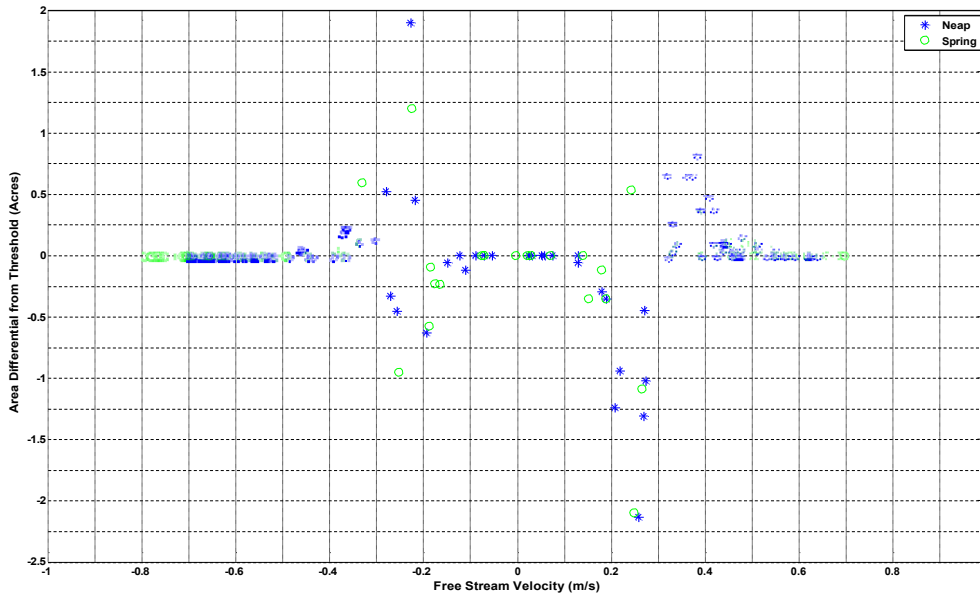


Figure 3-15. Scatterplot of difference in area coverage between the with CWW intake flow and without CWW intake flow cases for bottom stress below the critical threshold level as a function of the free stream bottom velocity.

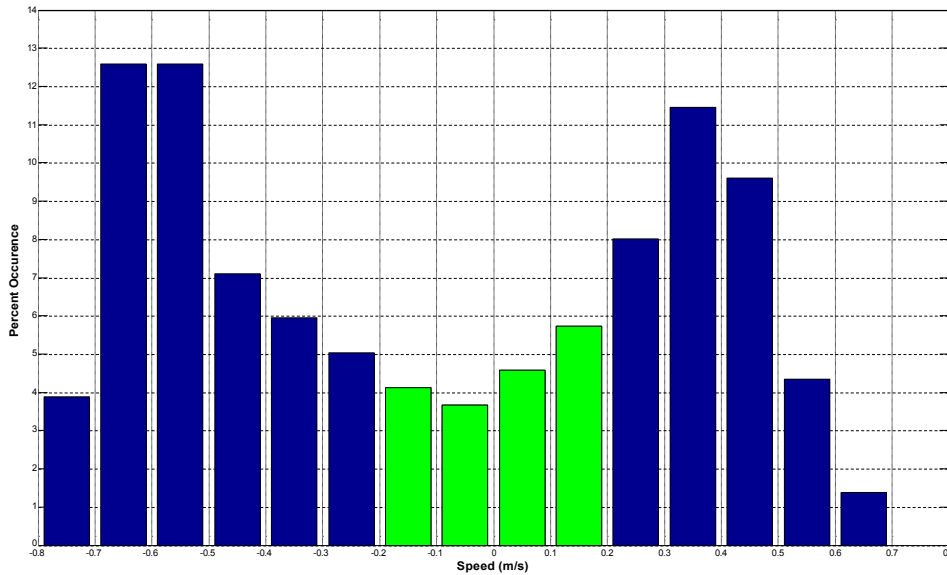


Figure 3-16. Frequency distribution of free stream bottom velocities in the study domain during the evaluation period.

3.2 COMPUTER MODELING OF FLOW AROUND CWW SCREENS USING FLUENT MODEL

For an even finer refinement of the localized effects attributable to the CWW arrays, a high resolution Computational Fluid Dynamics (CFD) model was used. The CFD model can typically resolve details of the flow to the level of small fractions of meters (feet). Enercon performed the CFD modeling using the ANSYS FLUENT model system and documented its efforts in a technical report (Enercon, 2012b). The purpose of the FLUENT model was to investigate the effect of the CWW screen risers on velocity and shear stress at or near the bottom of the river. The fine resolution CFD results were ultimately combined with the lower resolution BFHYDRO model results and reported in Section 3.3.

3.2.1 DESCRIPTION OF MODEL AND APPLICATION

The modeling approach simulated the velocities around the 72-CWW-screen arrays for each of the two IPEC units separately. Figure 3-17 shows the grid mesh defining the CWW screen array for one of the units. Velocity and pressure are determined for each cell in the grid mesh based on the governing hydrodynamic equations. The FLUENT model was run in steady state mode, i.e. a series of constant River velocities were applied to the open boundaries of the model grid and the model solver iterated on the solution until convergence was reached. The constant river velocities were chosen as selected percentiles of speed found from the analysis performed by Normandeau of the measured currents from the ADCP deployment described in Appendix B. The analysis used River speeds measured at a height of 3 m (10 ft) above the bottom coincident with the centerline elevation of the CWW screens. The range of speeds modeled varied from 0.01 to 0.89 m/s (0.04 to 2.9 ft/s) for Unit 2 and from 0.01 to 0.97 m/s (0.04 to 3.2 ft/s) for Unit 3.

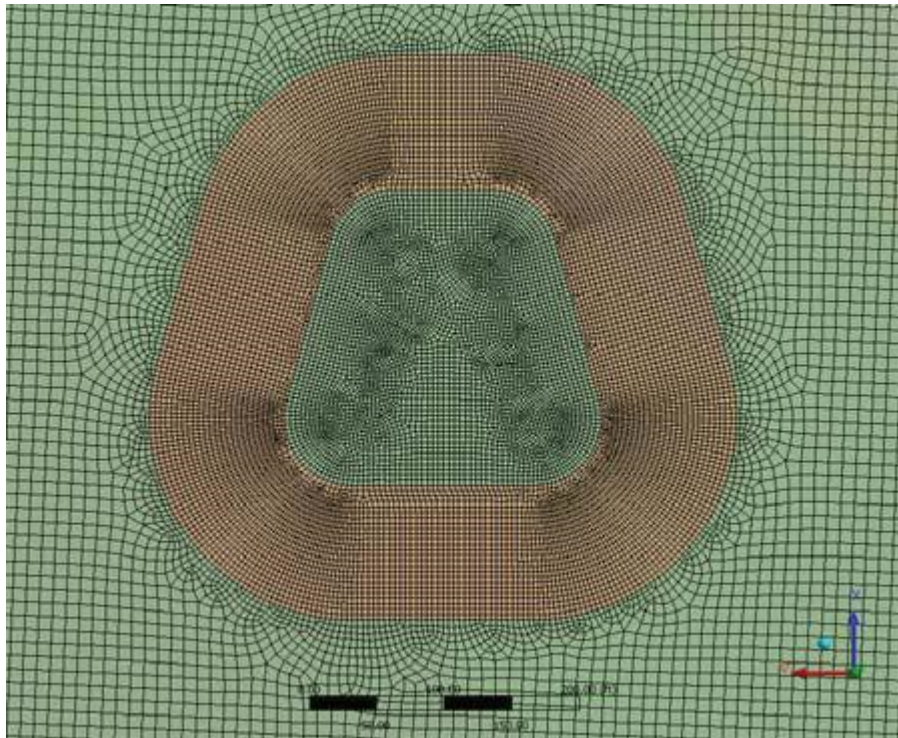


Figure 3-17. Grid mesh detail around the CWW screen array (reproduced from Enercon [2012b] Figure 5.8) for a typical unit.

In order to perform the stress calculation described in Appendix D it was necessary to extract the model predicted velocity 1 m (3.3 ft) off the bottom. Enercon provided ASA with a spreadsheet containing velocity components and the coordinates of the location where they were calculated for each River velocity scenario modeled. The next sections present the velocity predictions and the subsequently calculated shear stress.

3.2.2 MODEL VELOCITY RESULTS

Twenty eight scenarios were modeled using FLUENT for each of the two IPEC Units, flood and ebb tide at seven velocities defined as the 1st, 10th, 25th, 50th, 75th, 90th, and 99th percentiles from the velocities in Table 5.2 of Enercon (2012b) and repeated here as Table 3-3 with the conversions to SI units. The flood tide velocities were consistently smaller than the ebb tide velocities for both units and all percentile levels.

Table 3-3. Percentiles of velocity observations for each unit and river tidal flow direction.

Unit	Tide	Percentiles of Velocity Observations (m/s)						
		1 st	10 th	25 th	50 th	75 th	90 th	99 th
2	Ebb	0.0159	0.0550	0.1159	0.2724	0.4502	0.6511	0.8907
2	Flood	0.0117	0.0405	0.0854	0.2007	0.3317	0.4796	0.6561
3	Ebb	0.0209	0.0770	0.1604	0.3010	0.4753	0.7063	0.9704
3	Flood	0.0133	0.0489	0.1019	0.1913	0.3021	0.4489	0.6167
Unit	Tide	Percentiles of Velocity Observations (ft/s)						
2	Ebb	0.0521	0.1805	0.3804	0.8936	1.4769	2.1360	2.9222
2	Flood	0.0383	0.1329	0.2801	0.6584	1.0881	1.5736	2.1524
3	Ebb	0.0687	0.2525	0.5261	0.9874	1.5595	2.3174	3.1837
3	Flood	0.0437	0.1605	0.3343	0.6275	0.9912	1.4728	2.0234

Figure 3-18 and Figure 3-19 illustrate a plan view of the different velocity patterns resulting from ebb (flow generally moving left and slightly up towards the top of the figure) and flood currents (flow generally moving right and slightly down towards the bottom of the figure), respectively. The 12 risers are shown as black circles in a 4 X 3 pattern for each of the 6 plenums. These figures were based on the 50th river velocity percentile at Unit 2, 0.2724 m/s (0.8936 ft/s) for ebb and 0.2007 m/s (0.6584 ft/s) for flood. Each figure shows a stagnation point right at the center of the upstream risers (those first affecting the flow) shown as a small blue area with a pattern of velocity increases around these risers (and some others) shown in yellow, decreasing velocities around subsequent risers shown as deeper blue, and wakes of lower velocities in the lee of the plenums shown in blue.

Velocity patterns between the flood and ebb tidal conditions were generally symmetrical as expected. During a flood tide (Figure 3-19), flow came unopposed to the risers (generally moving right and slightly towards the bottom of the figure), encountered the risers and slowed. This increased the velocity around the first few risers on the left side of each plenum, and generally decreased the velocity around subsequent risers on that plenum. The lowest velocity (thus the greatest area of possible sedimentation) occurred behind the last risers on the right side of each plenum. During an ebb tide the opposite occurred (Figure 3-18); areas with the lowest velocity during the flood now had the highest velocities.

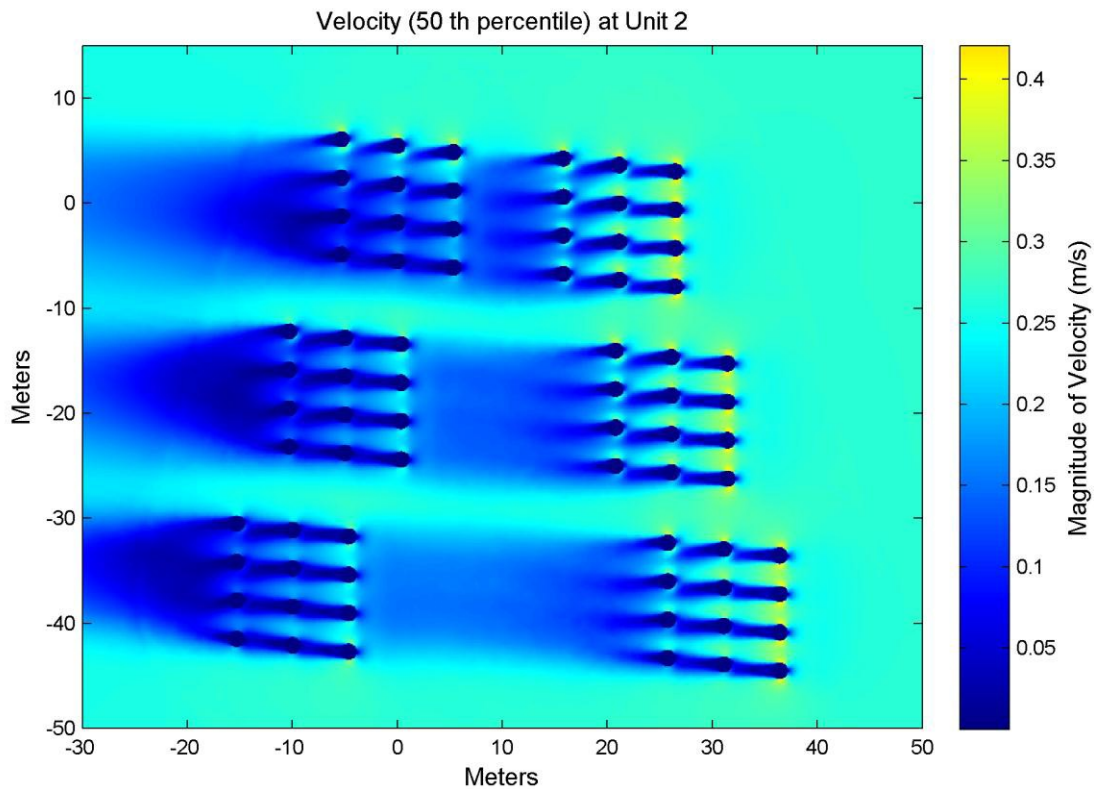


Figure 3-18. Velocity variations at Unit 2 during ebb tide at the 50th percentile of River velocity (0.2724 m/s [0.8936 ft/s]). Ebb tide velocity is generally moving left and slightly up towards the top of the figure.

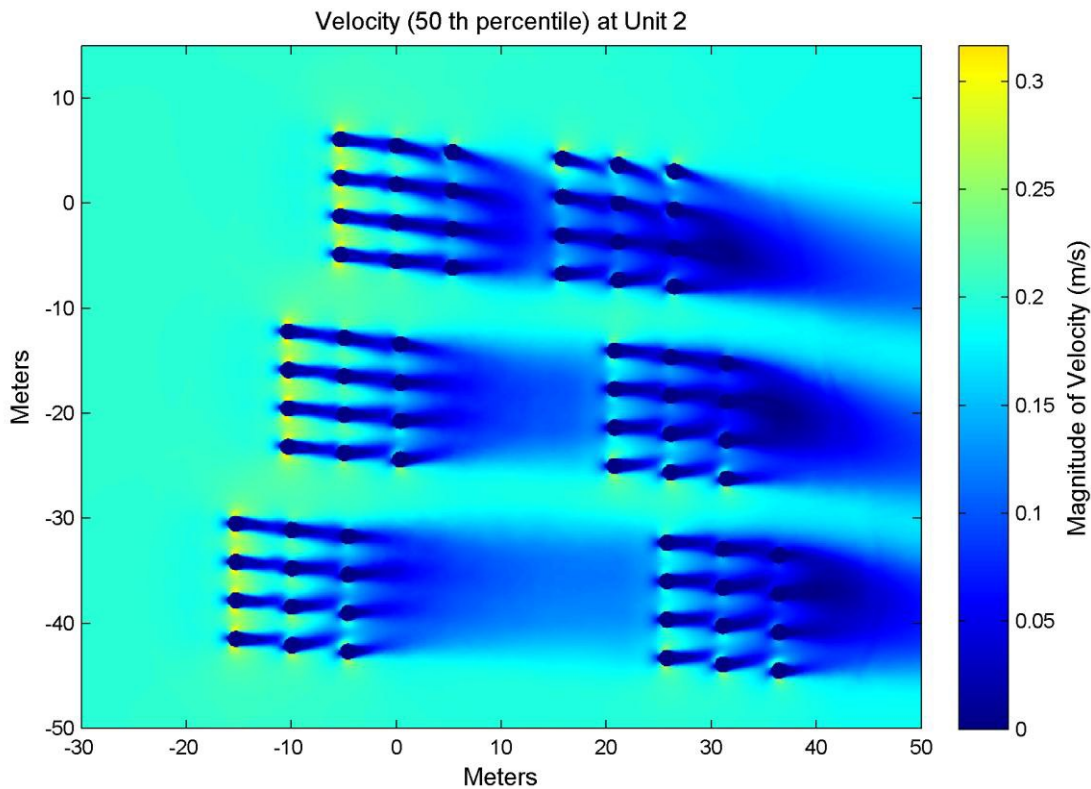


Figure 3-19. Velocity variations at Unit 2 during flood tide at the 50th percentile of River velocity (0.2007 m/s [0.6584 ft/s]). Flood tide velocity is generally moving right and slightly down towards the bottom of the figure.

The velocity patterns as a function of River velocities at higher percentiles are shown in Figure 3-20 through Figure 3-22 and illustrate the 10th, 50th, and 90th percentile river velocity cases at Unit 3 during flood tide (flow generally moving right and slightly down towards the bottom in the figures). The results for the ebb tide were generally symmetrical (opposite to the flood results). Note that each figure has a unique color coded scale for velocity so that the flow variations can be seen. The area of increased velocity at the leading risers at the upstream (approximately from the left in the figures) plenums scales similarly relative to the baseline River velocity for each case although at the 10th percentile the flow direction of the wakes are more variable. The decrease in velocity seen in the subsequent risers also follows a similar pattern for each 10th to 50th to 90th percentile case.

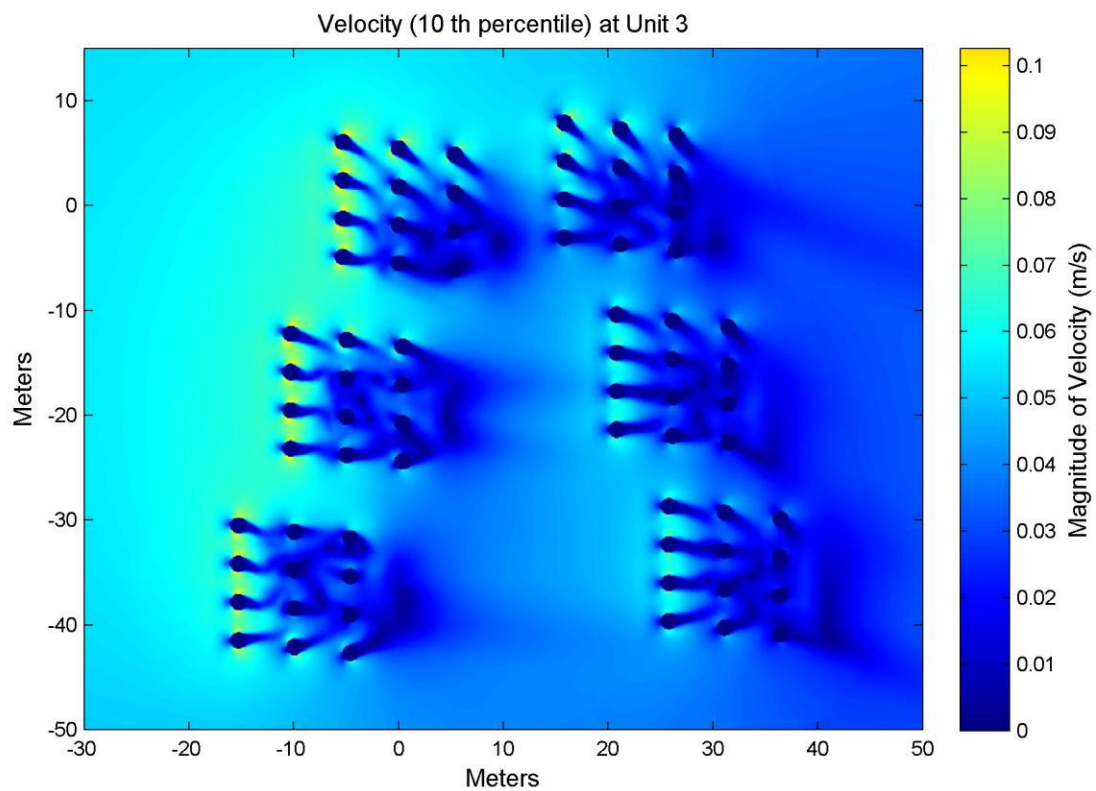


Figure 3-20. Velocity variations at Unit 3 during flood tide at the 10th percentile of River velocity (0.0489 m/s [0.1605 ft/s]). Flood tide velocity is generally moving right and slightly down towards the bottom of the figure.

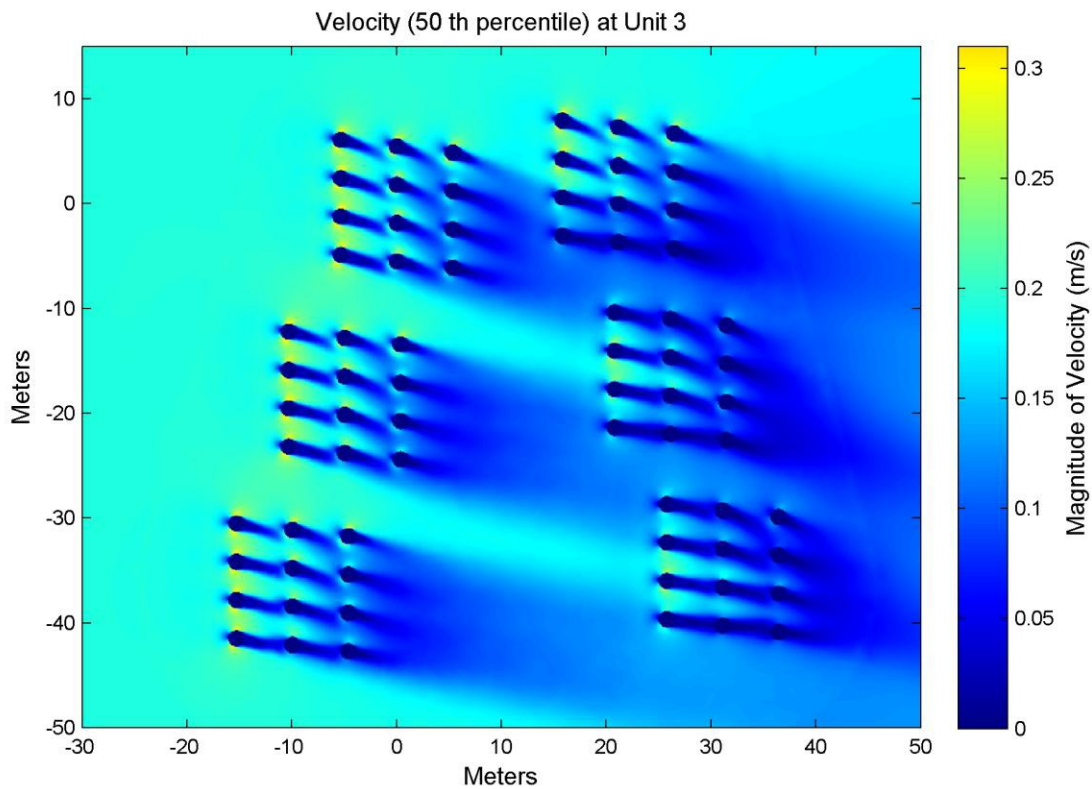


Figure 3-21. Velocity variations at Unit 3 during flood tide at the 50th percentile of River velocity (0.1913 m/s [0.6275 ft/s]). Flood tide velocity is generally moving right and slightly down towards the bottom of the figure.

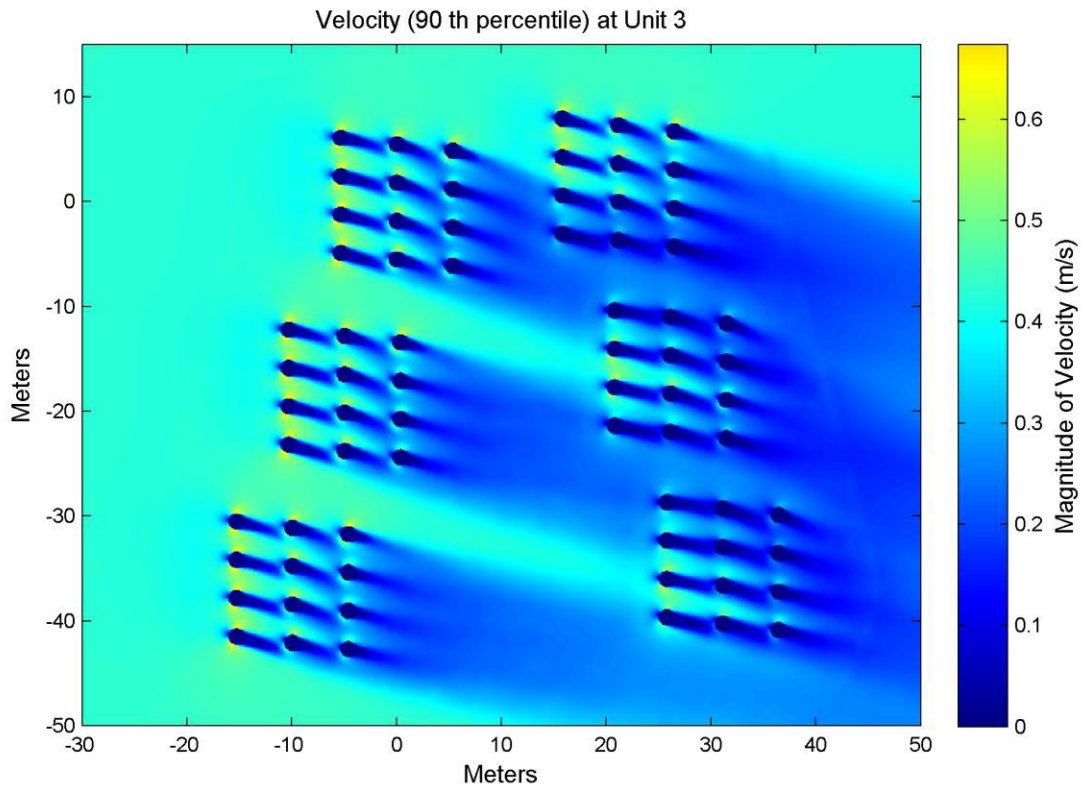


Figure 3-22. Velocity variations at Unit 3 during flood tide at the 90th percentile of River velocity (0.4489 m/s [1.4728 ft/s]). Flood tide velocity is generally moving right and slightly down towards the bottom of the figure.

The same basic pattern was found for both units, for both flood and ebb tides, and through the range of percentile velocities. This pattern included a lowering of the velocity at the most upstream point on each riser, then an increase in velocity along the sides and then another low velocity area behind rise. The riser array together showed an increased velocity around the first few risers on the upstream side of each plenum, which generally decreased around subsequent (downstream) risers on that plenum. The lowest velocity (thus the greatest area of possible sedimentation) occurred behind the last risers on the downstream side of each plenum.

3.2.3 BOTTOM SHEAR STRESS CALCULATION

Using the CFD model results of velocity at 100 cm (3.3 ft) above the bottom (U_{100}), shear stress ($\tau_{\text{fluent,cal}}$) is calculated using the equation:

where ρ is density ($1,014 \text{ kg/m}^3$ [63.30 lb/ft^3]) and C_D is the drag coefficient (0.0019) calculated in Appendix D. The relationship between velocity and shear is quadratic; meaning that when velocity increases the shear increases by the square of velocity. Thus, at higher velocities, the risers and plenum chambers increased their local effect on the River velocity.

An example comparison between calculated shear and that directly calculated in the FLUENT model itself (τ_{fluent}) is shown in Figure 3-23 below for the 50th percentile ebb tide for Unit 2. (The flood tide results are symmetrical (opposite) with the ebb tide results, which are not shown.) The basic pattern between the two shear calculations was very similar. However the shear calculated in the model, being a more direct calculation, had more intricate structures in the shear as well as slightly different magnitudes. The values differ only slightly and therefore the internally calculated shear will be used in the subsequent analysis.

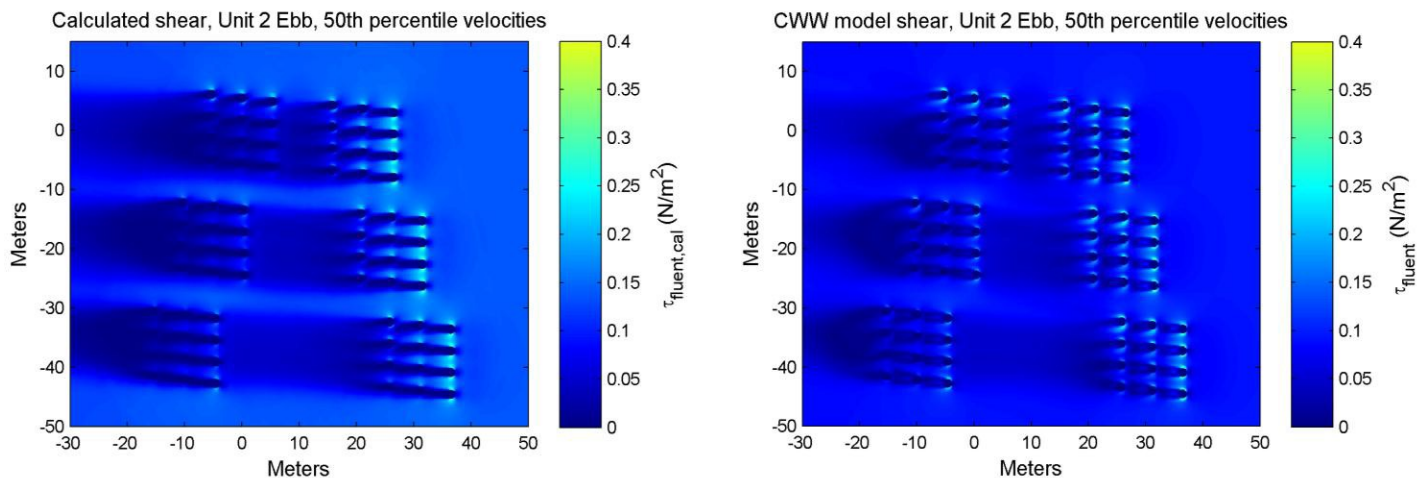


Figure 3-23. Calculated shear (from velocity at 1 m (3.3 ft) in the CWW model) on the left and shear output directly from the FLUENT model on the right. Both are for Unit 2 during ebb tide at the 50th percentile of River velocity. Ebb tide velocity is generally moving left and slightly up towards the top of the figure.

Shear stress greater than the critical shear stress ($\tau_{\text{crit}} = 0.077 \text{ N/m}^2$ [0.11 psi]), caused by velocities at or above 0.2 m/s (0.66 ft/s), is likely to resuspend sediments. The anticipated ambient shear (τ_{amb}) from flow upstream of the potential plenum structures is shown below in Table 3-4. These ambient shear stress values were extracted from the CWW model results in a location upstream of the flow interaction with the plenums. It is important to note many of the

ambient velocity conditions were above the critical shear stress threshold without the effects of the CWW installation.

Table 3-4. Summary of ambient shear stress in (N/m^2) associated with unaltered conditions at selected percentiles for the free stream River velocity. Bolded green text indicates ambient shear stress is greater than the critical shear stress.

Unit	Direction	Percentiles of Ambient Shear Stress τ_{amb} (N/m^2)						
		1 st	10 th	25 th	50 th	75 th	90 th	99 th
2	Ebb	0.00	0.01	0.02	0.10	0.23	0.45	0.79
2	Flood	0.00	0.00	0.01	0.06	0.13	0.26	0.45
3	Ebb	0.00	0.01	0.04	0.11	0.25	0.51	0.91
3	Flood	0.00	0.00	0.02	0.05	0.11	0.22	0.40

Figure 3-24 through Figure 3-25 illustrate the effect of the risers on ambient shear stress conditions around Unit 3 during flood tide with 10th, 50th and 90th background River velocity percentiles, respectively. (The flood tide results are symmetrical (opposite) with the ebb tide results, which are not shown.) The colorbar shows computed shear stress from the FLUENT model minus the ambient values shown in Table 3-4:

A white color indicates no change from ambient (present) conditions, red indicates an increase in shear stress, and blue indicates a decrease in shear stress from ambient conditions. Colorbar scales change between figures to highlight the variation in stress. It is shown that there were small regions of increased shear stress around the leading risers (in red), but larger areas of decreased shear stress occurred in the wake of the risers (in blue). This effect was enhanced as the River velocity percentile increased. As with velocity, the 10th percentile stress difference shown in Figure 3-36 was more variable due to the low velocity at that percentile.

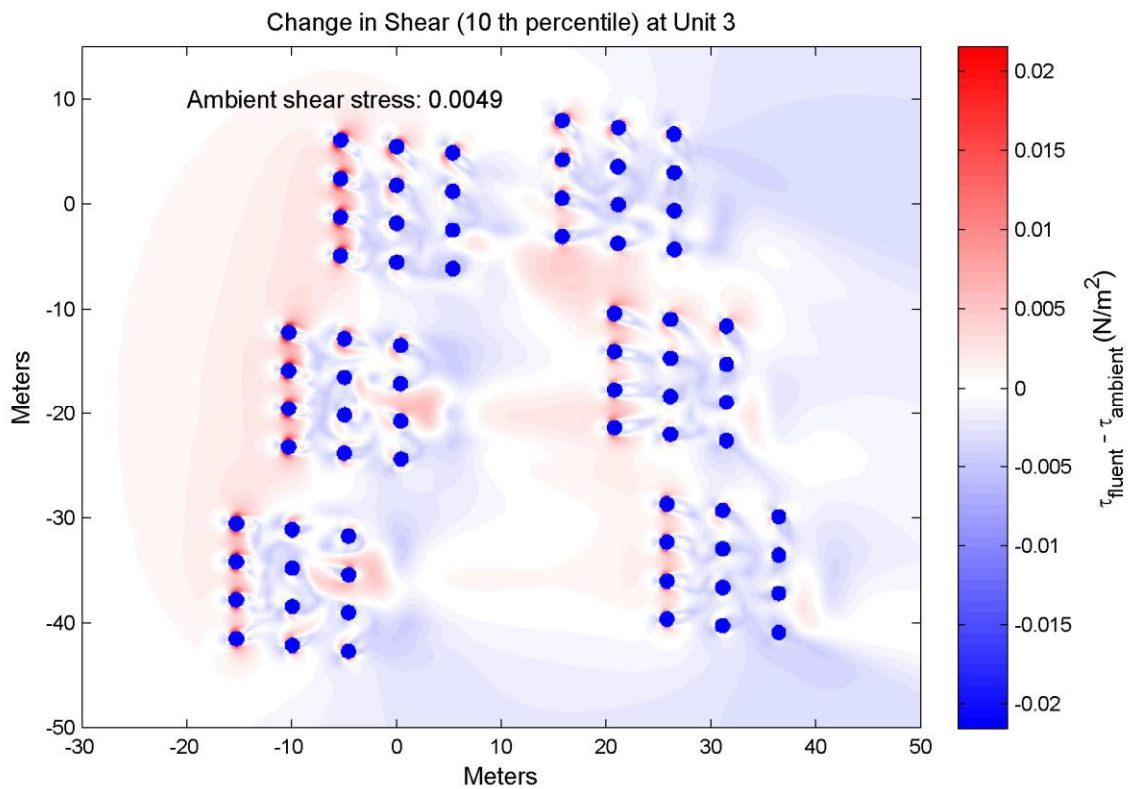


Figure 3-24. Change in shear stress from ambient (present) conditions due to the risers at Unit 3 with 10th percentile velocities during flood (0.0489 m/s [0.1605 ft/s]). Flood tide velocity is generally moving right and slightly down towards the bottom of the figure.

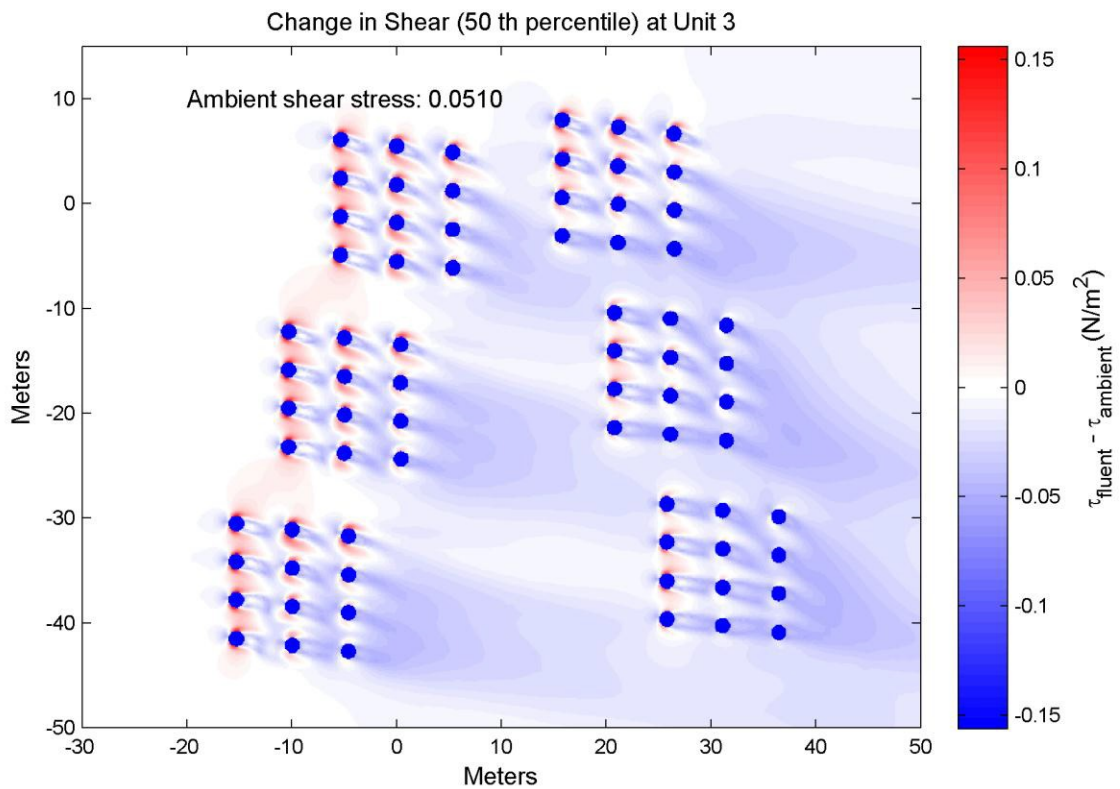


Figure 3-25. Change in shear stress from ambient (present) conditions due to the risers at Unit 3 with 50th percentile velocities during flood (0.1913 m/s [0.6275 ft/s]). Flood tide velocity is generally moving right and slightly down towards the bottom of the figure.

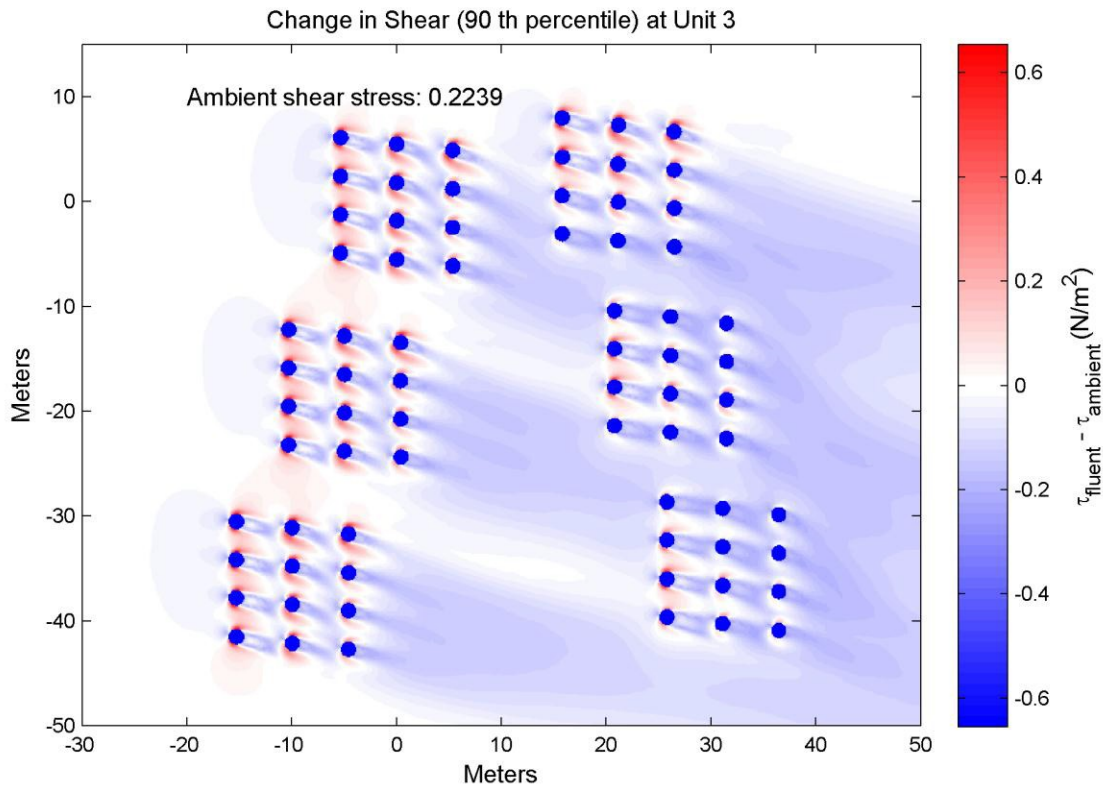


Figure 3-26. Change in shear stress from ambient (present) conditions due to the risers at Unit 3 with 90th percentile velocities during flood (0.4489 m/s [1.4728 ft/s]). Flood tide velocity is generally moving right and slightly down towards the bottom of the figure.

For low velocities (10th percentile) the change in shear due to the risers was very small, usually less than 0.01 N/m² (0.15 x 10⁻⁵ psi). These values remained small, and well below the resuspension threshold. For the 50th percentile and 90th percentile, the increase in shear was a small area around the risers, but left greater regions of lower shear in the wake of the plenums. In many of these instances the shear fell below the threshold of resuspension, and any blue regions shown in these plots indicate an increase in the area and time that would allow for additional deposition to occur over ambient (present) conditions.

Figure 3-27 and Figure 3-28 illustrate examples of the effect of the plenums during conditions resulting in greater depositional potential. The example figures are again of Unit 3 during flood tide with 50th and 90th background velocity percentiles, respectively. The 10th percentile velocity was completely below the resuspension threshold, and therefore was not shown. (The

flood tide results are symmetrical (opposite) with the ebb tide results, which are not shown.) The colorbar shows computed shear stress from the CFD model minus the threshold value of 0.077 N/m^2 ($1.1 \times 10^{-5} \text{ psi}$). This resultant is often called the excess shear stress.

White colors indicate no change, red indicates the model shear stress was greater than the critical shear stress (resuspension), and blue indicates the shear stress was less than the critical shear stress (deposition). In both cases, the risers allow for more sedimentation than ambient conditions by lowering the shear stress at the risers below the freestream stress.

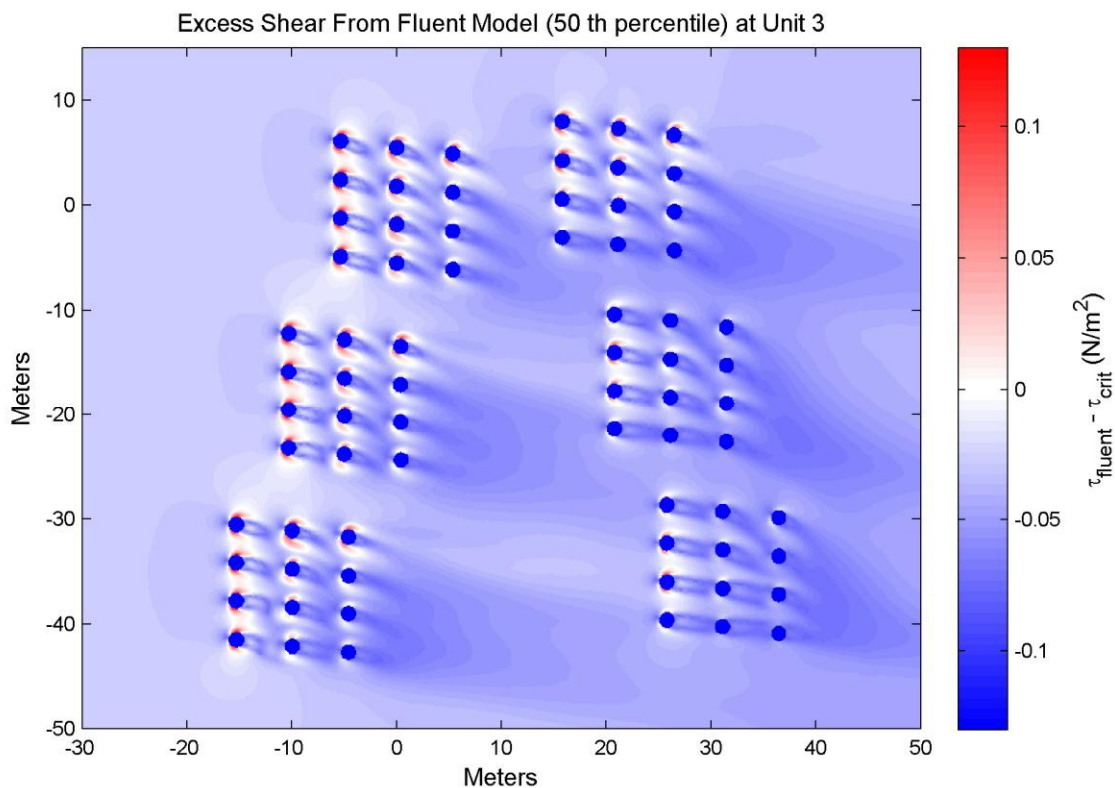


Figure 3-27. Excess shear stress experienced at Unit 3 during flood tide at the 50th percentile (0.1913 m/s [0.6275 ft/s]). Flood tide velocity is generally moving right and slightly down towards the bottom of the figure.

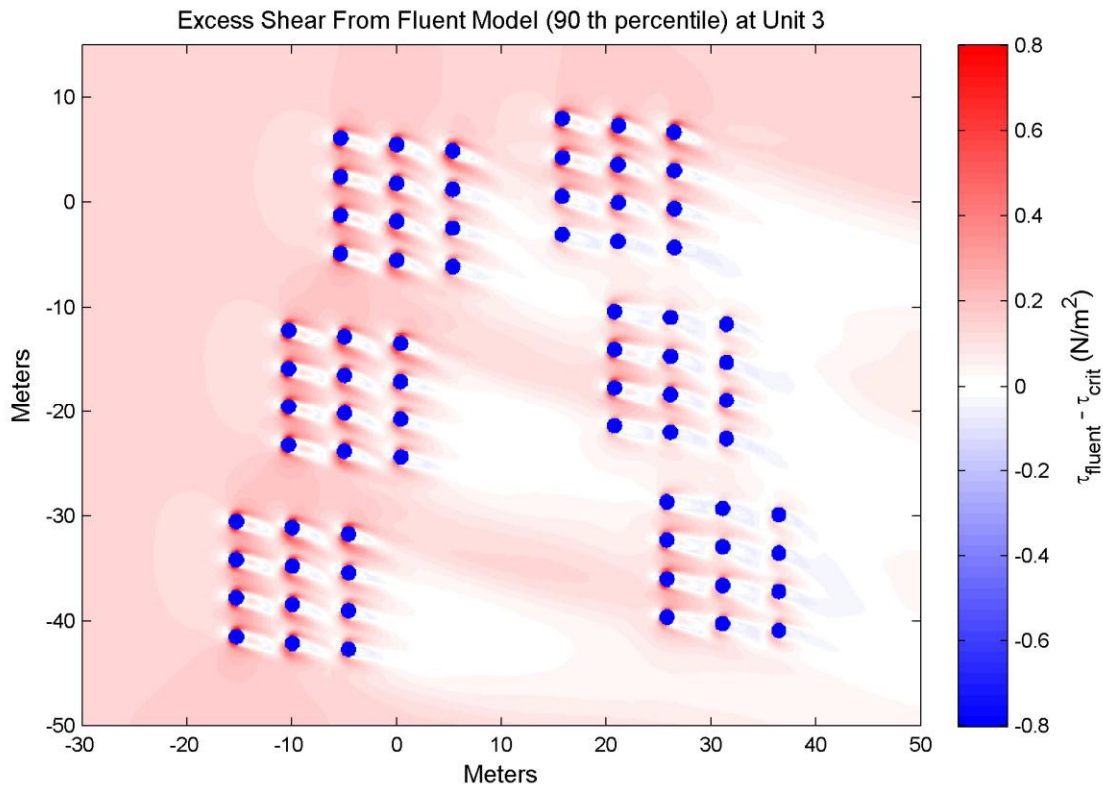


Figure 3-28. Excess shear stress experienced at Unit 3 during flood tide at the 90th percentile (0.4489 m/s [1.4728 ft/s]). Flood tide velocity is generally moving right and slightly down towards the bottom of the figure.

At the 50th percentile ambient velocity conditions (Figure 3-27) the risers decrease stress over most areas (in blue) and allowed for more sedimentation to occur. Only small areas at the leading risers have increased stress (in red). At the 90th percentile background velocity, the background velocity itself is large enough to resuspend material (in red), and after the leading risers shear is reduced significantly to the point where sedimentation is possible at some locations (in blue).

3.3 INTEGRATION OF BFHYDRO AND FLUENT MODEL RESULTS

The predictions from both the FLUENT and BFHYDRO models were synthesized to take into account the potential large scale and near field effects of the CWW arrays. This section documents the combination of the large scale, bathymetric effects from the BFHYDRO model described in section 3.1 and the high resolution, near field, results from the CFD FLUENT model described in section 3.2. Specifically, this analysis includes the presence of the plenum structures and intake flow (BFHYDRO model) and all risers in each 72-CWW screen array (FLUENT).

3.3.1 RESULTS OF CWW SCREEN ARRAY OPERATION

The BFHYDRO model output showed an incremental increase in shear stress, in most cases, around the plenums as they were slightly above grade and exposed to the flow. The incremental shear stress predictions are summarized in Table 3-5 (Unit 2) and Table 3-6 (Unit 3) for the six plenum locations designated as Flags A through F and the two mattress locations with geotech mattresses installed. The tables summarize incremental stress for both Flood and Ebb tidal conditions at both the 50th and 90th percentile velocities. The plenum and mattress locations are shown in Figure 3-29.

Table 3-5. Unit 2 incremental stress from BFHYDRO model results for various locations in the area of the CWW screen array.

Tide	Velocity Percentile	Plenum Flag A	Plenum Flag B	Plenum Flag C	Plenum Flag D	Plenum Flag E	Plenum Flag F	Mattress Left	Mattress Right
Ebb	50	0.007	0.000	0.007	0.008	0.000	0.000	0.006	0.000
Ebb	90	0.000	0.035	0.034	0.035	0.018	0.016	0.000	0.033
Flood	50	0.000	0.006	0.000	0.000	0.000	0.000	0.000	0.006
Flood	90	0.013	0.026	0.027	0.027	0.000	0.000	0.011	0.013

Table 3-6. Unit 3 incremental stress from BFHYDRO model results for various locations in the area of the CWW screen array.

Tide	Velocity Percentile	Plenum Flag A	Plenum Flag B	Plenum Flag C	Plenum Flag D	Plenum Flag E	Plenum Flag F	Mattress Left	Mattress Right
Ebb	50	0.000	0.008	0.015	0.016	0.015	0.007	0.015	0.008
Ebb	90	0.057	0.076	0.077	0.079	0.077	0.018	0.056	0.058
Flood	50	0.000	0.000	0.007	0.007	0.000	0.000	0.000	0.006
Flood	90	0.014	0.028	0.029	0.030	0.028	0.013	0.027	0.028

The larger scale incremental increase in stress from the BFHYDRO model results was added to the FLUENT model predictions in the region around the arrays to get a more accurate estimate of total increase in stress due to the presence of both the risers and the plenums. Figure 3-29 and Figure 3-30 illustrate the addition of total shear stress for the 50th and 90th percentile background velocities at Unit 3 during ebb tide, respectively. The incremental shear stress reflecting the BFHYDRO model predictions of the exposed plenum chambers increased the stress only slightly from that predicted from the FLUENT model.

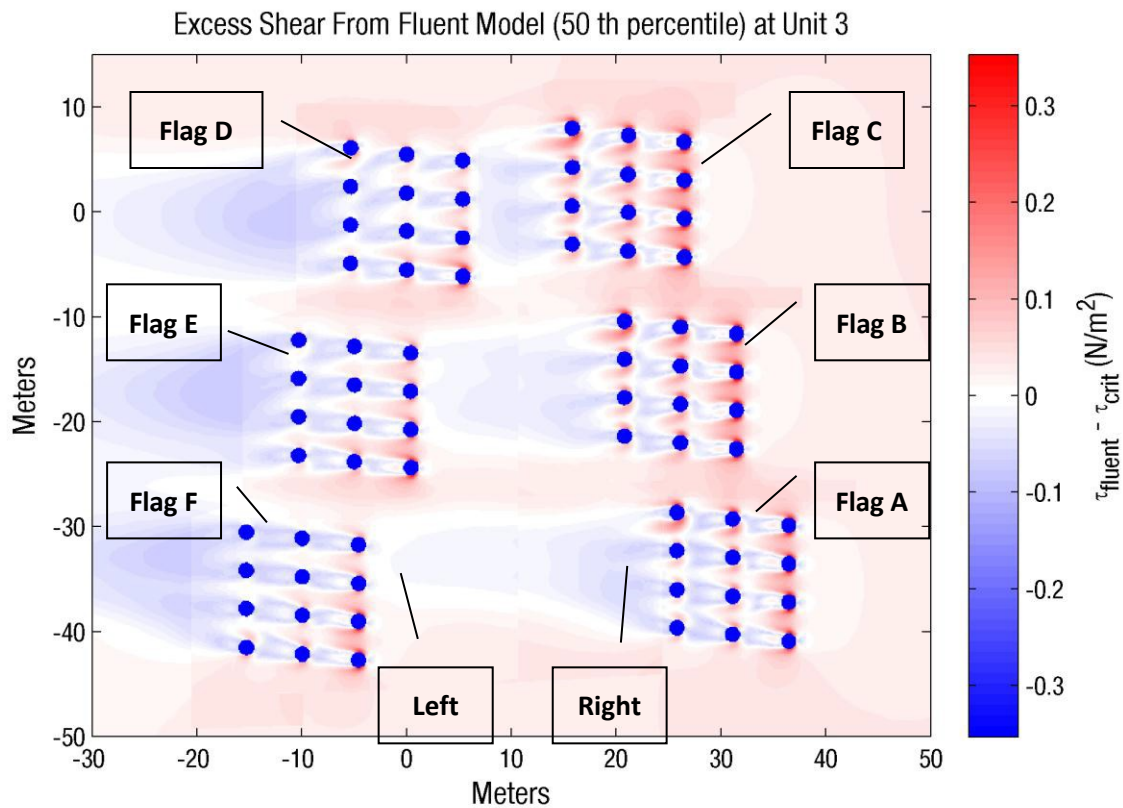


Figure 3-29. Excess shear stress experienced at Unit 3 CWW array during ebb tide at the 50th percentile velocity, with added stress from Table 3-6. Ebb tide velocity is generally moving left and slightly up towards the top of the figure.

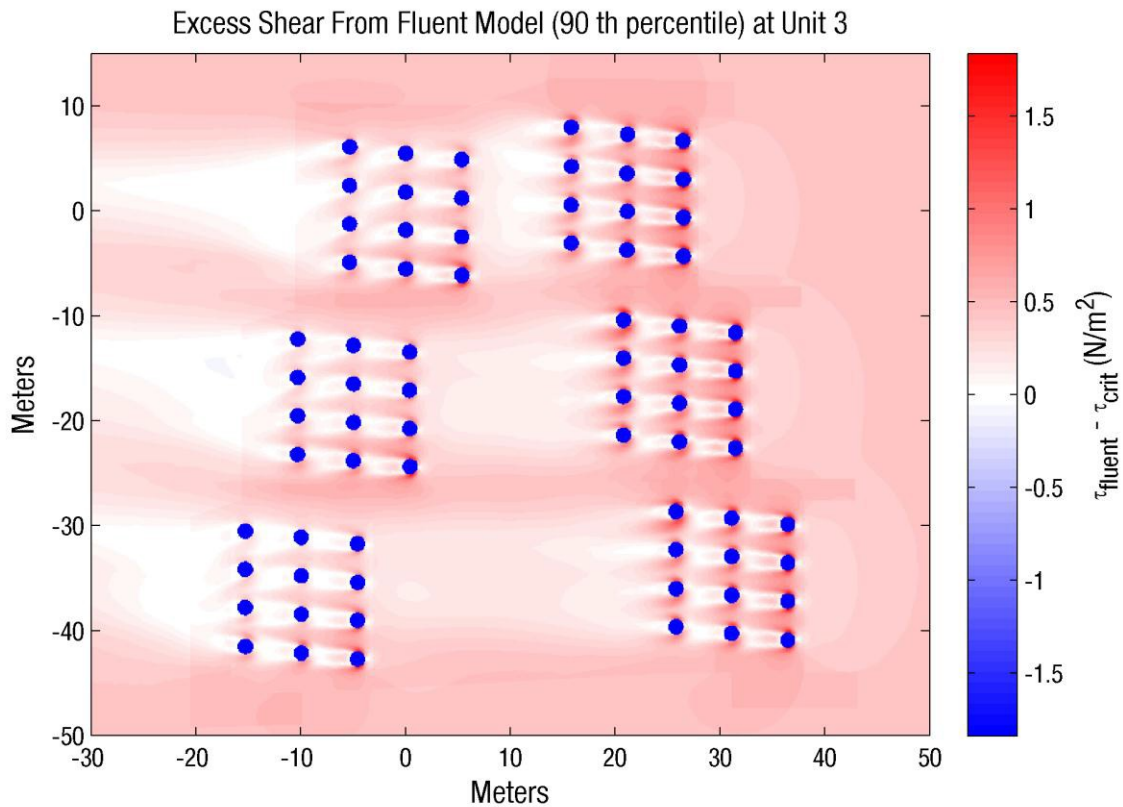


Figure 3-30. Excess shear stress experienced at Unit 3 CWW array during ebb tide at the 90th percentile velocity, with added stress from Table 3-6. Ebb tide velocity is generally moving left and slightly up towards the top of the figure.

The resulting grid of spatially varying shear stress levels was then used to calculate the total area that remained below the resuspension threshold ($\tau_{ex,flu}$), indicating that material could potentially deposit in those areas; the resulting areas for each scenario are summarized in Table 3-7. The region over which these areas were calculated included the plenums, rip-rap and mattresses near the CWW screen arrays serving the plant units minus the area of the risers. The total area summed is 2,700 m² (0.66 ac) around each CWW unit, including the unit itself.

Table 3-7. Area (acres) with shear stress below resuspension threshold values for scenarios using the 50th and 90th velocity percentiles.

Unit	Tide	Velocity Percentile	Plenum Box (ac)	Mattress (ac)	Rip-Rap / Backfill (ac)	Total Deposition Area	Total CWW Array Area (ac)	% Area Deposition
2	Ebb	50	0.15	0.17	0.00	0.32	0.66	49%
2	ebb	90	0.01	0.00	0.00	0.02	0.66	2%
2	Flood	50	0.27	0.23	0.12	0.63	0.66	95%
2	Flood	90	0.04	0.04	0.02	0.10	0.66	15%
3	Ebb	50	0.12	0.13	0.04	0.28	0.66	42%
3	Ebb	90	0.00	0.00	0.00	0.00	0.66	1%
3	Flood	50	0.27	0.23	0.13	0.64	0.66	96%
3	Flood	90	0.03	0.00	0.00	0.03	0.66	4%

During times of high background flow at the 90th percentile, regions where the baseline would currently be 100% resuspension (0% deposition), were estimated to be lower, with up to 15% depositional area potentially created by the installment of the CWW systems.

4. SUMMARY AND CONCLUSIONS

ASA assessed historical sedimentation in the area of the River where the CWW screen intake structures would be placed, and determined the area that would likely be permanently impacted by the operation of the CWW screen intake system. Our conclusions are as follows:

(1) Sediment in the area offshore IPEC was found to be predominantly muddy (silt and clay >90%) with areas of sandy mud (sand >10%) in elongated patches. Using bathymetric data comparisons, radiocarbon dating and sediment cores, it was estimated that sediment accumulated to thicknesses between 0 and 1.5 m (0 to 5 ft) from the 1930's to 2001 within the Indian Point reach.

Sub-bottom profiles, trace metals concentrations and horizons in sediment cores from additional independent studies were used to establish an average sedimentation rate of 3 mm/yr (0.12 in/yr) in the Indian Point Channel segment of the River during the last 70 years of the 20th century although deposition rates are highly variable within the region (RM 40.5 to 42.0). Using sidescan sonar images from the most recent surveys, it was concluded that the proposed sites for the CWW arrays in the Reach were within an area of "reduced current velocities and deposition". The area outside the screen array locations were characterized as erosional.

(2) An assessment was made to determine the potential influence of the exposed parts of the Unit 2 and Unit 3 CWW plenum chambers on the local currents and bottom stress using the BFHYDRO model applied to the Hudson River. The first purpose of the study was to assess the potential changes to the sediment deposition / resuspension environment in the River at these locations. The model was used to predict the currents for the present bathymetry and for the hypothetical case where the bathymetry includes the flat top of the plenum chambers. The difference in the velocity field between the two cases was then determined.

The model results indicated that only very small differences exist between the case with the plenum structures and without. The maximum difference seen is approximately 0.014 m/s (0.046 ft/s) for the Unit 2 plenums and 0.028 m/s (0.092 ft/s) for Unit 3, which would be roughly 2% and 4% of the peak speeds. The area covered by a difference of 0.01 m/s (0.033 ft/s) or greater is approximately 1,200 m² (0.3 ac) in the Unit 2 area and 3,000 m² (0.74 ac) in the Unit 3 area. The difference between the Unit 2 and Unit 3 speed and area results is primarily due to the difference in depths at the two sites, where the Unit 2 intake would be situated in significantly deeper waters.

The change in bottom stress was also estimated for the area of maximum current speed difference around each Unit's CWW intake structure from the BFHYDRO model results. The maximum bottom stress estimates with the CWW plenum chambers in place were 0.819 and

1.063 N/m² (1.18 and 1.54 x 10⁻⁴ psi) for Units 2 and 3, respectively. The corresponding bottom stress estimates for the present bathymetry, (i.e. no CWW plenum chambers), were 0.784 and 0.984 N/m² (1.14 and 1.43 x 10⁻⁴ psi), respectively. The resulting increase in the maximum bottom stress for the Unit 2 and Unit 3 areas were 0.035 N/m² (0.508 x 10⁻⁵ psi) for Unit 2 and a larger increase of 0.079 N/m² (1.15 x 10⁻⁵ psi) for Unit 3, equating to only 4% and 8% of the peak values estimated for present conditions, respectively.

(3) A second BFHYDRO analysis was then performed to simulate both the plenum chambers and the intake flow effects on the local velocities and bottom stress. The intake flow was held constant at 100 m³/s (2,282 MGD) distributed evenly over 16 model cells, representing the locations of the two plenum chamber arrays. The model was run for two sets of cases, the "with CWW screen intake flow" and "without CWW screen intake flow" conditions for a spring tide and a neap tide regime, respectively. The difference between the two cases was calculated and the maximum area with speed changes greater than 0.02 m/s (0.066 ft/s) was estimated at 15,000 m² (3.6 acres) and 7,000 m² (1.7 acres) for Unit 3 and Unit 2 CWW screen arrays, respectively.

The relationship between the current speeds and area coverage indicated that low speed (less than 0.2 m/s [0.66 ft/s]) produced large areas below critical shear and increasing speeds quickly reduced the area to zero, which was reached at approximately 0.4 m/s (1.31 ft/s). The area difference plots indicated that for free stream velocities less than +/- 0.2 m/s (0.66 ft/s), the "without" CWW intake flow cases had the larger associated areas (negative difference) whereas for velocities greater than +/- 0.2 m/s (0.66 ft/s) the "with" CWW cases had larger areas (positive difference). A frequency distribution of the period studied indicated that the current velocities were less than +/- 0.2 m/s (0.66 ft/s) only 18% of the time.

(4) The second model, ANSYS FLUENT, is a fine resolution Computation Fluid Dynamics (CFD) model that can simulate the detailed flow around each CWW screen in the arrays supplying cooling water for each IPEC unit. This modeling was performed by Enercon using a flat bottom approximation and constant River velocities. The range of constant River velocities modeled was based on the occurrence percentiles determined from the ADCP observations averaged at the centerline elevation of the CWW screens (3 m [10 ft]) calculated by Normandeau. Velocities at a 1 m (3.3 ft) elevation were extracted from the model output by Enercon for each of the model runs. During a flood tide, River currents flowed unopposed towards the upstream array of risers and then decreased quickly on the upstream side of the first row of risers. This increased the velocity around the sides of the first row of risers, and generally decreased around subsequent rows of risers until the lowest velocities were reached (thus greatest area of possible sedimentation) behind the last row of risers on the downstream side. The wake behind each riser in the downstream direction also showed a velocity decrease. During an ebb tide the flow was downstream, and areas with the slowest flow during the flood were now areas of fastest flow, in a symmetrical (opposite) pattern with respect to flood conditions.

Bottom shear stress was then calculated from the CFD model-predicted velocities at 1 m (3.3 ft) elevation. Consistent with the velocity patterns, the bottom shear stress differences showed reductions in the lee of the risers with increases along the sides of the risers.

(5) The results of both models were then combined to provide an integrated estimate of the changes in shear stress between present conditions and with the CWW screen array system in place. From the combined shear stress changes, estimates of resuspension areas and deposition areas were made. A range from 45.5 to 96.2% of the combined area (5340 m² [1.32 ac]) including the plenum chambers, the riprap and the mattresses between the plenum chambers, less the riser area for both units, was depositional for the 50th percentile River velocity, consistent with the median velocity in the River. During times of very high River flow, at the 90th percentile, consistent with maximum flood and ebb velocities, regions where the baseline (without any CWW array structures) would be 100% resuspension (0% deposition) the deposition areas increased to a maximum of 15% of the combined area.

In conclusion, the installation and operation of the CWW screens would cause a local decrease in velocity and bottom shear stress leading to more areas of likely deposition than with no structures present. However, the decrease is not large and the likely deposition small, particularly in the tidal environment where peak tides may resuspend previously deposited material.

5. REFERENCES

- Bokuniewicz, H.J., 2005. Sedimentary processes in the Hudson River estuary. In “The Hudson River Estuary Ecosystem”, J. Waldman and J. Levinton Eds., Cambridge University Press, p. 39-50.
- Coastal Engineering Research Center, Volume 1. 1984. Shore protection manual. US Government Printing Office, Washington, DC.
- Cheng, R.T., C.H. Ling, J.W. Gartner, and PF Wang. 1999. Estimates of Bottom Roughness Length and Bottom Shear Stress in South San Francisco Bay, California. *Journal of Geophysical Research*, volume 104, no. C4, p. 7715–7728.
- Dyer, K.R., 1986. Coastal and estuarine sediment dynamics, John Wiley and Sons Ltd., p. 342.
- Enercon, 2010. Evaluation of Alternative Intake Technologies at Indian Point Units 2 & 3. Prepared for Entergy Nuclear Indian Point 2, LLC and Entergy Nuclear Indian Point 3, LLC, Prepared by Enercon Services, Inc., Kennesaw, GA. 12 February 2010.
- Enercon, 2012a. Technical Design Report for Indian Point Units 2 and 3 Implementation of Cylindrical Wedge Wire Screens. Prepared for Entergy Nuclear Indian Point 2, LLC and Entergy Nuclear Indian Point 3, LLC, Prepared by Enercon Services, Inc., Kennesaw, GA. Report ENTGIP152-PR-CWW-06, 2012.
- Enercon, 2012b. Phase 1 Technical Report – CFD Models for Circulation Water Intake CWW Screen Arrays at Indian Point Units 2 & 3. Report ENTGIP152-PR-CWW-M-05. Prepared for Entergy Nuclear Indian Point 2, LLC and Entergy Nuclear Indian Point 3, LLC, Prepared by Enercon Services, Inc., Kennesaw, GA. January 2012.
- Gartner, J.W., 2004. Estimating suspended solids concentrations from backscatter intensity measured by acoustic Doppler current profiler in San Francisco Bay, California. *Marine Geology*, v. 211, p. 169-187.
- Geyer, W.R. and R. Chant, 2006. The Physical Oceanography Processes in the Hudson River Estuary. In Levinton, Jeffrey S., Waldman, John R. Eds. *The Hudson River Estuary*. Cambridge University Press.
- GZA Geoenvironmental, 2012. Phase 1 Geotechnical Report – Cylindrical Wedgewire Screen Project – Entergy Nuclear Indian Point, Units 2 and 3, Buchanan, New York. Prepared by GZA Geoenvironmental of New York for Enercon Services, Inc. April 2012.
- Holdaway, G. P., Thorne, P. D., Flatt, D., Jones, S. E., and Prandle, D., 1999. Comparison

- between ADCP and transmissometer measurements of suspended sediment concentration. *Continental Shelf Research*, 19: 421-441.
- Kim, Y.H., 2006. Circulation and material transport in a partially stratified estuary: Winyah Bay, SC, Ph.D. Dissertation, Univ. S. Carolina.
- Kim, Y.H. and Voulgaris, G., 2003. Estimation of suspended sediment concentration in estuarine environments using acoustic backscatter for an ADCP. *Coastal Sediments 2003*.
- Klingbeil, A.D. and C.K. Sommerfield, 2005. Latest Holocene evolution and human disturbance of a channel segment in the Hudson River Estuary. *Marine Geology*, Volume 218, issue 1-4 (June 30, 2005), p. 135-153.
- Nitsche, F.O., T.C. Kenna, M. Haberman, 2010. *Quantifying 20th Century Deposition in Complex Estuarine Environment: An Example from the Hudson River*. *Estuarine and Coastal Shelf Science*, Vol. 89 (2010), p. 163-174.
- Nitsche, F.O., W.B.F. Ryan, S.M. Carbotte, R.E. Bell, A. Slagle, C. Bertinado, R. Flood, T. Kenna, and C. McHugh, 2007. *Regional Patterns and Local Variations of Sediment Distribution in the Hudson River Estuary*. *Estuarine Coastal and Shelf Science*, Vol. 71 (2007), p. 259-277.
- Nitsche, F.O. and T.C. Kenna, 2007. Distribution, timing, and dynamic of deposition in the Hudson River Estuary. Hudson River Foundation, Final report 008/05A, Lamont-Doherty Earth Observatory of Columbia University, Palisades, NY. .
- Nitsche, F.O., R. Bell, S.M. Carbotte, W.B.F. Ryan, and R. Flood, 2004. *Process Related Classification of Acoustic Data from the Hudson River Estuary*. *Marine Geology*, Vol. 209 (2004), p. 131-145.
- Normandeau, 2011. Analysis of near-bottom flow in the Hudson River at Indian Point Energy Center from data collected by acoustic Doppler current profilers 4 March through 2 November 2011. Final Report, R-21825.001.
- Parchure, T.M. and A.J. Mehta, 1985. Erosion of soft sediment deposits. *Journal of Hydraulic Engineering*, v. 111, p. 1308-1326.
- Sanford, L.P. and J.P. Halka, 1993. Assessing the paradigm of mutually exclusive erosion and deposition of mud, with examples from upper Chesapeake Bay. *Marine Geology*, v. 114. p. 37-57.
- Soulsby, R. L., and S. Clarke, 2005. Bed Shear-stress Under Combined Waves and Currents on Smooth and Rough Beds, HR Wallingford Report TR137.

Swanson, C., D. Mendelsohn, Y. Kim, and D. Crowley, 2010. Hydrothermal Modeling of the Cooling Water Discharge from the Indian Point Energy Center to the Hudson River. ASA Project 09-167. Prepared for Elise Zoli, Goodwin Procter, Boston, MA. 22 March 2010.

Swanson, C., D. Mendelsohn, N. Cohn, D. Crowley, Y. Kim, L. Decker, and L. Miller, 2011. 2010 Field Program and Modeling Analysis of the Cooling Water Discharge from the Indian Point Energy Center. Final Report for ASA Project 09-167. Prepared for Indian Point Energy Center, Buchanan, NY. 31 January 2011.

Thorne, P.D., and D.M. Hanes, 2002. A review of acoustic measurements of small-scale sediment processes. Continental Shelf Research 22, p. 603-632.

APPENDIX A: DESCRIPTION OF PROPOSED USE OF CYLINDRICAL WEDGEWIRE SCREEN ARRAY SYSTEM TO SUPPLY IPEC COOLING WATER

LIST OF FIGURES

Figure A-1. General site plan constructed layout of CWW screen array (reproduced from Enercon Drawing ENTGIP152-CWW-C-002 Rev A).....	3
Figure A-2. Screen layout plan for Unit 2 CWW screen array (reproduced from Enercon Drawing ENTGIP152-CWW-C-005 Rev A).....	3

The IPEC plant consists of two active units, each having its own circulating water system cooling water intake structure (CWIS). The New York State Department of Environmental Conservation (NYSDEC) is conducting a proceeding to update its best technology available determination for IPEC's CWIS in connection with the renewal of IPEC's State Pollutant Discharge Elimination System (SPDES) permit. In response Entergy retained Enercon Services, Inc. (Enercon) to conduct an evaluation (Enercon, 2010) of alternative intake technologies and found that CWW screens are technologically feasible for use at IPEC. A total of 144 CWW screens are required to maintain low through-screen slot velocity. Each screen is 1.8 m (6 ft) in diameter and 6.5 m (21.4 ft) long.

Enercon prepared a technical report providing design details of the proposed CWW arrays (Enercon, 2012a). Each IPEC unit would employ 72 CWW screens that would be arrayed 12 each on six plenums. Each screen would be mounted on a 1.5 m (5 ft) diameter riser with its centerline 3 m (10 ft) above the top of the plenums. The plenums would be mostly below grade in the River sediments so that all the plenum tops for each unit would be located at 20.4 m (67 ft) (Unit 2) and 15.8 m (52 ft) (Unit 3) below Mean Sea Level (MSL). The bottom slopes down in the offshore direction so the range of water depths where the plenums are below grade range from 19.2 to 21.9 m (63 to 72 ft) below MSL (Unit 2) and from 14.9 to 17.4 m (49 to 57 ft) below MSL (Unit 3). This configuration would result in one plenum almost entirely below grade, one partially below grade and four exposed between 0 and 1.5 m (0 and 5 ft) above the local undisturbed bottom for each unit. During construction of each 72 screen array, fill (gravel) will be placed in between and around the plenums so that marine mattresses placed on the gravel and between groups of three plenums where the top of the mattress is level with the top of the plenums. All plenum top surfaces will be at the same elevation and the fill (gravel) will be level within the array (non-perimeter edges) to the height of the plenum top surfaces. Immediately outside the screen array (perimeter edges), the fill (rip-rap) profile will gradually blend into the pre-construction river bottom profile. Rip-rap would consist of graded angular stone with maximum sizes between 13 and 18 cm (5 and 7 in). Marine mattresses are planned to be installed above the header pipes and an intervening layer of graded crushed rock. They would consist of geogrids (made of reinforced polymer material) filled with 8 to 15 cm (3 to 6 in) diameter stone and would be 20 to 30 cm (8 to 12 in) thick.

Figure A-1 shows the plan view of the CWW screen arrays, the plenums, riprap and marine mattresses for both units. Figure A-2 shows a more detailed plan view for Unit 2.

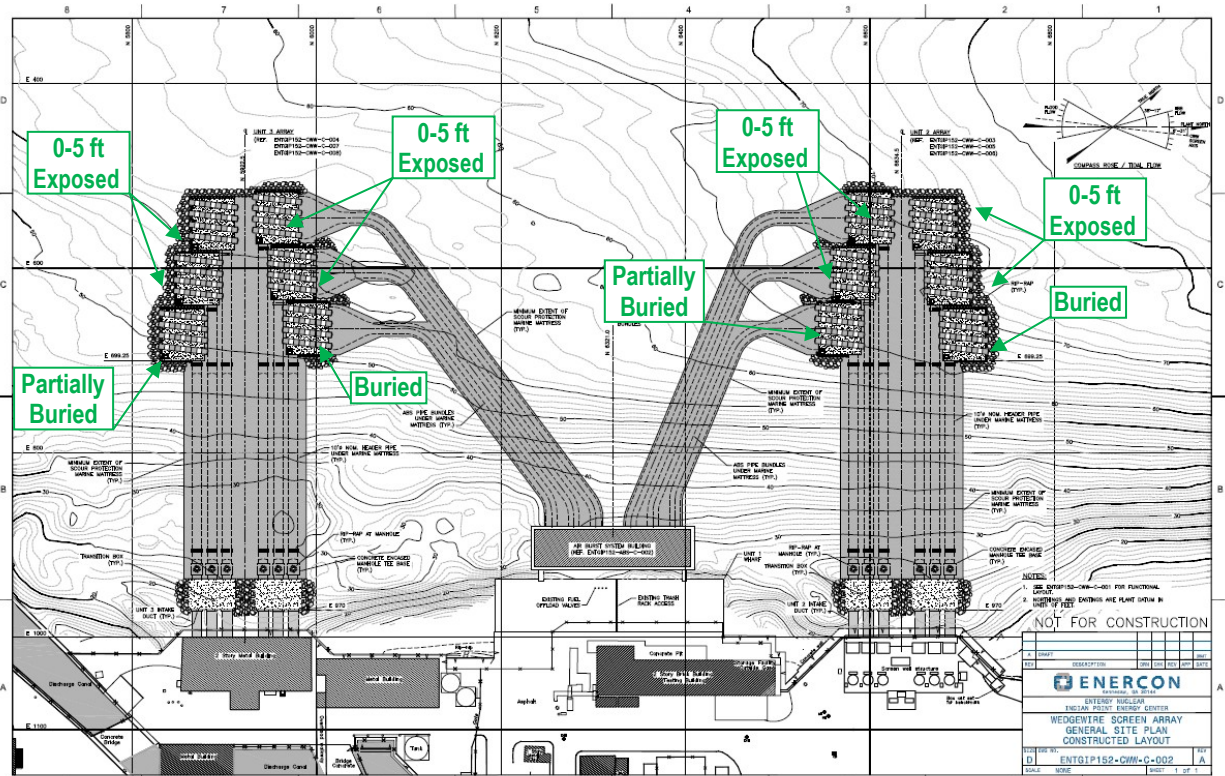


Figure A-1. General site plan constructed layout of CWW screen array (reproduced from Enercon Drawing ENTGIP152-CWW-C-002 Rev A).

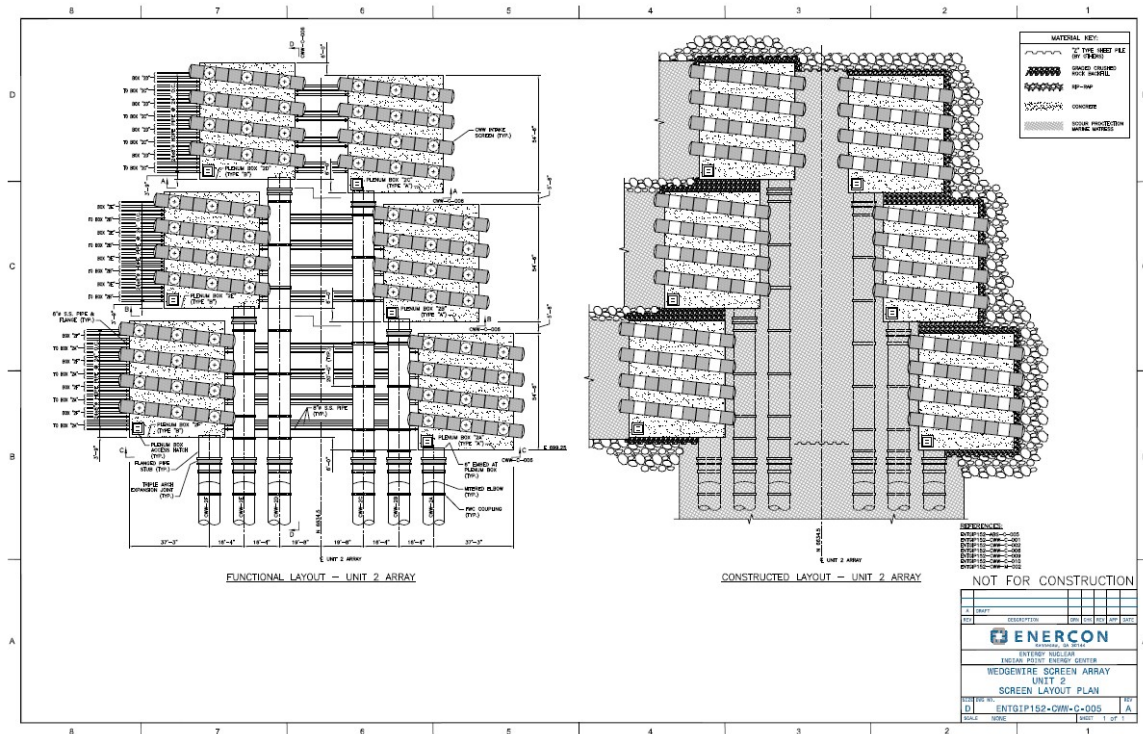


Figure A-2. Screen layout plan for Unit 2 CWW screen array (reproduced from Enercon Drawing ENTGIP152-CWW-C-005 Rev A).

In addition there would be 12 header pipes carrying the cooling water connecting the plenums to four structures (transition boxes) located approximately 9 m (30 ft) in front of the present CWISs with 12 intake ducts to be connected to the CWISs (see Figure A-1). The header pipes would be protected from scour by marine mattresses.

An Air Burst System (ABS) may be used to clear any accumulated material from the CWW screen slots. The system would consist of six buried bundles of 24 pipes each that extend from the new ABS building and platform to six pairs of plenums and then into each of the 144 CWW screens (see Figure A-1). High pressure air (up to 1.4 MPa [200 psi]) would provide sufficient force to dislodge material in the slots. Only one CWW screen on each unit would be “burst” at a time. The piping for the system would all be installed below the natural bottom and protected from scour by marine mattresses.

APPENDIX B: DATA COLLECTION ACTIVITIES IN PROPOSED AREA OF CWW SCREENS

TABLE OF CONTENTS

Table of Contents	1
List of Figures	1
B.1 Side Scan And Sub Bottom Surveys	2
B.2 Sediment Sampling	5
B.3 Acoustic Doppler Current Profiling	5
B.3.1 Water Column Currents	6
B.3.2 Backscatter and Total Suspended Solid Concentrations.....	9

LIST OF FIGURES

Figure B-1. Backscatter intensity from sidescan survey and sediment grain size distributions determined from samples collected as part of the Hudson River Estuary Program studies and reported by Nitsche et al. (2004). The light gray area (low backscatter intensity) directly in front of the IPEC was interpreted as recent deposition while the dark gray areas (high backscatter intensity) was interpreted as areas of erosion	2
Figure B-2. Sidescan imagery from the April 2010 survey performed by Substructure Inc. Gray color indicates the degree of acoustic backscatter from sediment on the river bed. Dark gray tones were considered to be areas of fine grained sediment while the light gray areas represented coarse grain deposits. Lines indicate water depth which decreases from upstream to downstream and near shore.....	3
Figure B-3. Areas covered by the November 2010 survey performed by Ocean Surveys Inc. Lines indicate the survey lines traversed by the survey vessel. Numbered vibra-core locations are also depicted. Geophysical data were not collected within the avoidance area surrounding a security barge onsite.....	4
Figure B-4. Multibeam data from the Ocean Surveys November 2010 survey of the area in front of the IPEC. Areas of deposition are dark gray with a smooth appearance while erosional areas are indicated by light gray tones. Depth contours are superimposed.	5
Figure B-5. Illustration of the location of the four ADCPs from the Normandeau field study.....	7
Figure B-6. Time series of bottom current speeds for the four Normandeau deployed ADCPs...	8
Figure B-7. Current rose of observed bottom currents from Normandeau field study. The rose is displayed in the oceanographic coordinate system.....	9

B.1 SIDE SCAN AND SUB BOTTOM SURVEYS

Using sidescan imagery, Nitsche, et al. (2004) delineated areas of riverbed as erosional (high backscatter, dark gray in Figure B-1) or depositional (light gray areas, low backscatter), defining acoustic facies that could be used to determine the predominant sedimentary process. Based on this analysis, the light gray area directly in front of the IPEC was interpreted to be depositional, but with thin (< 0.5 m [< 1.6 ft]) sediment accumulations, while the surrounding darker areas were thought to be erosional.

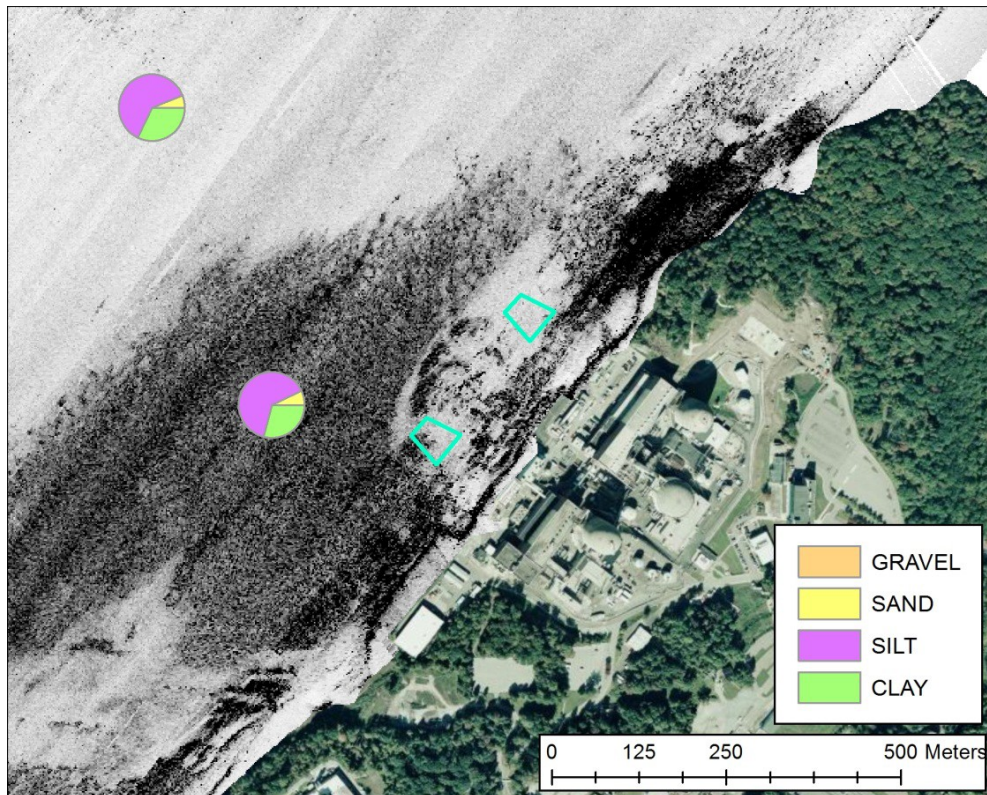


Figure B-1. Backscatter intensity from sidescan survey and sediment grain size distributions determined from samples collected as part of the Hudson River Estuary Program studies and reported by Nitsche et al. (2004). The light gray area (low backscatter intensity) directly in front of the IPEC was interpreted as recent deposition while the dark gray areas (high backscatter intensity) was interpreted as areas of erosion.

Substructure Inc. conducted a multibeam and sub-bottom profile survey on 12-13 April 2010, in the area directly in front of the IPEC. The data, shown in Figure B-2, provided a higher resolution image of the area than the Nitsche et al. data, but because sediment samples were not collected, it was not correlated to grain size or sediment type. Substructure inferred that areas of high backscatter (light gray in the image) depicted coarse grain sediment while the low backscatter regions (dark gray) depicted fine grain sediment.



Figure B-2. Sidescan imagery from the April 2010 survey performed by Substructure Inc. Gray color indicates the degree of acoustic backscatter from sediment on the river bed. Dark gray tones were considered to be areas of fine grained sediment while the light gray areas represented coarse grain deposits. Lines indicate water depth which decreases from upstream to downstream and near shore.

Ocean Surveys Inc. collected sub-bottom survey data in the area of the IPEC in November 2010 (track lines shown in Figure B-3). Sediment vibra-cores were also collected as part of this study that could correlate acoustic data with sediment data.

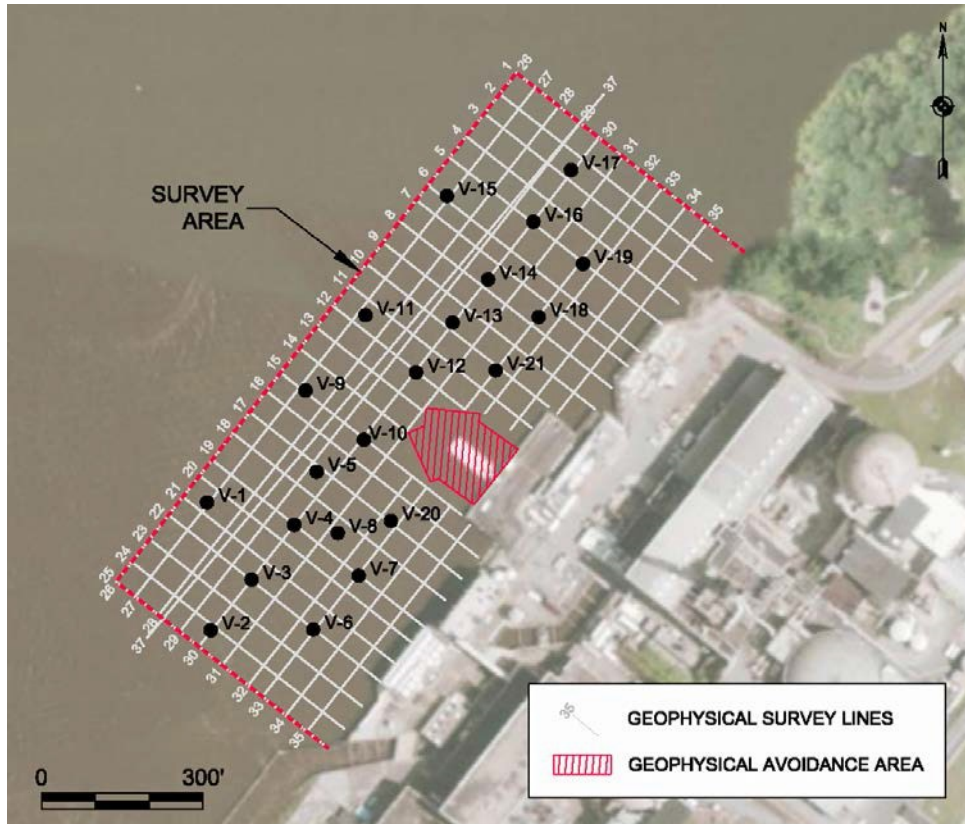


Figure B-3. Areas covered by the November 2010 survey performed by Ocean Surveys Inc. Lines indicate the survey lines traversed by the survey vessel. Numbered vibro-core locations are also depicted. Geophysical data were not collected within the avoidance area surrounding a security barge onsite.

Using the sidescan images from the Substructure Inc. field study in combination with results of the historical hydraulic physical modeling of the river interacting with plant cooling water systems performed with initial plant construction, GZA refined the interpretation of sedimentary environments provided by Nitsche et al. (2004) to characterize the river bed sedimentary environments (Figure B-4). GZA concluded that the proposed sites for the CWW arrays were within an area of “reduced current velocities and deposition.” The area outside the screen array locations was characterized as erosional.

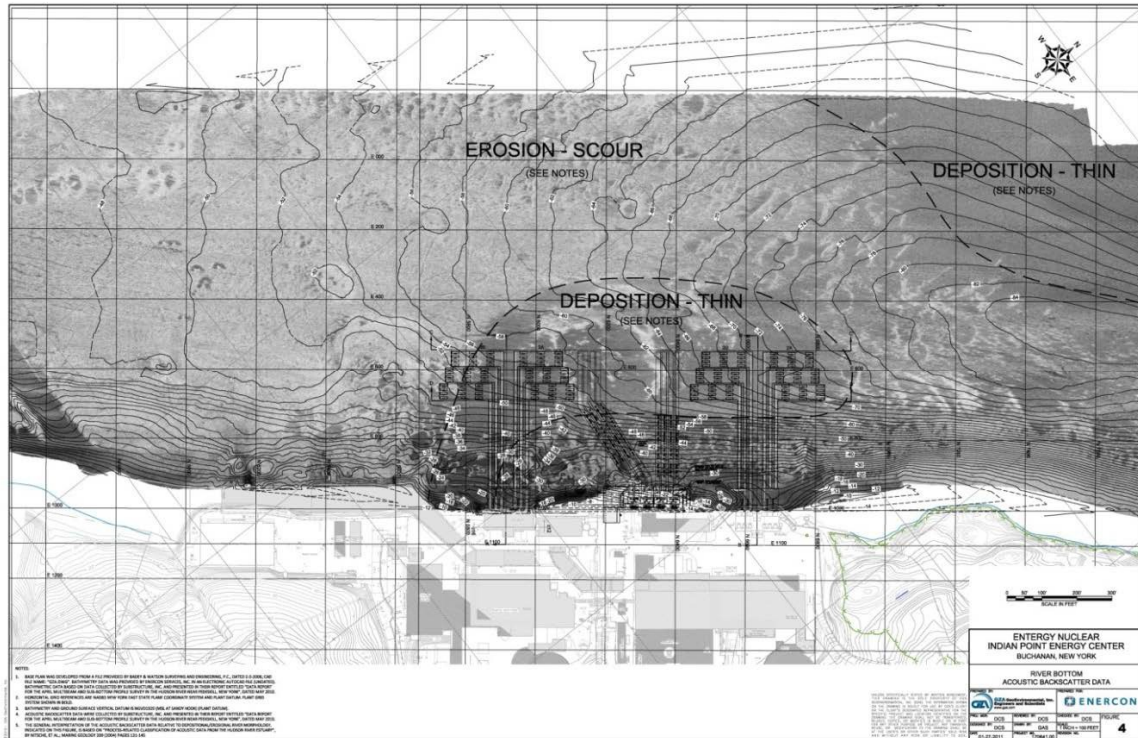


Figure B-4. Multibeam data from the Ocean Surveys November 2010 survey of the area in front of the IPEC. Areas of deposition are dark gray with a smooth appearance while erosional areas are indicated by light gray tones. Depth contours are superimposed.

B.2 SEDIMENT SAMPLING

The most comprehensive sampling within this area was done as part of the November 2010 study performed by GZA during which Ocean Surveys Inc. collected 21 vibra-cores at the site (see Figure B-3). The GZA report provided laboratory analysis results from a handful of samples taken from the vibra-cores and estimated the fraction of silt and clay in many portions of the cores. These data showed that surface sediment within the area surrounding the proposed CWW intake structures was predominantly (90% or more) silt and clay, with a small number of samples containing 40% or more of sand and gravel.

B.3 ACOUSTIC DOPPLER CURRENT PROFILING

In support of preliminary design of the CWW installation, Entergy retained Normandeau to perform a study of the water column current characteristics in the area of the proposed CWW screen installation through both field observations and data analysis (Normandeau, 2011). This section describes the Normandeau field study data.

B.3.1 WATER COLUMN CURRENTS

The Normandeau study included a field observation program and data analysis; the field program was carried out to obtain the necessary information to map the three-dimensional current structure at the location of the future installation of the CWW screen arrays. This was accomplished through deployment of four separate ADCPs which continuously monitored water column currents. The ADCPs were located at sites representative of the location of the proposed future CWW screen arrays as shown in Figure B-5.

The ADCPs used in the field study were upward-looking Teledyne RD Instruments known as Workhorse Sentinel ADCP (either 600 or 1200-kHz). They were deployed in multiple separate installations over a period of 4 March 2010 – 1 November 2010. At different points during this period, the instruments were temporarily retrieved to allow for data transfer and then immediately redeployed in the same location. The observations were taken via a number of vertically stacked bins and the observations recorded every five minutes as the average velocity over the five minute period for each bin. For the most part the bins were 0.5 m (1.6 ft) in size (vertical thickness); however, a few individual deployments utilized 1-m (3.3-ft) bins. The bin center of the bottom bin was typically ≈ 1 m (3.3 ft) above the sea floor. Since the focus of the study pertained to the environment in the immediate vicinity of the future CWW arrays, the Normandeau study focused on currents only in the bottom ≈ 11 m (36 ft) of the water column, and of particular interest were the bottom 5 bins (1 to 3 m [3.3 to 10 ft] above the River bed), which represented boundary layer conditions of the flow (e.g., Dyer, 1986) as well as the depths corresponding to the location of CWW screen arrays.

Figure B-6 illustrates time series of the observed bottom currents from the four deployed ADCPs during the length of the field program and Figure B-7 displays a scatter plot of observed current speed plot on a compass rose (displayed in the oceanographic coordinate system) where the location of the observation indicates the direction toward which the current was heading. The relatively linear pattern demonstrated the tidal nature of the currents, with slightly more directional variability on flood when the current was moving upstream.



Figure B-5. Illustration of the location of the four ADCPs from the Normandean field study.

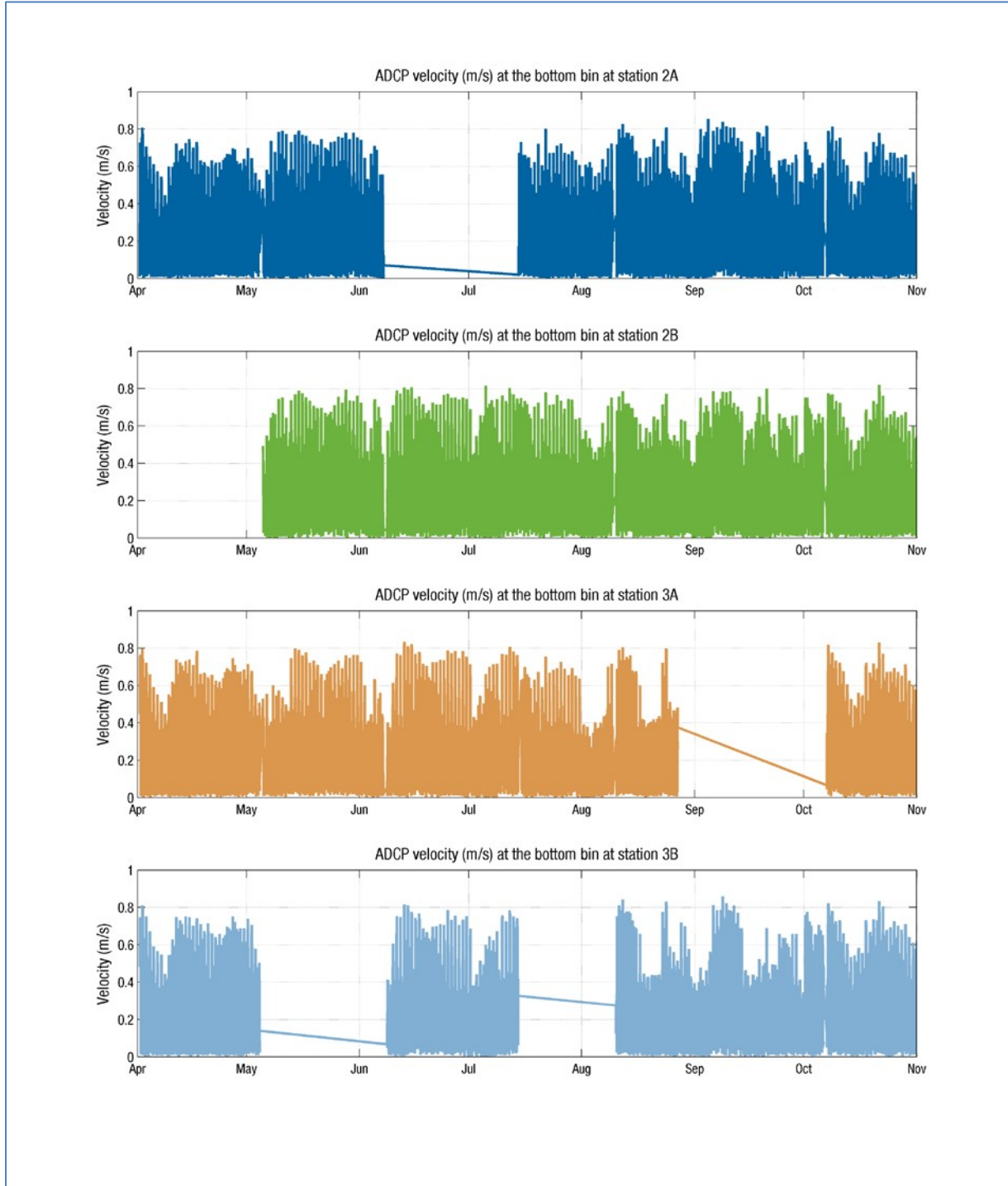


Figure B-6. Time series of bottom current speeds for the four Normandeau deployed ADCPs.

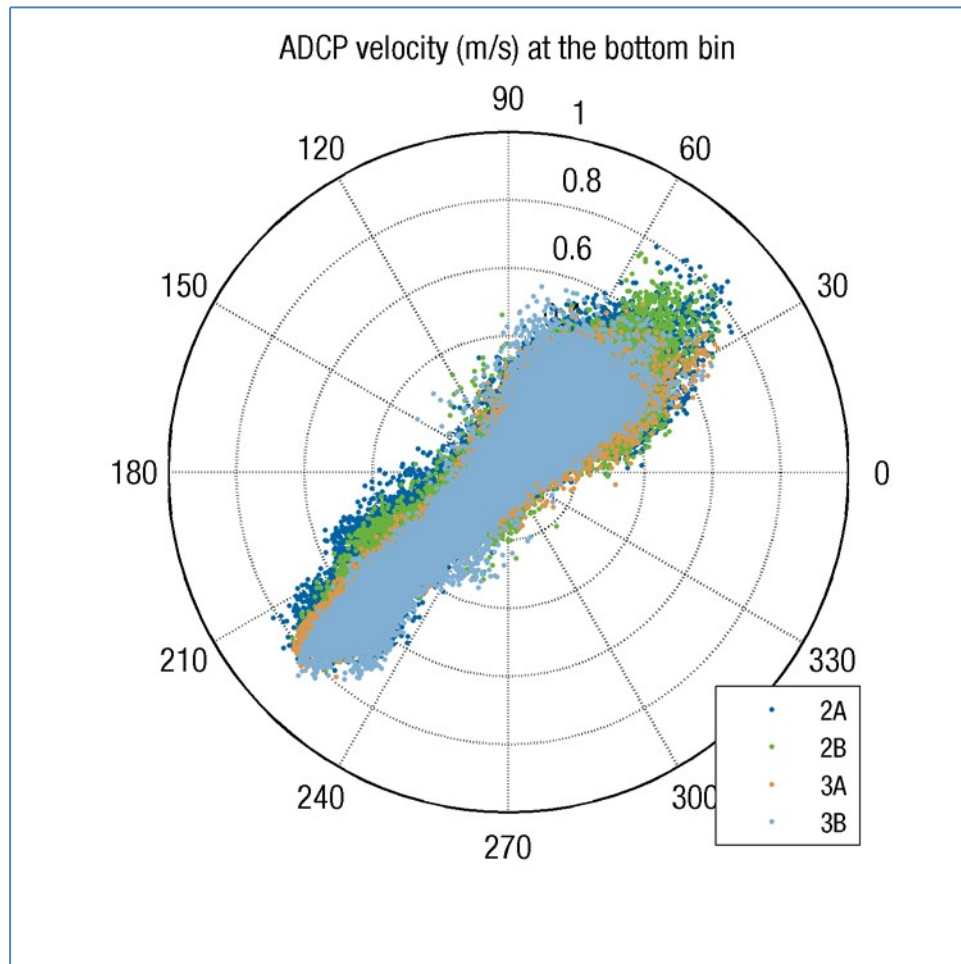


Figure B-7. Current rose of observed bottom currents from Normandeu field study. The rose is displayed in the oceanographic coordinate system.

B.3.2 BACKSCATTER AND TOTAL SUSPENDED SOLID CONCENTRATIONS

While not the intention of the Normandeu study, ADCPs can be used to estimate the degree of suspended solids (sediments) in the water column. ADCPs use acoustic waves to measure current velocity profiles in rivers, estuaries, and the ocean. This is accomplished by measuring the frequency shift, via the Doppler effect, of sound backscattered from particles (scatterers) in the water. The intensity of the sound that is backscattered off particles can be related to concentration of total suspended solids (TSS) through a calibration procedure which utilizes water column samples from which total suspended solids are measured to calibrate the instrument backscatter values to concentrations. This technique was developed to estimate suspended sediment concentrations (SSC) using backscatter intensity (e.g., Holdaway et al., 1999; Kim and Voulgaris, 2003; Gartner, 2004; Kim, 2006). This approach is similar to the use of higher frequency, acoustic backscatterance sensors (reviewed in Thorne and Hanes, 2002) developed specifically for TSS concentration measurements.

The method described in Kim (2006) was applied to the backscatter (also referred to as Echo Intensity) data acquired along with current observations from the Normandeau field program. Since the field program was not aimed at obtaining estimates of suspended solids concentrations, it did not include water samples of TSS concentrations and therefore the instruments were not calibrated to obtain absolute values of TSS. However, the echo intensity data was used to develop a relative index of TSS where the echo intensity signal could be analyzed to determine periods of relatively higher or lower TSS concentrations

APPENDIX C: SHEAR STRESS AND EROSION/DEPOSITION OF BOTTOM SEDIMENTS

LIST OF FIGURES

Figure C-1. Time series of current-derived bottom shear stress and echo intensity from ADCP 2A during July 2010	4
Figure C-2. The relationship between bottom shear stress and echo intensity from all four ADCP observations during July 2010	5
Figure C-3. Hjulstrom diagram showing the relationship between grain size and threshold erosion velocity	5

Analysis of Sedimentation Effects of Proposed CWW Screens at IPEC

A useful parameter for determining the potential of either erosion or deposition is the magnitude of bottom shear stress. Bottom shear stress is a function of the vertical structure of the water column currents, the water density and a drag coefficient. The frictional drag is dependent on the magnitude of shear stress of the flow, which depends on the viscosity of the fluid, the roughness of the surface and on the detailed form of the near surface flow. This shear stress can be derived by the interaction of wave and current in the coastal and estuarine environments. The combined wave and current shear stress (τ_{wc}) can be estimated:

$$\tau_{wc} = \tau_{curr} + 1.2 \cdot \tau_{curr} \cdot \left(\frac{\tau_{wave}}{\tau_{curr} + \tau_{wave}} \right)^{3.2}$$

where τ_{curr} is the shear stress due to current and τ_{wave} is the wave-induced shear stress (Soulsby and Clarke, 2005).

The current-driven shear stress on the bottom (τ_{curr}) has been experimentally observed to be proportional to the square of the velocity as

$$\tau_{curr} = \rho \cdot C_D \cdot u_{100}^2$$

where ρ is the fluid density, C_D is the drag coefficient, and u_{100} represents the velocity at 100 cm (3.3 ft) above the bottom (Dyer, 1986; Soulsby and Clarke, 2005). The drag coefficient is

$$C_D = \frac{U_*^2}{\langle u_{100} \rangle^2}$$

where $\langle u_{100} \rangle$ is the mean velocity at 100 cm (3.3 ft) above the bottom, and U_* is the friction velocity

$$U_* = \frac{K u_z}{z_0}$$

where u is velocity (cm/s), z is height above the bottom (cm), K is the Van Karman constant ($K = 0.42$) and z_0 is bottom roughness (cm). The bottom roughness is estimated using the extension of the velocity profile to the z axis to acquire the intercept.

The wave-related bottom shear stress (τ_{wave}) can be calculated as

$$\tau_{wave} = 0.5 \cdot \rho \cdot f_{wave} \cdot u_{wave}^2$$

Analysis of Sedimentation Effects of Proposed CWW Screens at IPEC

where f_{wave} is the dimensionless wave friction factor and u_{wave} is the amplitude of the bottom orbital velocity due to wave motion (Soulsby and Clarke, 2005).

A sediment particle on a river bottom will experience drag and lift force when exposed to a flowing fluid and this drag and lift force is a function of the bottom shear stress. For any given sediment type, there is a shear stress (or near bottom velocity) that is sufficient to dislodge sediment particles from the bottom; this value is referred to as the threshold shear stress (or threshold velocity) for erosion. When the shear stress is larger than this threshold value, the bottom is characterized as mobile, and may be erosional or depositional. When the shear stress is smaller than the threshold, the bottom is characterized as being in equilibrium or depositional. A similar concept can also be applied for the depositional processes, so called a threshold shear stress for deposition.

Previous studies show that the threshold for deposition is lower than or equal to that for erosion in estuarine conditions like the Hudson River (e.g., Parchure and Mehta, 1985; Sanford and Halka, 1993). For the purpose of this analysis, given the assumptions of simple 1-D sediment transport (i.e., vertical exchange of sediments between the water column and the sediment on the bottom) and constant sediment properties in the vicinity of the CWW screen plenum chambers, the bottom shear stress was used as a proxy for determining the potential for erosion or deposition conditions through comparison of the bottom shear stress to the threshold value.

The threshold shear stress was estimated based on ADCP observation data in this study. As described in Appendix B, echo intensity measured by an ADCP can be used for a proxy of suspended particulates in the water column. Figure C-1 shows time series of current-derived shear stress and echo intensity from the first bin (~1 m [3.3 ft] above the bottom) of ADCP 2A during July 2010. The data in this figure spanned one typical tidal cycle, including one maximum flood and ebb tidal flow, and is shown on a timeline referenced to hours after the slack before flood. Higher values of echo intensity represent periods of relatively higher amounts of suspended particles in the water column. This figure shows two distinct events of elevated echo intensity above the background values (e.g., hour 1 and 10). The onset of the resuspension events occurred when the shear stress exceeded 0.1 and 0.05 N/m^2 (1.5×10^{-5} and 0.73×10^{-5} psi), respectively. The coincidence between increase in current velocity and elevated value in echo intensity implies that the suspended matters in the water column are derived from resuspension from the bottom rather than advection from other sources. Thus, the relationship between the shear stress derived from the observed currents and the echo intensity depict the thresholds when sediments are resuspended, representing a period of erosion.

Figure C-2 shows the relationship between the shear stress and echo intensity for the entire data set of four ADCP stations during the July 2010 deployment. This figure indicates that the increase of echo intensity generally occurred when the shear stress was larger than 0.04 - 0.12 N/m^2 ($0.58 - 1.74 \times 10^{-5}$ psi). These ranges corresponded to current speeds of 0.15 - 0.25 m/s (0.06 - 0.10 in/s), which is consistent with the typical value in the literature where the erosion

of a mixture of silt/sand deposit occurred (e.g., Dyer, 1986, Soulsby and Clarke, 2005). This range also matched the value in the well-known Hjulstrom diagram (Figure C-3) which illustrates the conditions associated with erosion or deposition as a function of velocity and grain size. So, the averaged value of the current speed range, 0.2 m/s, will be used for the critical shear velocity in this report.

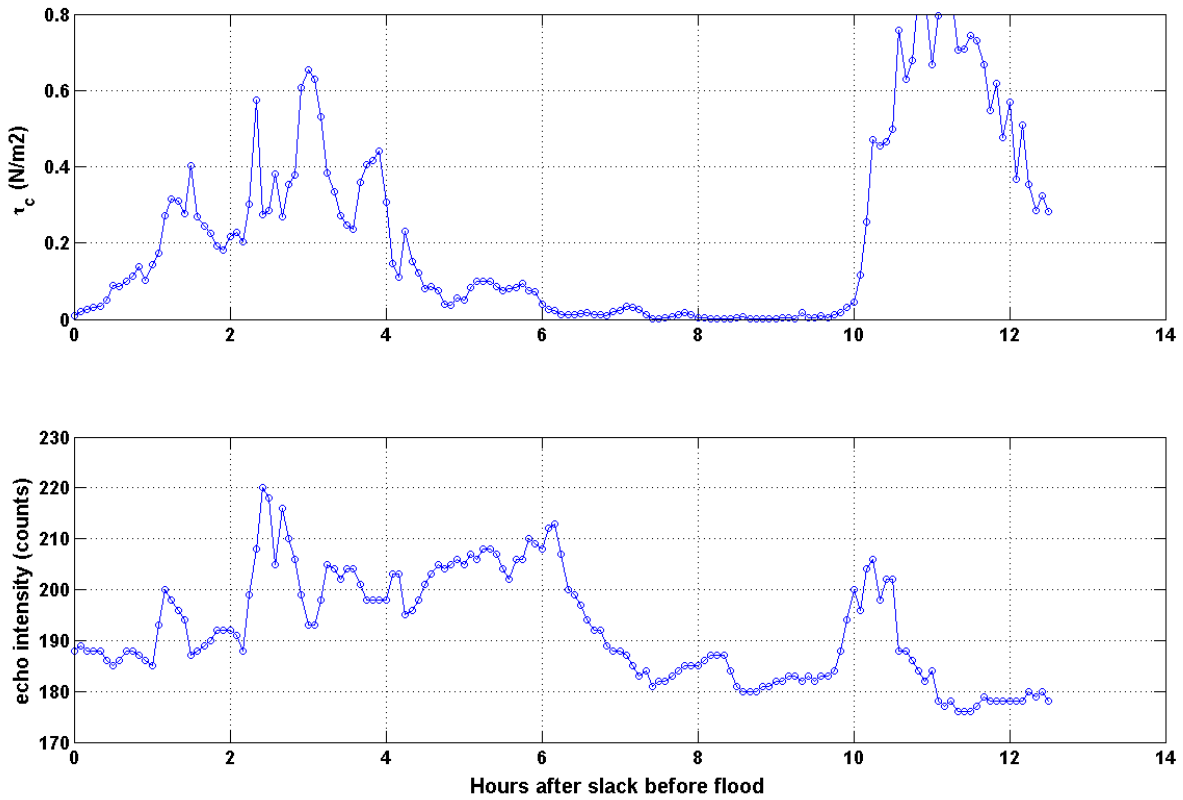


Figure C-1. Time series of current-derived bottom shear stress and echo intensity from ADCP 2A during July 2010.

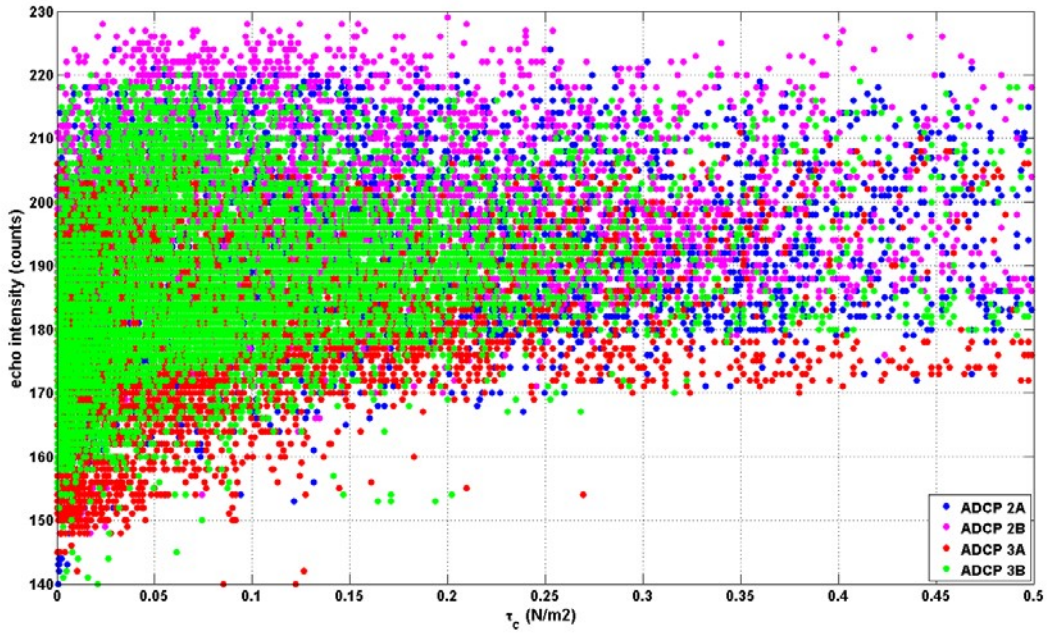


Figure C-2. The relationship between bottom shear stress and echo intensity from all four ADCP observations during July 2010.

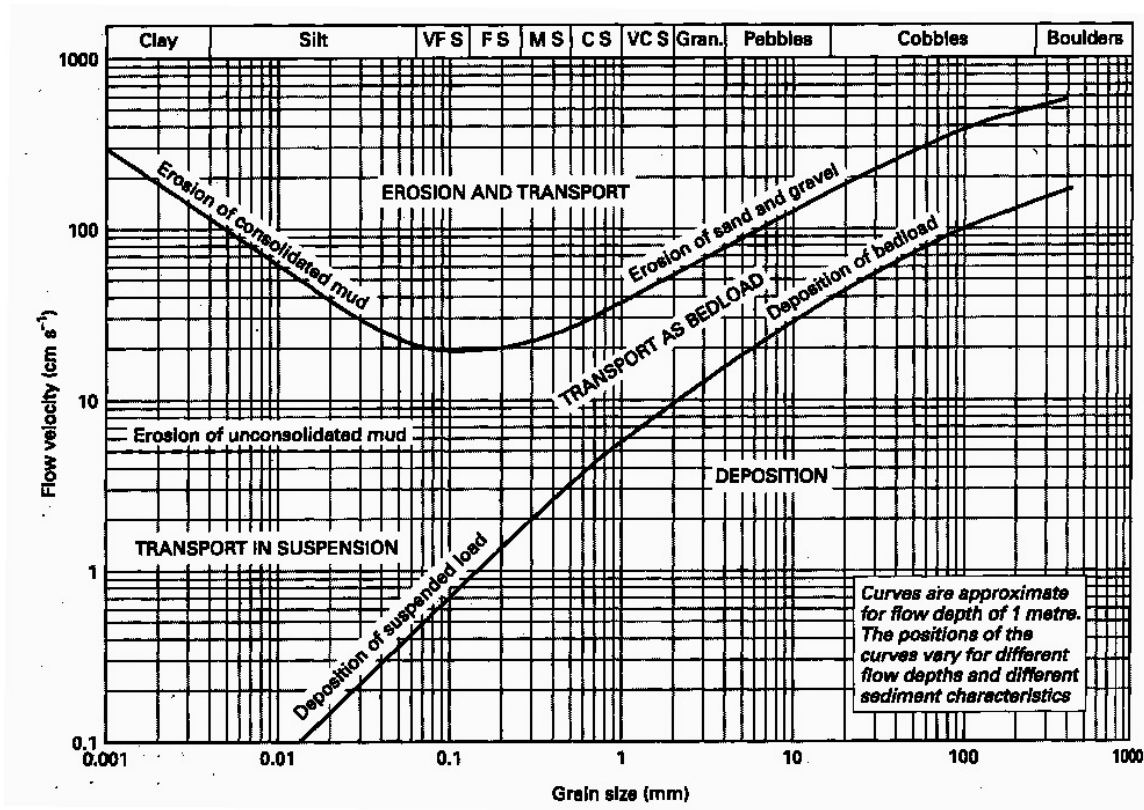


Figure C-3. Hjulstrom diagram showing the relationship between grain size and threshold erosion velocity.

APPENDIX D: ESTIMATION OF BOTTOM STRESS

TABLE OF CONTENTS

Table of Contents	1
List of Figures	1
List of Tables.....	1
D1. Current – Based Bottom Stress	2
D2. Wave – Based Bottom Stress.....	7

LIST OF FIGURES

Figure D-1. Velocity profiles between the bottom ADCP bin at 1 to 10 m (3.3 to 33 ft) above the bottom. Data is averaged over the deployment from April to November for each of the stations 2A, 3A and 3B, and from May to November for station 2B	3
Figure D-2. Velocity profiles from ADCP data with the reference to the depth below the water surface. Data are averaged over the deployment from April to November for each of stations 2A, 3A and 3B, and from May to November for station 2B	5
Figure D-3. Instantaneous shear experienced at each station over the entire deployment based on the velocity observed in the ADCP bottom velocity bin for each station.	6
Figure D-4. Wind rose from HPN (White Plains) for the period of July 1996 through March 2010.	8
Figure D-5. Illustration of potential fetch relative to IPEC	9

LIST OF TABLES

Table D-1. Time periods for each ADCP station deployment	2
Table D-2. Derived values for friction velocity (U^*), bottom roughness (z_0), and drag coefficient (C_D) from ADCP data.	3
Table D-3. Average calculated shear stress for each ADCP station	5
Table D-4. Summary of wind wave induced bottom stress potential in the area of interest based on wind observations at HPN and scaling factor from SPM for different fetches and wind speeds.....	9
Table D-5. Summary of wind wave induced bottom stress potential in the area of interest based on wind observations at IPEC for different fetches and wind speeds	10

D1. CURRENT – BASED BOTTOM STRESS

An estimate of bottom stress from the currents measured at the four Normandeau ADCP sites (2A, 2B, 3A, and 3B) near the proposed CWW installations was made. In order to estimate bottom stress, the drag coefficient at each ADCP location was calculated. As part of this estimate, the drag coefficients at these locations were calculated (since they were needed along with bottom velocity to estimate the bottom shear stress).

Data from the four bottom mounted Normandeau ADCP stations: 2A, 2B, 3A, and 3B were used in this analysis. ADCPs 2A and B were located in slightly deeper water (~20 m [66 ft]) and better represent the River channel, while stations 3A and B were located in approximately 17 m (56 ft) of water representing shoal condition when compared to the stations 2A and B. Each station location had observations from multiple short term deployments interrupted by brief periods of instrument retrieval for data transfer. For this analysis the individual deployment records were combined together to provide continuous six- to seven-month time series (Table D-1). There were some slight differences in the bin depths between deployments, so observations from similar depth bins were identified and concatenated to generate long term records at representative depth along the vertical profile. The observed data were averaged in time to create a mean vertical profile for each of the four stations; profiles are shown in Figure D-1. The vertical profiles extend from 1 to 10 m (3.3 to 33 ft) above the local bottom. Near the bottom, all stations show similar velocities, 0.23 to 0.25 m/s (0.75 to 0.82 ft/s) but the stations 2A and B diverge from stations 3A and B with maximum mean velocities at 10 m (33 ft) reaching 0.33 m/s (1.08 ft/s) and 0.38 m/s (1.25 ft/s), respectively, in a near linear manner.

Table D-1. Time periods for each ADCP station deployment.

Station	Start Date	End Date
2A	1 April 2010	1-November-2010
2B	5 May 2010	1-November-2010
3A	1 April 2010	1-November-2010
3B	1 April 2010	1-November-2010

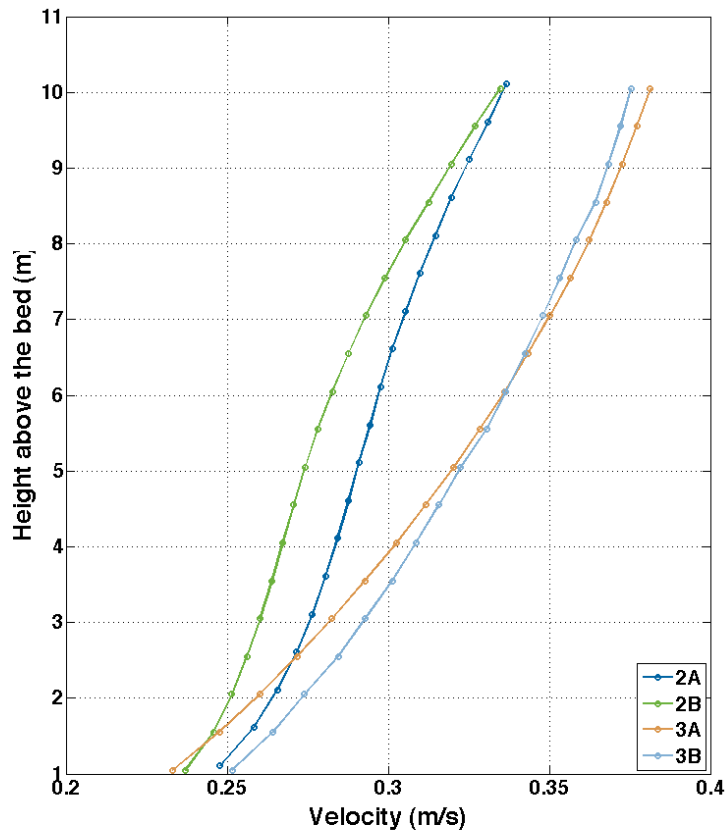


Figure D-1. Velocity profiles between the bottom ADCP bin at 1 to 10 m (3.3 to 33 ft) above the bottom. Data is averaged over the deployment from April to November for each of the stations 2A, 3A and 3B, and from May to November for station 2B.

The friction velocity (U^*), bottom roughness (z_0), and drag coefficient (C_D) were calculated using the bottom 5 bins (1 - 3 m [3.3 – 9.8 ft]) of the averaged profiles with the equations described in the previous section. The results of these calculations are summarized in Table D-2.

Table D-2. Derived values for friction velocity (U^*), bottom roughness (z_0), and drag coefficient (C_D) from ADCP data.

Station	U_{100} (cm/s)	U^* (cm/s)	z_0 (m)	C_D
2A	24.5	1.16	0.014	0.0023
2B	23.6	0.90	0.002	0.0015
3A	23.1	1.95	0.734	0.0071
3B	25.0	1.63	0.171	0.0042

The bottom roughness (z_0) values were estimated as the intercept of vertical velocity profiles on y-axis in Figure D-1 . The results are listed in Table D-2, ranging 0.002 – 0.734 m. The bottom roughness values calculated for locations 3A and 3B were unreasonably high (0.734 and 0.171

m [2.41 and 0.561 ft]) when compared to typical values from previous studies in estuarine settings (e.g., order of 0.01 m [0.4 in] or less reported in Cheng et. al., 1999). The observations were acquired by bottom-moored ADCPs so that the height above the bottom was used for the vertical reference in the analysis (see Figure D-1). Figure D-2 shows the same velocity profiles presented in Figure D-1 but with the water depth rather than the height above the bottom as the vertical axis. Figure D-2 shows that the water depth of the stations 3A and 3B are approximately 4 m (13 ft) shallower than for stations 2A and 2B. The shape of velocity profiles look almost identical in the water depth range from 10 to 15 m (33 to 49 ft) (Figure D-2). Based on the shape of the profiles, the bottom boundary layer was well developed below 14 m (46 ft) on locations 2A and B, whereas it was not fully developed in any depth of locations 3A and 3B probably due to abrupt bathymetry change. In other words, although the stations 3A and 3B are located in the transition region between channel and shoal system, the flow structure is still under the influence of the channel regime.

It should be noted that the equation for estimating the drag coefficient and bottom roughness was developed given the assumption of local dissipation of the total turbulent energy due to the bottom boundary. The condition in station 3A and B does not comply with this assumption, and the unreasonably high value of bottom roughness supports this incompliance. Thus, the estimated values of shear stress and drag coefficient from 3A and 3B were excluded in further analysis. On the contrary, drag coefficient and bottom roughness values calculated from the data of stations 2A and 2B are consistent with typical literature values (~ 0.002 and ~ 0.01 m, respectively) as well as the hydrodynamic modeling performed for this project. Given the similarities of both the ADCP profiles at 2A and 2B and their resulting drag coefficients, an average of the two stations ($C_D = 0.0019$) will be used in the bottom shear stress calculations. By applying this drag coefficient and the critical shear velocity of 0.2 m/s, the critical shear stress can be estimated as 0.077 N/m^2 ($1.117 \times 10^{-5} \text{ psi}$) for the further analysis.

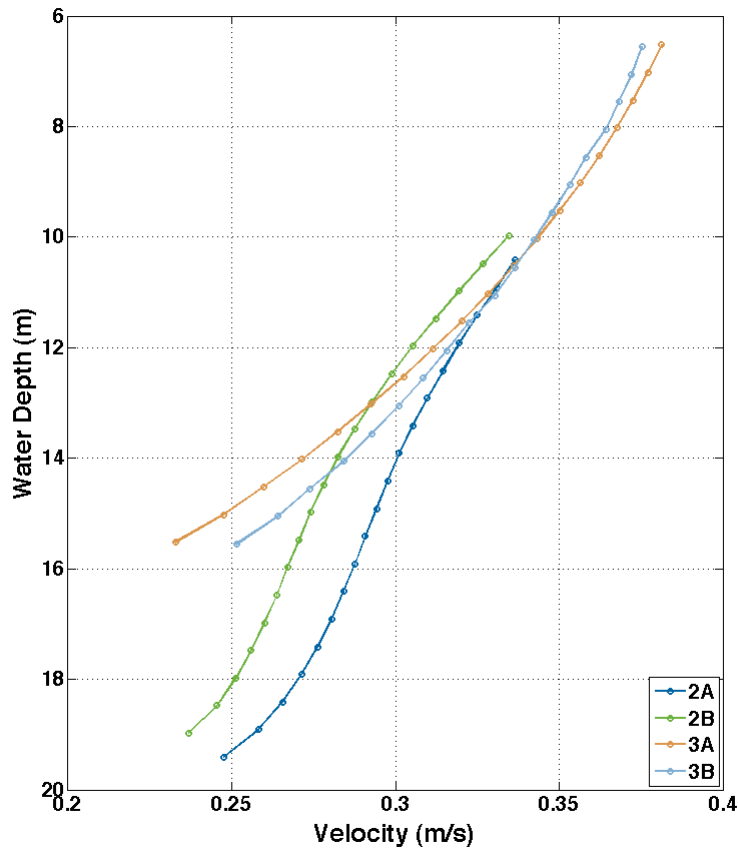


Figure D-2. Velocity profiles from ADCP data with the reference to the depth below the water surface. Data are averaged over the deployment from April to November for each of stations 2A, 3A and 3B, and from May to November for station 2B.

The estimates of average drag coefficients were subsequently used along with the ADCP velocities observed at 1 m (3.3 ft) and a water density of 1014 kg/m^3 (63.30 lb/ft^3) to estimate instantaneous shear stress at each of the ADCPs with the time series of these estimates at each location shown in Figure D-3. The average shear stress over the observation period at each location is summarized in Table D- 3.

Table D-3. Average calculated shear stress for each ADCP station.

Station	Mean Shear Stress
2A	0.177 N/m^2 ($2.57 \times 10^{-5} \text{ psi}$)
2B	0.165 N/m^2 ($2.39 \times 10^{-5} \text{ psi}$)
3A	0.159 N/m^2 ($2.31 \times 10^{-5} \text{ psi}$)
3B	0.179 N/m^2 ($2.60 \times 10^{-5} \text{ psi}$)

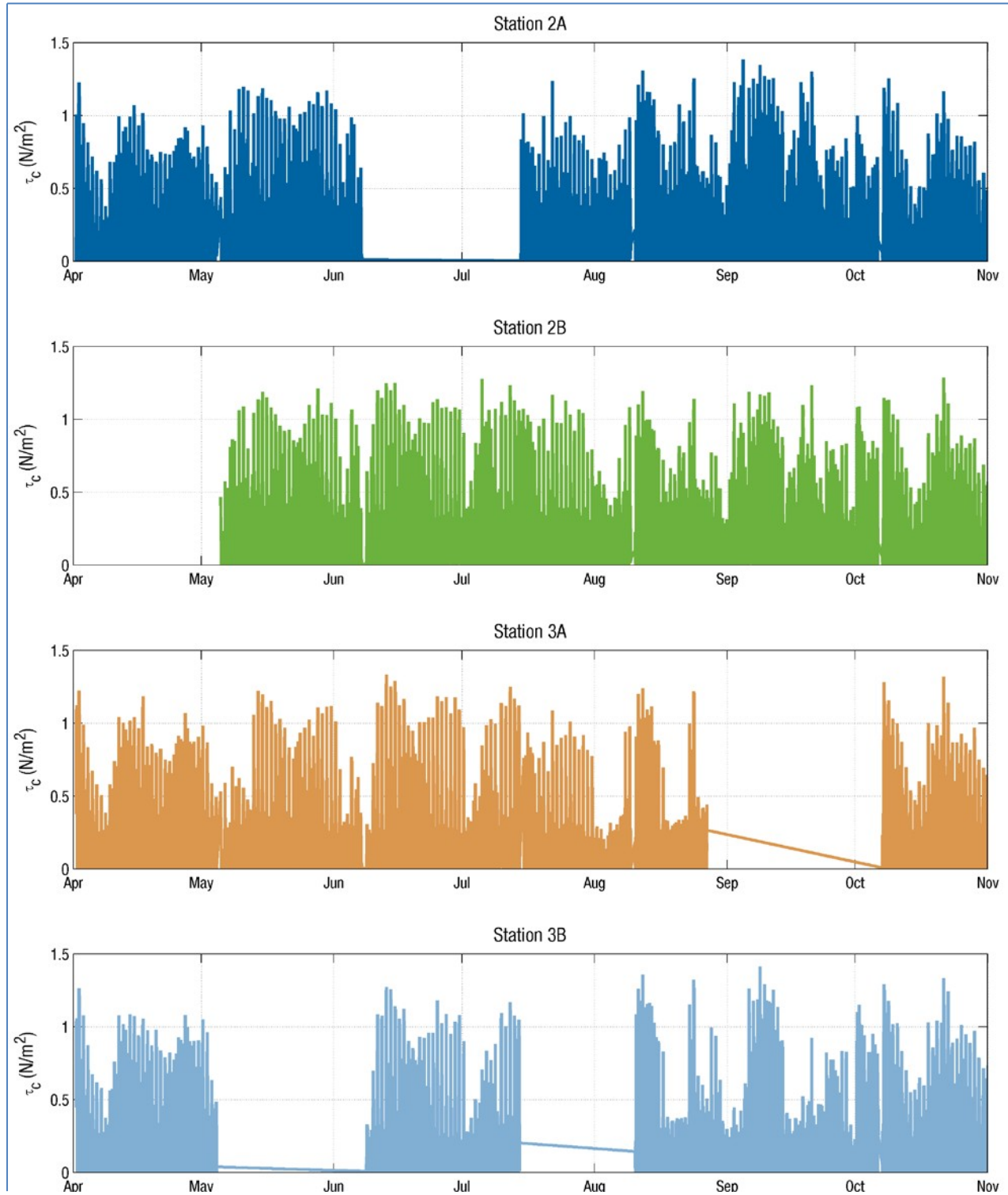


Figure D-3. Instantaneous shear experienced at each station over the entire deployment based on the velocity observed in the ADCP bottom velocity bin for each station.

D2. WAVE – BASED BOTTOM STRESS

An analysis of the bottom stress in the River due to wind driven wave action was also performed. Estimates of significant wave height and period as well as bottom orbital water velocity were made using formulations from the Shore Protection Manual (SPM) (Coastal Engineering Center, 1984) for fetch limited waves in shallow waters. These formulations are appropriate for this site, based on the geometry of the shoreline, which limits the fetch in any orientation to relatively small distances (less than 3 km [1.9 mi]), and the bathymetry in the area which is within the threshold for the assumption of shallow waters (15 to 21 m [50 to 70 ft] at the site, which is less than the 90 m [295 ft] threshold). Significant wave height and period, bottom water particle orbital velocity, water depth, water density, and sediment grain size as defined by the d_{50} (median) grain size were then used as input to formulations for the wave related bottom shear stress (Soulsby and Clarke, 2005) presented in Appendix C. Estimates of bottom shear stress resulting from a range of wind speeds and fetch (for varying direction) were made based on this approach.

The area of the analysis is located less than 150 m (500 ft) from the eastern shore of the River in front of the existing IPEC intake units. Water depths in the area range from approximately 15 – 21 m (50 – 70 ft). Depth influences the significant wave height estimates as well as the bottom orbital velocity; however depth has a greater influence on bottom orbital velocity where orbital velocity increases as depth decreases. For this analysis to be conservative, the shallower depth of 15 m (50 ft) was used.

The wind record from the White Plains Airport (HPN) from the period from July 1996 through March 2010 was analyzed to determine the patterns of wind speed and direction in the region; this record contains hourly wind speed and direction observations at an elevation of 10 m (~ 33 ft) above grade. This was the data set used in the hydrothermal model application (Swanson et al., 2010 and Swanson et al., 2011) for IPEC. Figure D-4 shows a wind rose from HPN which indicates that the wind at HPN was typically from the northwest, and analysis of the data showed that the median (P50) wind speed was approximately 3.1 m/s (10.2 ft/s) and that the peak (P99) wind speed was observed to be approximately 10.3 m/s (33.8 ft/s).

Due to orographic effects, the wind direction and speed at the area of interest on the River may be somewhat different than those observed at HPN; however, the patterns of winds are anticipated to be similar. Wind induced waves increase with higher wind speeds and in order to account for the potential increases in wind speed in the area compared to the land-based observations, the observations were scaled based on guidance from the SPM Coastal Engineering Center, 1984) on relating land-based observations to coastal waters. The SPM provides a curve of estimated amplification factors of wind speed as a function of land wind speed observed with recommended amplification values decreasing with increasing wind speed. Using this approach the amplification factors for the average (P50) and extreme (P99) observed wind speeds were estimated at 2.0 and 1.2, respectively, which resulted in an average and extreme wind affecting the River of 6.2 m/s (20.3 ft/s) and 12.4 m/s (40.7 ft/s), respectively. In order to account for potential directional differences the analysis was run for

different fetches reflecting all possible directions of winds blowing towards the area of interest. Figure D-5 shows an aerial view of the study site with buffer rings at 500-m (1640-ft) increments from the area; this figure illustrates that the fetch ranges from 1.5 km (4,900 ft) to 3.0 km (9,800 ft).

Estimates of shear stress were made using the extremes of these inputs as well as the assumption that water density was 1014 kg/m^3 (63.30 lb/ft^3) and the sediment d_{50} was 0.002 mm ($8 \times 10^{-5} \text{ in}$). Table D- 4 provides a summary of the relevant assumptions and incremental results used in the analysis as well as the final calculated values of bottom shear stress based on these input parameters. The fetch limited significant wave height ranged from $0.13 - 0.35 \text{ m}$ ($0.43 - 1.14 \text{ ft}$). The associated anticipated range of bottom stress from wind induced waves is between 0.010 and 0.045 N/m^2 (0.15×10^{-5} and $0.65 \times 10^{-5} \text{ psi}$).

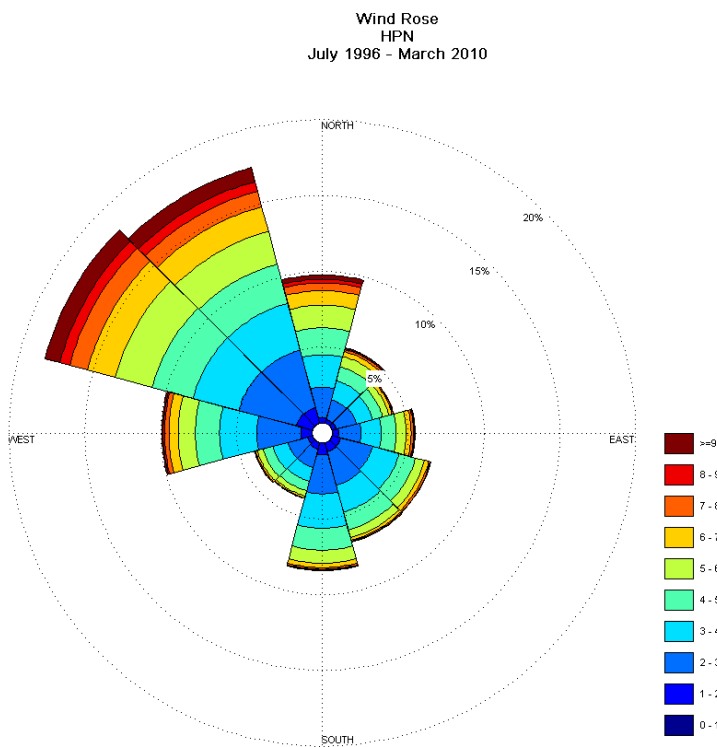


Figure D-4. Wind rose from HPN (White Plains) for the period of July 1996 through March 2010.

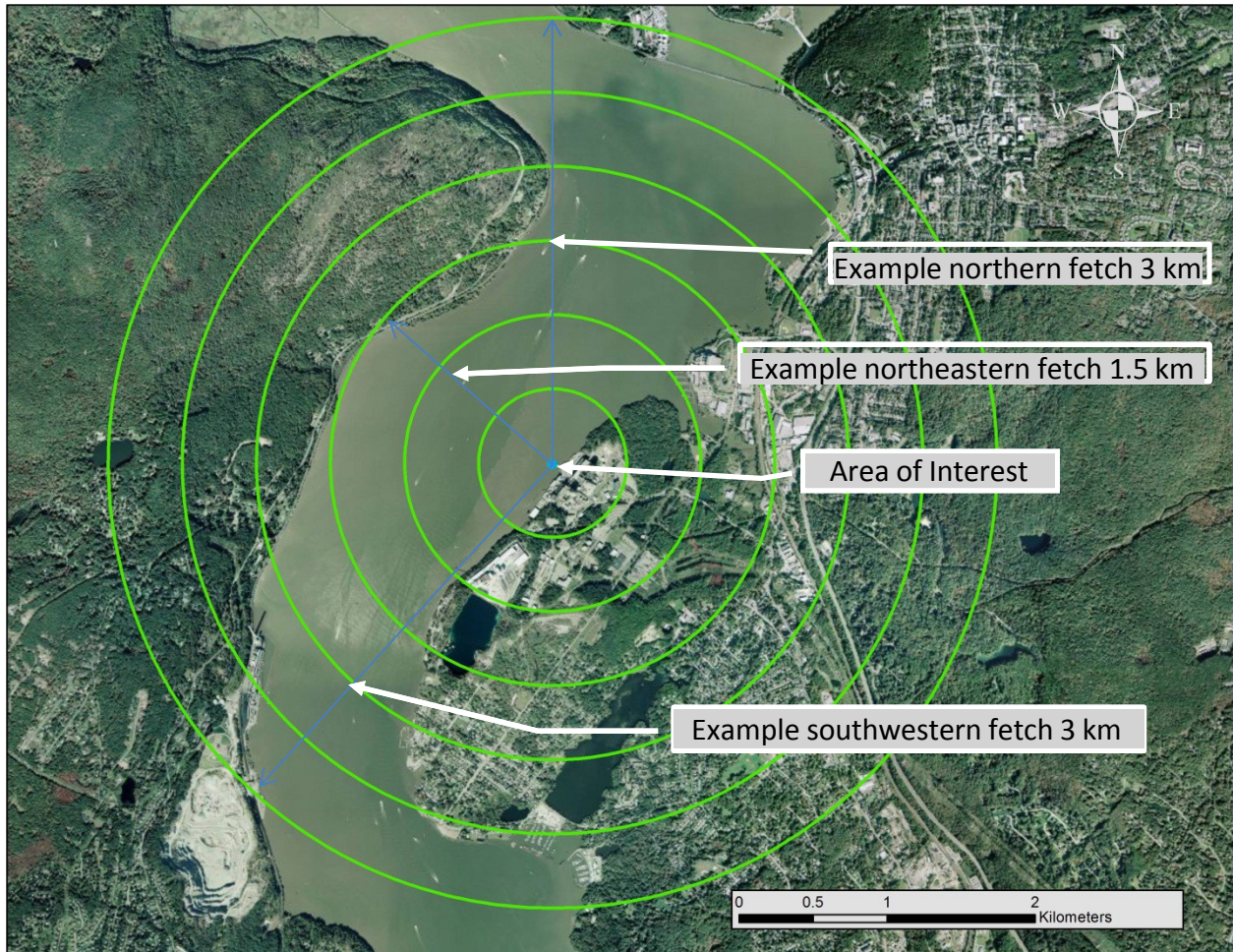


Figure D-5. Illustration of potential fetch relative to IPEC.

Table D-4. Summary of wind wave induced bottom stress potential in the area of interest based on wind observations at HPN and scaling factor from SPM for different fetches and wind speeds.

Parameter	Units	Case 1	Case 2	Case 3	Case 4
Fetch	km	1.5	3	1.5	3
Wind Speed	m/s	6.2	6.2	12.4	12.4
D50	mm	0.002	0.002	0.002	0.002
Water Depth	m	15	15	15	15
Significant Wave Height	m	0.13	0.19	0.31	0.35
Significant Wave Period	s	1.30	1.61	1.75	2.17
Orbital Wave Velocity	m/s	0.044	0.075	0.124	0.175
Bottom Stress	N/m ²	0.010	0.015	0.030	0.045

To assess the potential for differences between the winds at HPN and the winds at IPEC, an additional analysis was performed based on the meteorological data set acquired at the plant. This record was shorter, from 1999 through 2008. The analysis showed that, based on local

measurements, the median (P50) wind speed was 4.3 m/s (14.1 ft/s) and the peak (P99) was 12.3 m/s (40.3 ft/s). As a comparison these speeds were, on average, greater than observed at HPN but less than the scaled (from land-based to coastal site) version of HPN used in the wave calculations. Furthermore the peak speed observed on site was greater than observed at HPN but was slightly less, though nearly equivalent, to the scaled version of HPN peak speeds used in the wave calculations. The onsite speeds were not scaled because they were observed onsite whereas the offsite speeds were scaled to account for known relationships between inland versus coastal wind speeds. Table D- 5 summarizes the relevant assumptions and incremental results used in the analysis as well as the final product of calculated values of bottom shear stress based on these input parameters using the speeds observed on site. Compared with the results based on HPN observations (Table D- 4) the bottom stress predictions are similar but smaller. It can be seen that while waves generate bottom oscillatory currents, which would contribute to the local velocity to a small extent, the waves do not contribute significant currents and can be ignored

Table D-5. Summary of wind wave induced bottom stress potential in the area of interest based on wind observations at IPEC for different fetches and wind speeds.

Parameter	Units	Case 1	Case 2	Case 3	Case 4
Fetch	km	1.5	3.0	1.5	3.0
Wind Speed	m/s	4.270	4.270	12.270	12.270
D50	mm	0.002	0.002	0.002	0.002
Water Depth	m	15	15	15	15
Significant Wave Height	m	0.08	0.12	0.31	0.35
Significant Wave Period	s	1.10	1.34	1.74	2.17
Orbital Wave Velocity	m/s	0.034	0.047	0.123	0.174
Bottom Stress	N/m ²	0.006	0.008	0.030	0.044

APPENDIX E: COMPUTER MODELING OF RIVER CURRENTS USING BFHYDRO

TABLE OF CONTENTS

Table of Contents	1
List of Figures	1
E1. Application to the River	2
E2. Comparison of Model Predictions to ADCP – Measured Currents.....	2

LIST OF FIGURES

Figure E-1. Fine resolution BFHYDRO hydrodynamic model grid and bathymetry	3
Figure E-2. Detail of the fine resolution grid and bathymetry showing the present intake locations with proposed CWW screen intake locations shown in gray.....	3
Figure E-3. Plan view of the IPEC area showing the approximate location of the ADCPs used to evaluate currents in the planned CWW screen area.	4
Figure E-4. Model-predicted versus observed current speeds at ADCP station 2A	5
Figure E-5. Model-predicted versus observed current speeds at ADCP station 2B	5
Figure E-6. Model-predicted versus observed current speeds at ADCP station 3A	6
Figure E-7. Model-predicted versus observed current speeds at ADCP station 3B	6

E1. APPLICATION TO THE RIVER

The refined BFHYDRO grid focused on the immediate area of the plant intakes in the IPEC reach of the River including the area for the potential CWW screen installation. The model application was based on the previous calibrated model grid that covers the entire River estuary (Swanson et al., 2010; Swanson et al. 2011). An illustration of the fine resolution grid and bathymetry is shown in Figure E-1 below. A detailed map of bathymetry in the IPEC area showing the location of the present intakes, indicated by the icons on shore, is presented in Figure E-2. This figure also shows the approximate area of the proposed CWW screen arrays, as indicated by the two grey shaded areas offshore of the present IPEC intakes.

The model application was set up with a tidal boundary condition downstream and a river flow boundary condition upstream. The tidal boundary condition was based on measured surface elevation at the Hastings on Hudson USGS gaging station, coincident with the downstream boundary of the model grid domain. The upstream boundary was set up to reflect the River discharge as observed at the Green Island USGS gaging station coincident with the upstream end of the model grid domain above Troy, NY. The model was run for a simulation period between 15 and 31 July 2010; this period had been previously used in the hydrothermal modeling and so synoptic input forcing and output comparison data sets were available.

E2. COMPARISON OF MODEL PREDICTIONS TO ADCP – MEASURED CURRENTS

A comparison of the model-predicted currents to observations in the area of the potential CWW screen arrays was made for the simulation period of 15-31 July 2010. During that time period, Normandeau had four ADCPs deployed in the vicinity of the CWW screen installation area (Normandeau, 2011) as discussed in Appendix B. A map of the approximate location of the deployed ADCPs, denoted as 2A, 2B, 3A, and 3B, is presented in Figure E-3. The number designation refers to the associated IPEC Unit number. The ADCPs were mounted on the bottom of the River to capture the currents at the depth of the CWW screen intake locations. The depth varied somewhat between 15 - 21 m (49 – 69 ft) as can be seen in model gridded bathymetry in the plot.

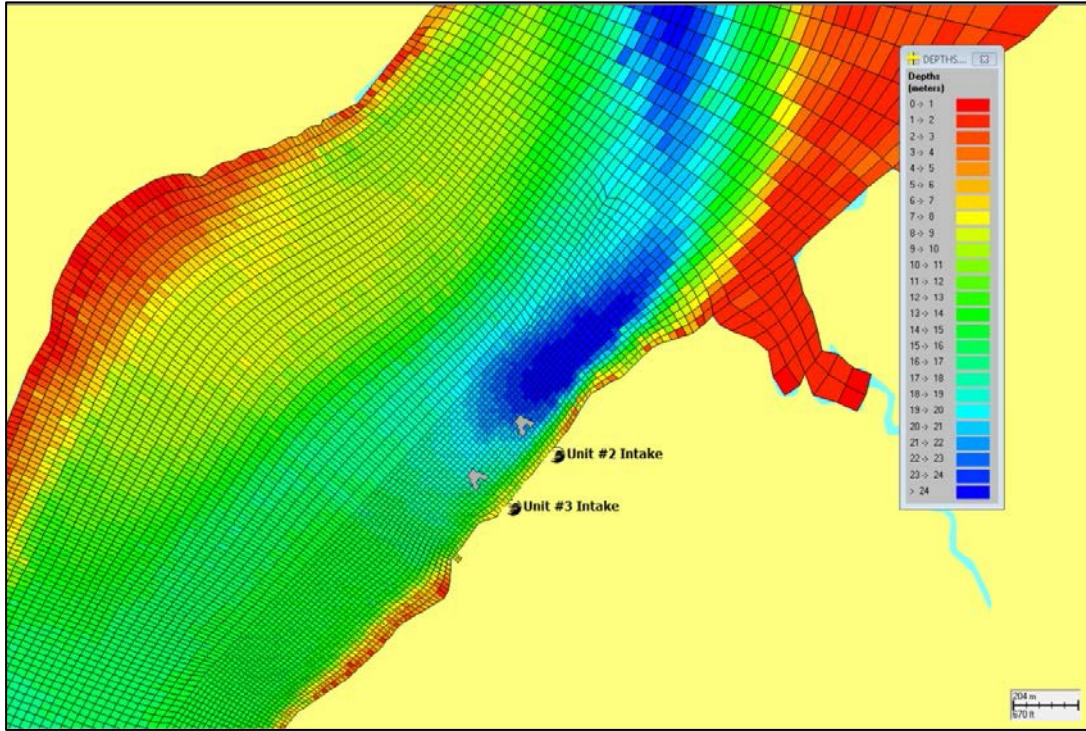


Figure E-1. Fine resolution BFHYDRO hydrodynamic model grid and bathymetry.

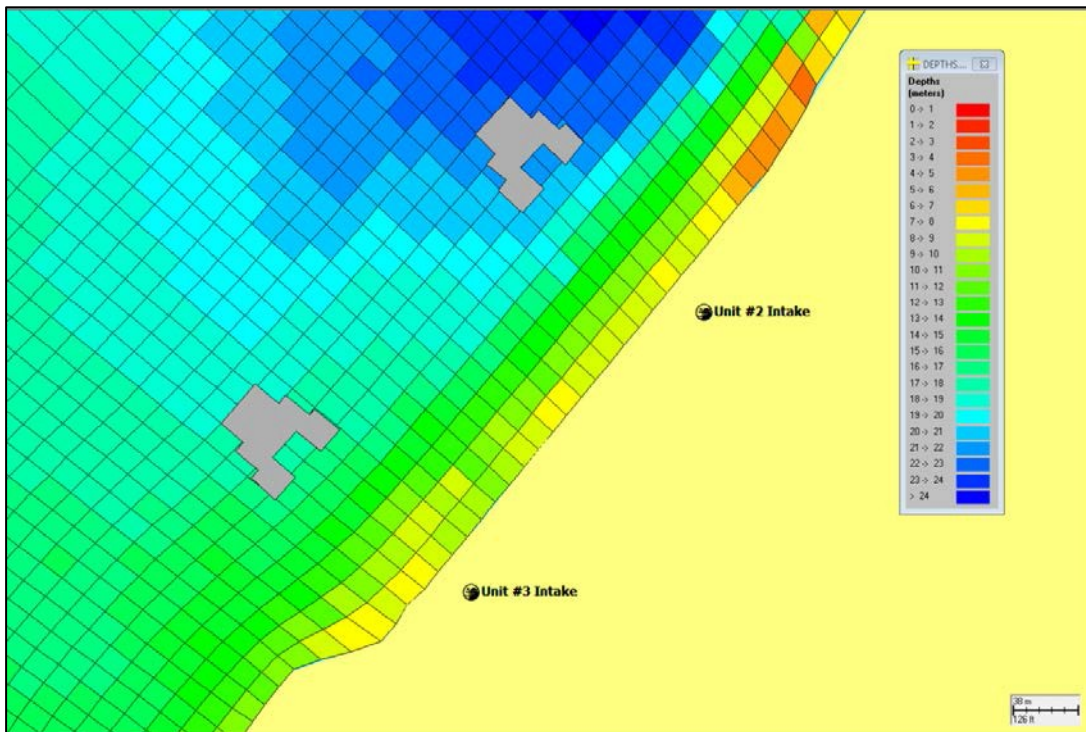


Figure E-2. Detail of the fine resolution grid and bathymetry showing the present intake locations with proposed CWW screen intake locations shown in gray.

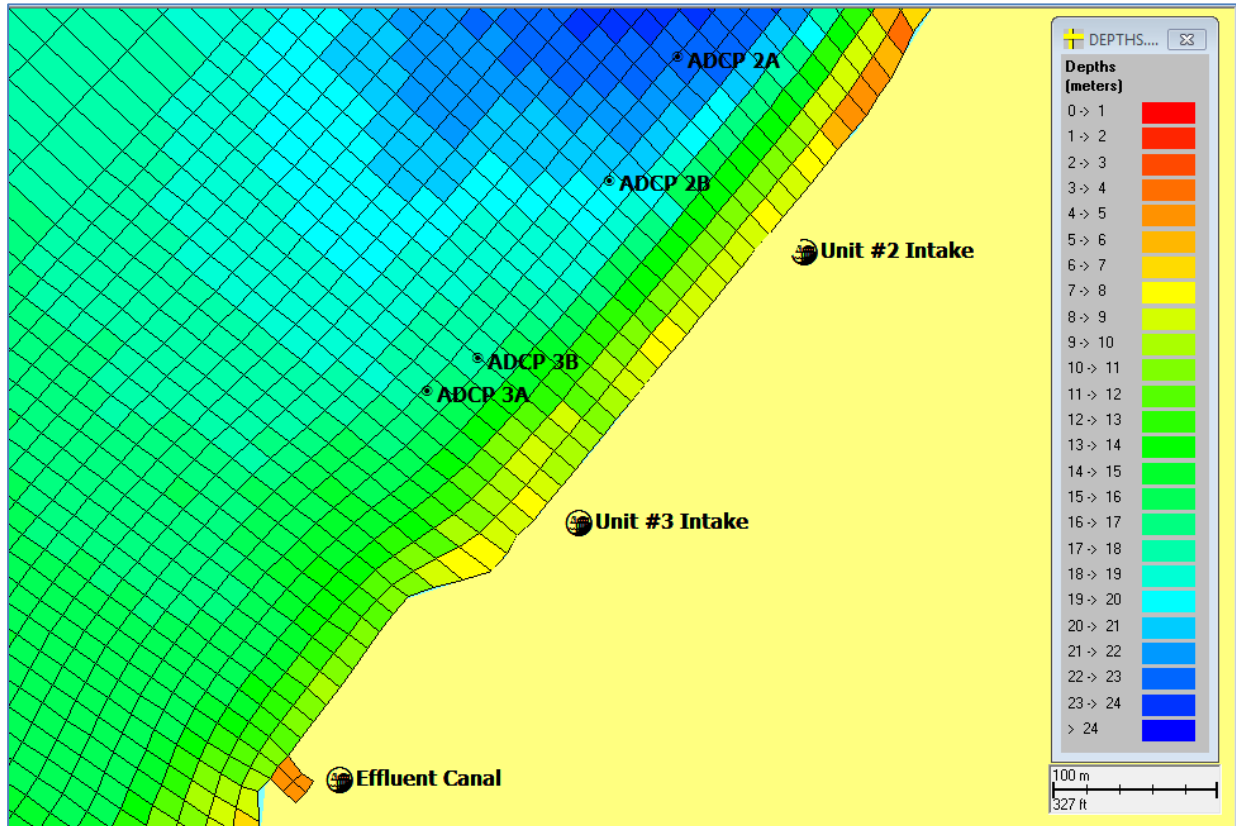


Figure E-3. Plan view of the IPEC area showing the approximate location of the ADCPs used to evaluate currents in the planned CWW screen area.

As the focus of the present analysis was on the potential for changes in the sediment deposition / suspension patterns in the area of proposed CWW screen installations, the bottom boundary layer current speeds and the associated shear stress were of interest. The comparison of model predictions to observations therefore focused on the bottom current speeds to verify the current magnitudes, but also looked at the surface speeds to verify the vertical profile in the CWW screen area. A comparison was made for each of the four ADCP locations, 2A through 3B, which are presented in Figure E-4 through Figure E-7, respectively.

Both the model predictions and the observations contain data at a five-minute timestep, which is presented in the time series plots. In each of the plots the surface speed comparison is in the top panel and the bottom speed comparison is in the bottom panel. It can be seen that the model-predicted current speeds generally matched the observed speed well, recreating both the ebb and flood differential, seen as alternating higher peaks and adjacent lower peaks, as well as the variability over the time period shown. The important aspect of the comparison was that the model predictions accurately captured the magnitudes of the peak speeds observed as well as the variability of those peaks, which affects the suspension / deposition balance in the area.

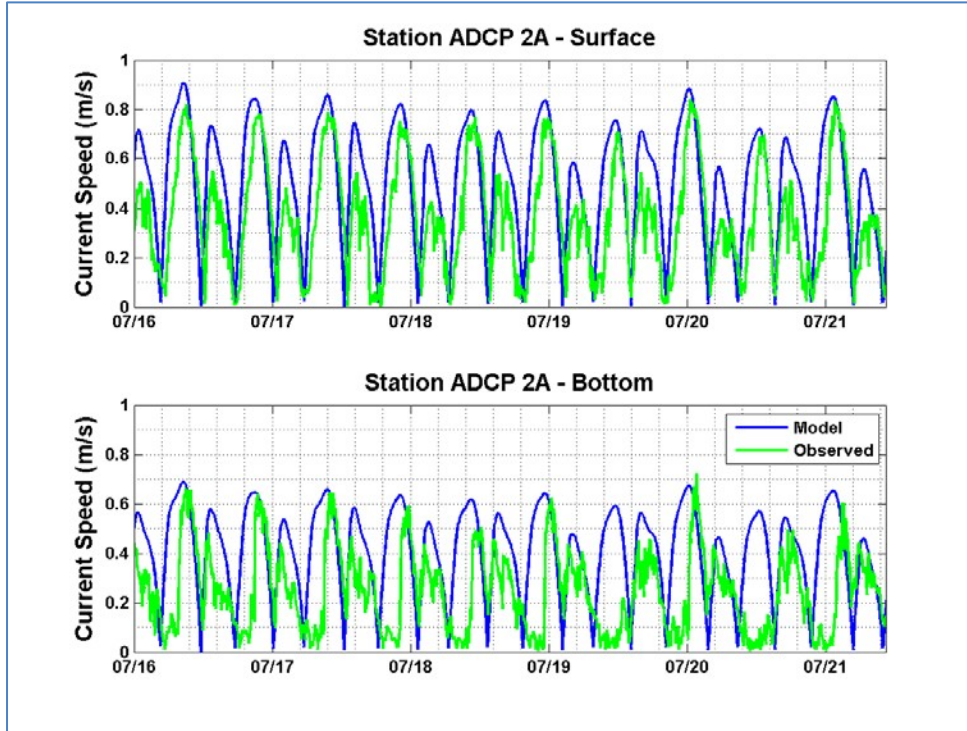


Figure E-4. Model-predicted versus observed current speeds at ADCP station 2A.

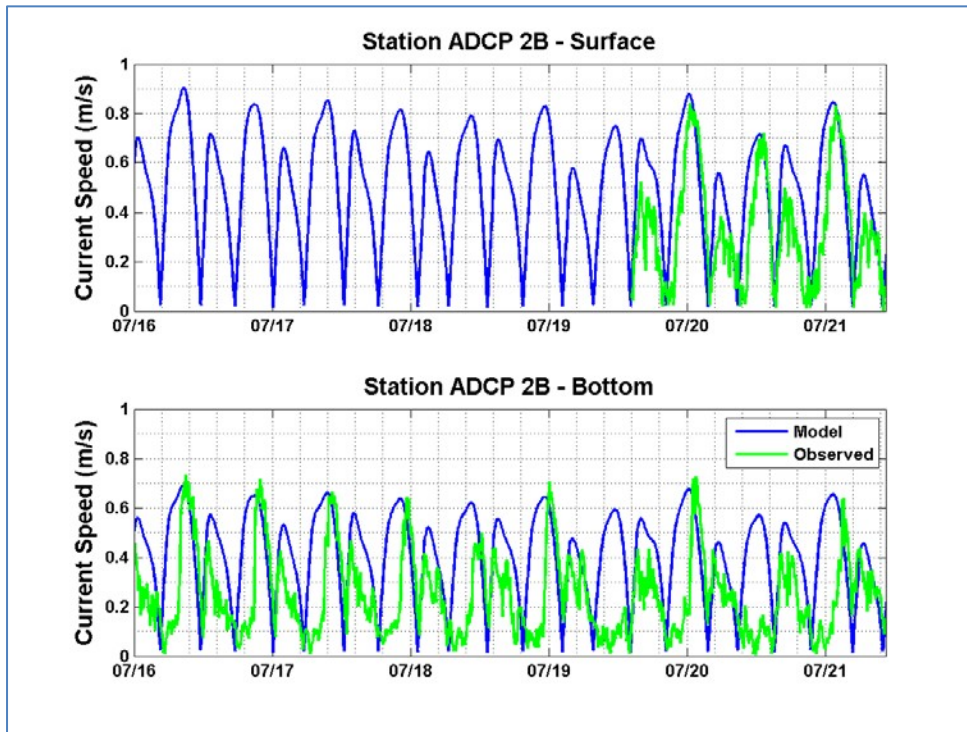


Figure E-5. Model-predicted versus observed current speeds at ADCP station 2B.

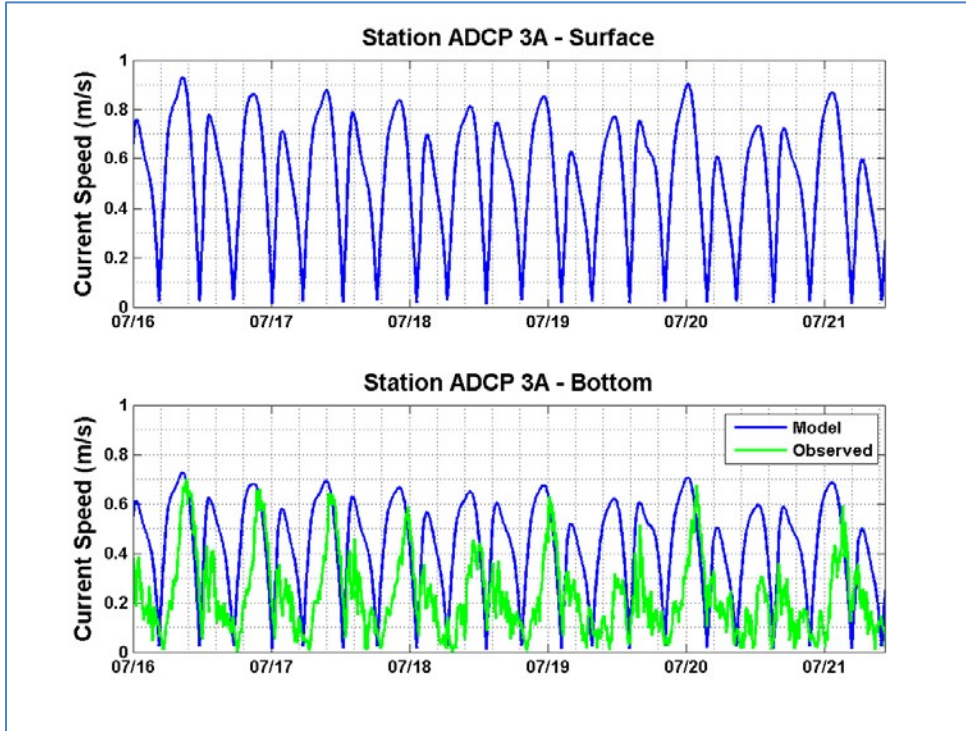


Figure E-6. Model-predicted versus observed current speeds at ADCP station 3A.

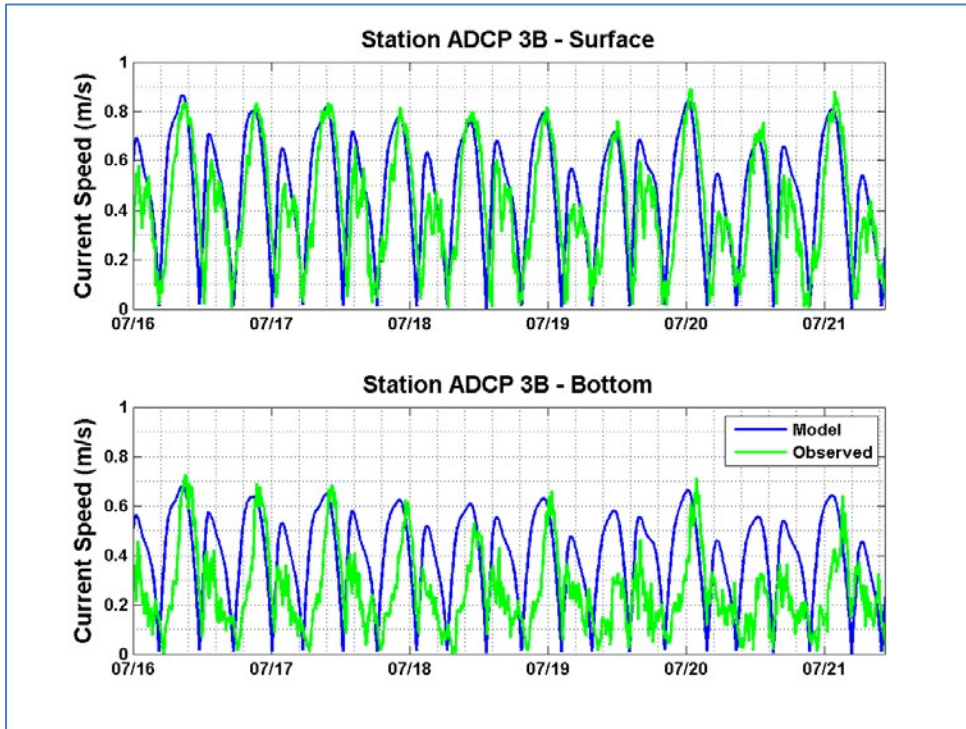


Figure E-7. Model-predicted versus observed current speeds at ADCP station 3B.